FAILURE MECHANISM OF SLOPE UNDER SEVERAL CONDITIONS BY TWO-DIMENSIONAL AND THREE-DIMENSIONAL DISTINCT ELEMENT ANALYSIS

LI NA

M.Phil

The Hong Kong

Polytechnic University

2013

THE HONG KONG POLYTECHNIC UNIVERSITY
DEPARTMENT OF CIVIL AND ENVIRONMENTAL ENGINEERING

FAILURE MECHANISM OF SLOPE UNDER SEVERAL CONDITIONS BY TWO-DIMENSIONAL AND THREE-DIMENSIONAL DISTINCT ELEMENT ANALYSIS

LI NA

A Thesis Submitted in Partial Fulfillment of the Requirements

For the Degree of Master of Philosophy

FEBRUARY 2013

CERTIFICATE OF ORIGINALITY

I hereby declare that the present thesis entitled "**Failure Mechanism of Slope under Several Conditions by Two-dimensional and Three-dimensional Distinct Element Analysis**" is my own work and that, to the best of my knowledge and belief, it reproduces no material previously published or written by other person, no material that has been accepted for the award of any other degree of diploma or other qualifications, except where due acknowledgement and reference has been made in the text.

Signed_____

Name _____Li Na_____

Abstract of thesis entitled

FAILURE MECHANISM OF SLOPE UNDER SEVERAL CONDITIONS BY TWO-DIMENSIONAL AND THREE-DIMENSIONAL DISTINCT ELEMENT ANALYSIS

submitted by Na Li

for the degree of Master of Philosophy

at The Hong Kong Polytechnic University in February 2013

Landslide is a major disaster resulting in considerable loss of human lives and property damages in hilly terrain in Hong Kong, China and many other countries. The factor of safety and the critical slip surface for slope stabilization have been the main considerations for slope stability analysis in the past, while the detailed post-failure conditions of the slopes have not been considered in sufficient details. There are however increasing interest on the consequences after the failure which includes the amount of failed mass and the runoff and the affected region. To assess the development of failure of slope in more details and to consider the potential danger of slopes, the slope stability problem is analyzed by the distinct element method (DEM) in the present research. There are very few studies about slope stability using the DEM in the past due to various difficulties in DEM modeling. To investigate the progressive failure of slope, the author has managed to model the complete failure processes under several

important conditions by particle flow analysis, and important new results have been obtained in the present study. In this study, Particle Flow Code (PFC) is used for the detailed investigation of the failure mechanism of slopes. Large displacement simulation of slope failure by distinct element analysis using PFC has been carried out for both two-and three-dimensional analysis to reveal the failure patterns of simple slope under the effect of self-weight, reinforced action of soil nails, buoyant force and seepage of water flow, local surcharge and also curvature effect on curvilinear slope.

In two-dimensional DEM analysis, firstly, it is found that for a slope with cohesionless soil, failure firstly occurs at the crest of the slope, and the failure gradually extends to the base of the slope until finally the slope angle is equal to the friction angle of the soil and slope is completely collapsed. The analysis successfully simulates the whole flow process of simple slope failure, and the modeling includes the flow of sand from crest to toe of slope. The large scale soil movement and major change of slope geometry have revealed some important stress change and soil movement due to soil failure and flow of soil not considered in the past which is one useful new contribution in this study. Secondly, soil nails can effectively reinforce the slope stability, especially when nail head is used, and the overall stability is greatly enhanced which is demonstrated by the numerical analysis using distinct element method in this study. It is demonstrated that the soil nail can greatly stabilize the stress change along the potential

failure surface even when large scale soil movement is mobilized which is another new contribution. Moreover, four influencing factors are considered in the study of the failure mode by rainfall induced water flow as followings: buoyant effect of ground water, seepage effect, strength reduction during slope failure and persistent rainfall effect. The simulation results show that the slope crest is scoured smoothly under continuous effect of rainfall induced water flow. More obvious settlements occur at the top of the slope, and extended failure zone and noticeable upheaval at the toe are developed compared with normal failure. Thus rainfall induced water flow can accelerate slope failure with an obvious decrease in the stability of the slope leading to collapse at the end. The detailed stress change and large soil movement under these cases are important and useful innovative works with no previous study.

Three-dimensional DEM analysis possesses many major difficulties and is not commonly considered. Practically, most of such studies are devoted to qualitative study with very few quantitative studies at present. In the present three-dimensional DEM analysis, the author has carried out a tedious and very time-consuming analysis together with laboratory test aiming at quantitative slope failure analysis which is an innovative and new work. The comparison of the physical modeling and numerical simulation indicates that the relations between the force against displacement curves are basically similar between the physical model test and the numerical model, and the final failure

loadings from the physical model test and the numerical model are also very close which is a success seldom accomplished in DEM studies. For the three-dimensional curvature influence on slope stability with or without localized loading, the study shows that the curvature defined by R_0/H_0 (where R_0: radius of curvature, H_0: height of slope) has a beneficial effect on the global stability of concave slopes, especially when the resistance of soil is relatively high and also arching effect is illustrated clearly for concave slope. As a result, only partial/localized failure is initiated in concave slope under local loading.

These studies which are seldom considered in microscopic scale in the past are both difficult to be considered as well as useful in giving clearer insights about the development of failure, microcosmic failure mechanism and the post-failure mechanism of slope. The various findings from the present work are pioneer works in slope stability analysis and they are very useful and important to the better understanding of the failure and post-failure condition of a slope.

Key words: slope stability, distinct element method, particle flow code, failure mechanism, two-dimensional analysis, three-dimensional analysis

LIST OF PUBLICATION

Journal Articles

1. Cheng Y.M., Chau K.T., Xiao L.J. and **Li N**. (2010), Flow pattern for silo with two layers of materials with single and double openings, Journal of Geotechnical and Geoenvironmental Engineering, ASCE, 136(9), 1278-1286.

2. Cheng Y.M., Lansivaara T., Baker R. and **Li N.** (2013) The use of internal and external variables and extremum principle in limit equilibrium formulations with application to bearing capacity and slope stability problems, Soils and Foundations, 53(1), 130–143.

3. Cheng Y. M., Au S.K., Pearson A. M. and **Li N.** (2013), An innovative Geonail System for soft ground stabilization, Soils and Foundations, 53(2), 282–298.

4. Li D.Z, Cheng Y.M., Wang J.A., Yang Y., **Li N.** (2013), Finite element based limit analysis with mesh adaptation and applications in geotechnical engineering, Chinese Journal of Geotechnical Engineering, 35(5), 922-929.

5. Cheng Y.M., Li D.Z., **Li N.**, Lee Y. Y., Au S. K. (2013), Solution of some engineering partial differential equations governed by the minimal of a functional by global optimization method, Journal of Mechanics, 29(03), 507-516.

6. Cheng Y. M., Li L., Li D.Z. and **Li N.** (2013), Simplified Approach for Locating the

Critical Probabilistic Slip Surface, Computers and Geotechnics (accepted but in press)

7. Cheng Y.M., **Li N**., Li D.Z. and Lansivaara T. (2012), Relation between Ultimate Bearing Capacity, Lateral Earth Pressure and Slope Stability by the Slip-line and Extremum Methods, Journal of Geotechnical and Geoenvironmental Engineering, ASCE (under review)

8. **Li N.** and Cheng Y.M. (2013), Failure Mechanism of Slope under External Surcharge by 3D-Distinct Element Analysis, Journal of Geotechnical and Geoenvironmental Engineering, ASCE (under review)

Conference Proceedings

1. Cheng Y.M. and **Li N**. (2010), A coupled global optimization algorithm for difficult problems, The Young Southeast Asian Geotechnical Conference, Taipei, Taiwan, May 9-12, p.22.

2. Cheng Y.M. and **Li N**. (2011), Particle flow pattern for silos with single opening, The 14th Asian Regional Conference on Soil Mechanics and Geotechnical Engineering, Hong Kong, China, 23 - 27 May 2011.

3. Cheng Y.M. and **Li. N**. (2011c), Parallel processing for three-dimensional slope stability analysis, International Conference on Future Computational Technologies and Applications, 37-41, Italy.

ACKNOWLEDGEMENT

My deepest gratitude goes first and foremost to my supervisor Dr. Y.M. Cheng, for his professional guidance, his teaching, his constant encouragement, his patience in supervisions and massive help during the past three years. Without his consistent and illuminating instruction, I would not have come so far in my education, and this thesis would not have reached its present form.

Second, I would like to express my sincere gratitude to other professors and teachers at the department of Civil and Environmental Engineering, Dr. Robina Wong etc, who have instructed and helped me a lot during my study. Also to the teachers in University in Shanghai for Science and Technology, China, for their kind support.

Moreover, I also own my heartfelt gratitude to my friends, my roommates, and my fellow classmates, Jiao Yang, Tina Wang, Ma Yao, Li Dazhong, Jessica Sun, Yang Dengbao, Yang Yi, who offer me their helps and times with their encouragement and great support and make my day in Hong Kong.

Lastly, my thanks would go to my beloved family, my parents, Peng Hua and Zhang Jingzhi, my uncle Peng Jian for their endless love and selfless support. Without them, there would be not who I am today.

CONTENT

LIST OF TABLES

LIST OF FIGURES

CHAPTER 1 INTRODUCTION

1.1 Background and motivation

Due to the rapid increase in population and huge demand for buildings in Hong Kong, China and many other developed cities, many buildings and highways are constructed uadjacent to natural slopes and cut slopes. Landslide has been a major cause of disasters resulting in considerable loss of human lives and property damages, and it is also one of the most serious disasters all over the world. To assess the potential dangerous of slopes, different slope stability analysis methods, such as Limit Equilibrium Method (LEM), Upper Bound and Lower Bound Method, Finite Element Method (FEM), Distinct Element Method (DEM), etc, have been developed and improved by researchers and engineers in the past. Among these methods, most of them suffer from the limitations that the post-failure condition is difficult to be assessed and the spread of the failure mass which is also important in many cases cannot be determined. DEM can consider the post failure condition and the spread of the failure mass in a natural way, but there are difficulties in connecting the micro-parameters to the macro-parameters in the analysis.

Due to its simplicity, ease of application and good accuracy, LEM is the most common way for slope stability analysis at present. Limit equilibrium methods for slope stability analysis do not, in general, satisfy the overall equilibrium conditions. Since this method is statically indeterminate by nature, assumptions regarding the inclination and location of the interslice forces have to be made, and there is also a need to search for the critical solution (critical failure surface). Furthermore, LEM is not suitable for the study of progressive failure

which is particularly important for loose fill slope.

Finite element method has been used successfully for the deformation analyses of slopes for about 20 years. The method has been developed to consider the flow rule, yield criterion and convergence criterion. Furthermore, the location of critical failure surfaces can be determined by the shear strain or shear strain increment contour without a need to search for the critical solution. Finite element methods are however computationally intensive requiring long computation time which may be more than 1 day time in some cases. Moreover, it is difficult to assess problems with multiple failure zones or failure surfaces for more complicated cases. The factor of safety is defined only in terms of the shear strength of soil, not the entire system. In this respect, some engineers are not satisfied with the use of the finite element slope stability analysis.

When a soil slope reaches its critical failure state, the critical failure surface is developed and FOS of the slope is 1.0. The continuum methods like FEM or LEM will fail to characterize the post-failure mechanisms in the subsequent failure process. For a rock slope comprising multiple joints sets which control the mechanism of failure, a discontinuum modeling approach is actually more appropriate. Discontinuum methods treat the problem domain as an assemblage of distinct, interacting bodies or blocks which are subjected to external loads and are expected to undergo significant motion with time. This methodology is collectively named as the discrete element method (DEM). DEM will be a more suitable tool for the study of progressive failure and the flow of the soil mass after initiation of slope failure, though this method is not efficient for the analysis of a stable slope.

The development of DEM represents an important step in the modeling and understanding of the mechanical behavior of joint rock masses or soil slope with FOS<1.0. Although continuum codes can be modified to accommodate discontinuities, this procedure is often difficult and time consuming. In addition, any modeled inelastic displacements are further limited to elastic orders of magnitude by the analytical principles exploited in developing the solution procedures. In contrast, discontinuum analysis permits sliding along and opening/closure between particles or blocks. Nowadays, discontinuum modeling starts to constitute the commonly applied numerical approach to rock slope analysis.

The progressive failure/ post failure phenomenon and the action of soil nail and water seepage are important problems in Hong Kong. At present, there is virtually no application of DEM to consider the important action of soil nail and effect of seepage, and there are many outstanding works to be considered in this respect. These outstanding problems will be assessed by the use of two-dimensional particle flow program PFC in present study.

Unlike idealized numerical modeling, most of the slope is three-dimensional in nature. There are far less three-dimensional slope stability studies than two-dimensional studies for all the methods. In this study, the effect of the curvature of slope and the presence of local surcharge will be considered. The beneficial action of soil nail under the effect of curvature which is another outstanding item will also be studied in the present work.

1.2 Objectives

This study will consider various aspects (which are not well considered in the past) about slope stability problems by Distinct Element Method in greater depth as follows:

1. To carry out slope stability analysis by distinct element based particle flow analysis, considering seepage force, soil/nail interface and progressive failure. This work will help to identify the failure mechanism of loose fill slope.

2. To analyze experimental results of slope failures induced from external surcharges, and make comparison with numerical model results to investigate the progressive failure mode of slope under local loading.

3. To extend the numerical study to three-dimensional analysis on the stability of slope to assess the effect of curvature and external surcharges.

1.3 Outline of thesis

This thesis is organized as follows:

Chapter 2 introduces Limit Equilibrium Method, Strength Reduction Method, Finite Element Method, Discrete Element Method and the theory of particle flow code. It also reviews rainfall induced slope stability analysis, and presents how to carry out rainfall-induced slope stability analysis

In **Chapter 3**, the numerical study on the progressive failure mechanism of slope is presented under several conditions including simple slope, soil-nailed slope and slope influenced by rainfall induced water flow by 2D DEM analysis. This analysis gives clearer insight about the development of failure, microcosmic failure mechanism and the post-failure mechanism for slope.

Chapter 4 is devoted to laboratory test and three-dimensional numerical simulation under discrete element method. Physical and numerical models are discussed and compared. Progressive failure mechanism of slope under local loading is analyzed. Furthermore, both qualitative and quantitative studies are performed in the following.

Chapter 5 investigates the influence of curvature on the stability and failure mode of concave slopes by three-dimensional Distinct Element Method. The special effects of the concavity and the progressive failure process have been studied for simple and locally loaded slope with curvature.

Chapter 6 presents the conclusions and summarizes the findings. The suggested further works are also proposed and discussed.

CHAPTER 2 LITERATURE REVIEW

2.1 Slope stability analysis

Slope stability problems have attracted considerable attention from many researchers and engineers, from the past till present. Even though this problem has been studied in great details in the past, there are still many new methods coming out for slope stability analysis at present. In general, slope stability analysis methods can be classified as: limit equilibrium method, finite element / finite difference (strength reduction), limit analysis method, variational method and distinct element method. Limit equilibrium method (LEM) has the advantages of efficiency and the ease to determine the factor of safety with good accuracy, so it is still favored by most of the engineers in routine analysis and design. LEM however requires assumptions on the distributions of the internal forces and location of the critical failure surface which can be critical and difficult for some complicated cases. Strength reduction methods (SRM) which is a stress field analysis usually do not suffer from convergence problem (except under limited cases), and the limitations of LEM do not apply to SRM in general. SRM however requires the assumption on the flow rule and more time in setting up and the solution of the problem. The powerful finite element method can determine the location of critical failure surfaces automatically by the shear strain or shear strain increment contour. For more complicated cases where there are multiple failure zones, it is possible that a particular failure zone may control the non-linear analysis so that only one failure zone is detected during the analysis. To assess the effect of the other failure zones which are not known from the analysis, the engineers may need to manually control the zones of

analysis which are however not known precisely from the initial analysis. LEM, SRM and FEM methods usually are continuum based method which is not suitable if the post-failure mechanism has to be assessed, and distinct element method (DEM) which is discontinuity based method will be more suitable for this case.

2.2 Limit equilibrium method

Up to the present, Limit Equilibrium Method (LEM) has been playing a dominant role in the stability analysis of geotechnical problems mainly due to its simplicity and the capability in obtaining approximate but realistic solutions. The LEM is well known to be a statically indeterminate problem, and method of slices based on the LEM is commonly used by engineers for assessing the factor of safety of slopes. To determine the factor of safety, assumptions on the distributions of internal forces (or thrust line) are required for the solution of the factor of safety. Morgenstern and Price (1965) adopted an assumption that the relation between the interslice normal and shear forces could be specified to make the stability problem statically determinate. In this method, the relation between the interslice normal and shear forces can be described as

$$X=\lambda f(x)E \qquad (2.1)$$

in which $\lambda f(x)$ is the inclination of interslice force and λ can be determined by the equilibrium conditions when a given f(x) is prescribed by the engineers.

Later, Spencer (1967) assumed that all the interslice forces could be assumed to be parallel to obtain the FOS. $\lambda f(x)$is hence actually specified to be 1, and $\lambda f(x)$ is constant in the Spencer's method. Some researchers have made different efforts on the investigation of interslice force function. Chen and Morgenstern (1983) have proposed the interslice force relations for the first and last slices should be based on the Mohr-circle consideration. Fan, Fredlund and Wilson (1986) have proposed a function similar to the error function which is derived from an elastic finite element stress analysis. The validity of this function should actually be questioned as the stress state for slope stability analysis should be the ultimate limit state instead of the elastic stress state. Liang, Zhao and Vitton (1997) adopted the hypothesis of least resistance which stated that among all the forces satisfying the geometrical boundary conditions of a system, the smallest interslice force derived from local moment equilibrium of a slice will be the required force. This method will eliminate the requirement for $f(x)$ at the expense that the hypothesis is not necessarily the true phenomenon. The moment equilibrium of the last slice is also not considered in this formulation, and this formulation is very similar to the original Janbu's rigorous method (1973) and can be modified from the Janbu's rigorous method (1973) by varying the thrust line until the smallest interslice force is obtained.

For "rigorous" methods, "failure to converge" is well known among many engineers, in particular, for complicated problems with heavy external loads or soil reinforcement. Cheng et al. (2008b) have carried out a detailed study on the convergence problem in stability analysis and have concluded that there are two reasons for failure to converge with the

rigorous methods. Firstly, the iteration method that is commonly used to determine the factor of safety may fail to converge because the interslice shear force is assumed to be zero in the first step of the iterative analysis. Cheng (2003) has developed the double QR method, which can evaluate the factor of safety and internal forces directly from a Hessenberg matrix. Based on this method, failure to converge in stability calculations due to the first reason can be eliminated. There are, however, many cases for which the double QR method determines that a physically acceptable answer does not exist for a given f(x), which means that no meaningful factor of safety will be available unless f(x) can be varied. Actually, some engineers have questioned the meaning of "no factor of safety available" for a given failure surface, as such a concept does not appear in structural engineering. So far, there is little previous study on this type of failure to converge, and no rigorous method can guarantee convergence for the general case. Since the critical failure surface may not necessarily converge according to the existing "rigorous" methods of analysis (Cheng et al. 2008b, 2010), there is always a chance that the critical failure surface may be missed during optimization analysis. It is also interesting to note that it has never been proved that a slip surface that fails to converge in stability analysis is not a critical slip surface, but all commercial programs will simply neglect those slip surfaces which fail to converge. Although this problem may not be critical in general, a failure surface with no FOS is still physically surprising. A system without factor of safety is not real and is just a human deficiency in making the wrong assumption, and this situation never appears in structural engineering or other similar disciplines. Factor of safety always exists for a problem, but it is possible that we are not able to determine it simply because of the use of wrong assumption, and this is supported by the

study by Cheng et al. (2008b) that many smooth slip surfaces can fail to converge using the popular Spencer's analysis.

The popularity of LEM resides in: (1) simple to be used for problems which include various loading conditions, complex geometries, and soil profiles; (2) ease to code into general engineering software, and this method has been implemented into many commercial codes, making the technique attractive to practitioners. Despite the wide acceptance and the accumulated experience in the applications of LEM, there remain several weaknesses inherited in this approach: (1) none of the equations of solid mechanics is explicitly satisfied everywhere inside or outside the slip surface; (2) equilibrium condition is satisfied only in a limited sense.

2.3 Strength reduction method

The strength reduction method (SRM) was first used in 2D slope stability analysis by Zienkiewicz et al. (1975). The concept of SRM analysis is to reduce the strength parameters by the factor of safety while the body forces due to weight of soil and other external loads are applied until the system cannot maintain a stable condition. This procedure can determine the safety factor within a single framework for both two and three dimensional slopes, and it is implemented in some commercial geotechnical programs for engineering uses. The advantages of the SRM are: (1) the critical failure surface can be found automatically from the application of gravity loads and/or the reduction of shear strength; (2) no assumption is requireed on the interslice shear force distribution; and (3) it can be applied to many complex

conditions and can get the information on stresses, movements, and pore water pressures. On the other hand, SRM suffers from long solution time and tedious effort required to develop the computer model, and SRM relies on the assumption of flow rule which is actually unknown in general. Although the flow rule is usually not sensitive to the factor of safety (similar to the situation of f(x)) in general, it is still an important drawback of the SRM.

In strength reduction analysis, the convergence criterion is the most critical factor for the assessments of the factor of safety. Different criteria for the ultimate state have been used in practice according to the choice of the program: (1) maximum number of iteration is reached; (2) formation of a continuous failure mechanism; (3) sudden change in the displacement for some selected points. For simple problems, there are no major differences between these criteria, while greater differences may be obtained by different convergence criteria for some special cases, particularly for those with soil nails or heavy external loads.

Recently, SRM appears to be a popular alternative to the LEM, but Cheng et al. (2007, 2008) and Wei et al. (2008) have carried out extensive SRM studies and have found that there are also many practical limitations to the SRM. Cheng et al. (2007, 2008) and Wei et al. (2008) concluded that both LEM and SRM are useful to slope stability analysis, and each method cannot totally replace the other method in practical use.

2.4 Finite element method

Finite element method is a very powerful computational tool in engineering. It gains its power from the ability to simulate physical behaviors using computational tools without the

need to simplify the problem. Indeed, complex engineering problems require finite element method to obtain more reliable and accurate results.

The finite element method (FEM) is more powerful than the limit equilibrium method (LEM) in slope stability analysis as the FEM satisfies the equilibrium at any point in the soil mass (local domain) and the surrounding soil (global domain), while the LEM satisfies the global force or moment equilibrium for the sliding mass only. After the stresses within the system are determined, it is required to determine the critical failure surface from the stresses along the trial failure surface until the minimum factor of safety is determined. Because of this requirement, very few engineers adopt this approach of FEM to assess the stability of slopes, and most of the engineers will prefer the SRM instead.

Selection of the constitutive models in finite element analysis is vital and should be based on the physical behavior of the studied problem. For example, the soil-hardening model gives more reliable results than the Mohr-Coulomb model when modeling soil excavations. Mohr-Coulomb model is a linearly elastic, perfectly plastic model where soil parameters are assumed to be constant during all stages of soil loading and unloading during the analysis. Soil hardening model is an elastoplastic model that simulates the behavior of soils in triaxial test (shear hardening) and in oedometer test under isotropic loading (compression hardening) where the yield cap is expanded due to plastic strains (Brinkgreve et al, 2001).

2.5 Discrete element method

2.5.1 Introduction

The Discrete Element Method (DEM) was initially developed by Cundall (1971, 1974) for the study of Rock Mechanics problems. The method was later enhanced to various applications (Cundall and Strack 1979). The DEM has been used extensively to study physical and geotechnical phenomena such as mechanisms of deformation, constitutive relations for soil, stability of rock masses, flow of granular media, ground collapse and other types of geotechnical phenomena.

The distinct-element approach describes the mechanical behavior of both the discontinuities and the solid material. This method is based on a force-displacement law which is specifying the interaction between the deformable rock blocks and a law of motion which is determining displacements caused in the blocks by out-of-balance forces. Joints are treated as boundary conditions. Deformable blocks are discretized into internal constant-strain elements (Eberhardt, 2003).

In the DEM, the medium under study is divided into discrete elements with arbitrary shapes. The interaction of these elements is viewed as a transient problem with the states of equilibrium developing whenever the internal forces are balanced (Cundall and Strack, 1979). The calculation cycle alternates between the sum of forces acting on an element resulting from a force-displacement law at the contacts, and the Newton's law is used to find the incremental displacements, velocities, and accelerations of the element. The time step is chosen to be small enough so that disturbances do not propagate to more than the adjacent

particles during each time step, and the accelerations can be assumed to be constant during that time step (Cundall and Strack 1979).

There are a series of computer codes available in the literature for the application of the DEM. Most of these codes follow the pioneering work by Cundall (1974, 1978) with variations either in the modeling of the contact forces or in the solution algorithm. The first DEM code was developed for the study of rock mass behavior by Cundall (1971, 1974). Cundall also developed the Universal Discrete Element Code (UDEC) to model jointed rock mass and BALL and TRUEBALL for the study of granular media. UDEC is suitable for highly jointed rock slopes subjected to static or dynamic external loading. Two-dimensional analysis of the translational failure mechanism allows for simulating large displacements, modeling deformation or material yielding (Itasca, 2000). Three-dimensional DEMs have been developed in the early 1990s. Three-dimensional discontinuum code 3DEC contains modeling of multiple intersecting discontinuities and therefore it is suitable for the analysis of wedge instabilities or the influence of rock support (e.g. rockbolts, cables) (Eberhardt, 2003).

Discontinuous rock mass can be modeled with the help of distinct-element method in the form of particle flow code, e.g. program PFC2D/3D (Itasca, 1999) or other codes. Spherical particles interact through frictional sliding contacts. Simulation of joint bounded blocks may be realized through specified bond strengths. The law of motion is repeatedly applied to each particle and force-displacement law to each contact. Particle flow method enables modeling of granular flow, fracture of intact rock, transitional block movements, dynamic response to blasting or seismicity, deformation between particles caused by shear or tensile forces. These

codes also allow to model subsequent failure processes of rock slope, e.g. simulation of rock fracture (Eberhardt, 2003). The method of particle flow code employs a time-stepping, explicit-calculation scheme (Cundall and Strack, 1979), which has advantages over traditional implicit calculation schemes in that it can handle a large number of particles with modest memory requirements because there are no matrices to be inverted because the solution scheme solves the full dynamic equations of motion by dynamic propagation of waves through the material, and the velocities of the waves are dependent on the stiffness, density and packing of particles (Hazzard et al., 1998). This also allows physical instabilities such as shear-band formation to be modeled without numerical difficulty because kinetic energy that accompanies shear-band formation is released and dissipated in a physically realistic way (Itasca, 1999a). On the other hand, the use of dynamic relaxation to solve the system equation in DEM requires extensive cycle time to reach the equilibrium state. If the time-step chosen is excessive, the results obtained from the analysis can be meaningless. In practical application, greater care, knowledge and judgment is required for DEM as compared with FEM, and a large problem using DEM may require days or even weeks for the solution.

While distinct element methods are powerful tools for numerical analysis of discontinuous material in geotechnical problems and geological mechanics, limitations are also appreciated to point out here. The granular materials are considered to be packed assemblies of particles in DEM simulation, and the mechanical interaction between particles is assumed to be simple. However, in reality, the contact between particles is highly complex and it's hard to be detected explicitly. Also it is difficult to generate complicated model

geometry. In addition, Thornton and Lanier (1997) mentioned development of accurate contact constitutive models for use in discrete element analysis is non-trivial. The effective stress in a soil will govern its response and including pore water pressures in a discrete element framework is non-trivial.

A central limitation of discrete element modeling is the difficulty associated with modeling the large number of particles that exist within soil volumes large enough to be of practical interest to engineers. A real soil specimen, with a distribution of particle sizes would contain many more particles than simulated model.

Also the computational power will limit the maximum number of particles in the numerical models, and duration of a virtual simulation. Moreover, it is difficult to provide the detailed information about the distribution and evolution of the contact forces and internal stresses available in a DEM analysis.

2.5.2 Particle flow code

A more recent development in the discontinuum modeling techniques is the application of distinct element methodologies in the form of particle flow codes, e.g. PFC2D/3D (Itasca 1999). This code allows the soil to be represented as a circular (2D) or spherical (3D) particle, or the rock mass as a series of circular or spherical particles, which interact through frictional sliding contacts (Figure 2.1). Clusters of particles may also be bonded together through specified bond strength in order to simulate joint bounded blocks. The calculation cycle then

involves the repeated application of the law of motion to each particle and a force-displacement law to each contact (Figure 2.2).

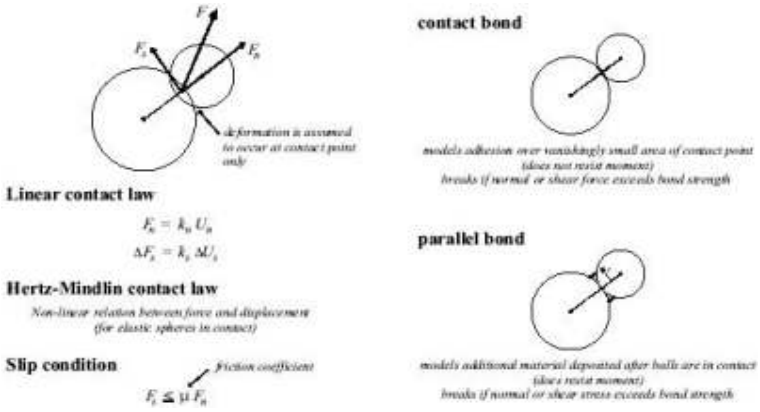

Figure 2.1 Contact and bonding logic of interacting particles used in the discrete element program PFC2D (from Itasca 1999)

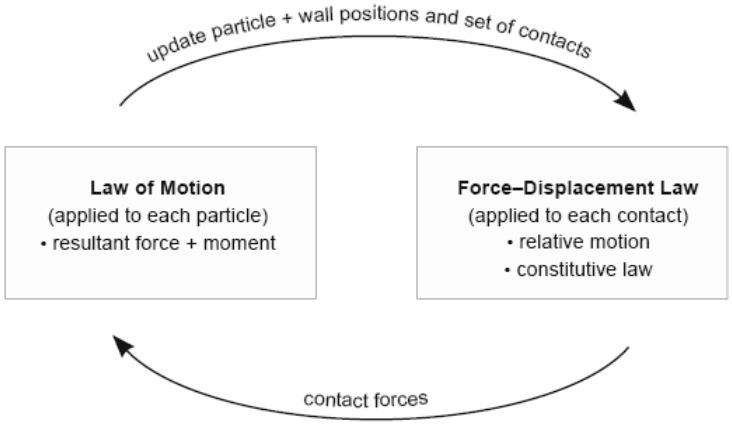

Figure 2.2 Calculation cycle used in PFC2D (from Itasca 1999)

Particle flow codes employ the distinct-element method with the following assumptions: (1) particles are circular in PFC2D / spherical in PFC3D and elastic; (2) contacts between particles occur over a vanishingly small area (i.e. at a point); (3) the magnitude of elastic particle 'overlap' of nominal radii is related to the contact force by a force-displacement law

similar to linear springs that mimic the physics of Hertz elastic spheres (Cundall, 1988); and (4) tensional and shear bonds can exist between particles.

With these codes, it is possible to model granular flow, translational movement of blocks, fracture of intact rock and dynamic response to blasting or seismicity. The breaking of bonds between circular particles roughly simulates intact rock fracture and failure (although not fracture propagation). Deformation between particles due to shear or tensile forces can also be included, where slip between adjacent particles is prescribed in terms of the frictional coefficients that limit the contact shear force.

Particle flow codes are thus able to simulate material from the macro level of fault- or joint- bounded blocks to the micro scale of grain-to-grain contact, with the main limiting factors being the computing time and memory requirements. In this sense, it becomes possible to model a number of soil/rock slope failure processes, and subsequently, the runout of the failed material down the slope. At present, these codes are predominantly a research tool, but its potential is being widely recognized in mining, petroleum and civil engineering.

General formulation

The PFC runs according to a time-difference scheme in which calculations include the repeated application of the law of motion to each particle, a force-displacement law to each contact, and a contact updating a wall position. Generally, there are two types of contact available in the program which are ball to wall contact and ball to ball contact. In each cycle,

the set of contacts is updated from known particle and known wall position. Force-displacement law is first applied on each contact. New contact force is calculated and replaces the old contact force. The force calculations are based on pre-set parameters like normal stiffness, density and friction. Next, law of motion is applied to each particle to update its velocity, direction of travel based on the resultant force, moment and contact acting on particle. Force-displacement law is then applied to continue the circulation.

The force-displacement law

The force-displacement law is described for both the ball-ball and ball-wall contacts. The contact arises from contact occurring at a point. For the ball-ball contact, the normal vector is directed along the line between the ball centers. For the ball-wall contact, the normal vector is directed along the line defining the shortest distance between the ball center and the wall. The contact force vector *Fi* is composed of normal and shear component in single plane surface

$$F_i = F_{ij}^n(t) + F_{ij}^s(t + \Delta t) \tag{2.2}$$

The force acting on particle i in contact with particle j at time t is given by

$$F_{ij}^n(t) = k_n(r_i + r_j - l_{ij}(t)) \tag{2.3}$$

where r_j and r_i stand for particle i and particle j radii, $l_{ij}(t)$ is the vector joining both centers of the particles and k_n represent the normal stiffness at the contact.

The shear force acting on particle i during a contact with particle j is determined by:

$$F_{ij}^{s}(t+\Delta t) = \pm \min(F_{ij}^{s}(t) + k_s \Delta s_{ij}, f \mid F_{ij}^{n}(t+\Delta t) \mid) \quad (2.4)$$

where f is the particle friction coefficient, k_s represents the tangent shear stiffness at the contact. The new shear contact force is found by summing the old shear force (min $F_{ij}(t)$) with the shear elastic force. Δs_{ij} stands for shear contact displacement-increment occurring over a time step Δt.

$$\Delta s_{ij} = V_{ij}^{s} \Delta t \quad (2.5)$$

where V_{ij}^{s} is the shear component of the relative velocity at contact between particles i and j over the time step Δt.

Law of motion

The motion of particle is determined by the resultant force and moment acting on it. The motion induced by resultant force is called translational motion. The motion induced by resulting moment is rotational motion. The equations of motion are written in vector form as follow:

- (Translational motion)

$$\sum_{j} F_{ij} + m_i g + F_i^{d} = m_i x_i^{''} \quad (2.6)$$

- (Rotational motion)

$$\sum_{j} r_i F_{ij} + M_i^{d} = I_r \theta_i^{''} \quad (2.7)$$

Where x_i'' and θ_i'' stand for the translational acceleration and rotational acceleration of particles i. I_r stands for moment of inertia. F_i^d and M_i^d stand for damping force and damping moment.

Measuring logic

A number of quantities in a PFC model are defined with respect to a specified measurement circle. These quantities include coordinate number, porosity, sliding fraction, stress and strain rate. The coordination number and stress are defined as the average number of contacts per particle. Only particles with centroids that are contained within the measurement circle are considered in computation. In order to account for the additional area of particles that is being neglected, a corrector factor based on the porosity is applied to the computed value of stress. The correction factor will be discussed in this section.

Since measurement circle is used, stress in particle is described as the two in-plane force acting on each particle per volume of particle. Average stress is defined as the total stress in particle divided by the volume of measurement circle. Thus, shape of particle is regardless of the average stress measurement because the reported stress is easily scaled by volume unity. The reported stress is interpreted as the stress per volume of measurement circle.

Contact constitutive models

The constitutive model acting at a particular contact consists of three parts: a stiffness model, a slip model and a bonding model. The stiffness model provides an elastic relation between the contact force and relative displacement. The slip model enforces a relation between the shear and normal contact forces such that the two contacting balls may slip relative to one another. The bonding model serves to limit the total normal and shear forces that the contact can carry by enforcing the bond-strength limits.

CHAPTER 3 STUDY ON THE FAILURE MECHANISM OF SLOPE UNDER SEVERAL CONDITIONS BY TWO-DIMENSIONAL DISTINCT ELEMENT METHOD

3.1 Introduction

Slope stability problem is always a main concern in geotechnical engineering. Natural or cut slopes have greatly influenced human's properties and life, and for area like Hong Kong, slope failures can be fatal. There have been many research works on the assessment of the stability of slopes under different geometries, soil properties and groundwater conditions in the past. Many slope stability analysis methods and tools have also been developed over the last forty years. Each stability analysis method differs from the others in some of the basic assumptions, but most of the stability analysis methods will give similar factors of safety for normal cases which are sufficient for normal engineering uses. Besides the factor of safety, the failure mechanism and post-failure mechanism are also important in some cases, and different methods of analysis are more suitable and efficient for specific aspects.

In practical applications, limit equilibrium method (LEM) based on the method of slices or method of columns and strength reduction method (SRM) based on the finite element method (FEM) or finite difference method are used for slope stability analysis. These two major analysis methods take the advantage that the insitu stress field which is usually not known with good accuracy is not required in the analysis. The uncertainties associated with the stress-strain relation can also be avoided by a simple concept of factor of safety. In

general, this approach is sufficient enough for engineering analysis and design. If the condition of the slope after failure has initiated is required to be assessed, these two methods will not be applicable. Even if the insitu stress field and the stress-strain relation can be defined, the post-failure collapse is difficult to be assessed using the conventional continuum based numerical method, as sliding, rotation and collapse of the slope involve very large displacement or even separation without the requirement of continuity. At these situations, Distinct Element Method (DEM) should be considered. Significant earthquakes have occurred in China in the past few years with major loss of lives and large scale slope failures. Actually, the debris flow of soil mass after slope failure has occurred is one of the major causes for the death in these major disasters. One of the important requirements for the slope stabilization works is the assessment of the post-failure conditions of the slopes, and this is a difficult task which is not easily considered by the classical slope stability analysis methods.

When soil mass is under self-weight or external loading, post failure begins at the time when a continuous yielding zone is formed. Yielding firstly appears at toe, then gradually extends to slope crest. Critical failure surface is generated after yielding line develops through the influenced area. FEM can continue performing the modeling till the moment when critical failure surface is formed. That is to say, post failure, also called progressive failure can be carried on with FEM. However after sliding has initiated, DEM is much better than FEM in modeling from the initiation to the eventual failure of the slope. Thus, the formation of critical failure surface is the demarcation point to differentiate FEM and DEM.

The Discrete Element Method (DEM) was initially developed by Cundall (1971, 1974)

for the study of Rock Mechanics problems. The method was later enhanced to various applications (Cundall and Strack 1979). The development of DEM represents an important step in the modeling and understanding of the mechanical behavior of joint rock masses or soil slope, particularly when there is large displacement taking place inside a soil mass. At present, there are only limited applications of the Distinct Element Method (DEM) to slope stability analysis, and DEM is more suitable for qualitative instead of quantitative assessment of the stability of slope.

The progressive failure/ post failure phenomenon and the action of soil nail and water seepage are important problems in Hong Kong. In the past, there has been very few applications of DEM in slope stability analysis, and it appears that there is no previous study about the stabilization action of soil nail or the effect of water flow on the stability of slope. These two outstanding works will be carried out in the present study. In this chapter, the slope stability problems are assessed by the use of two-dimensional particle flow program PFC2D in the following section.

3.2 Large displacement simulation of slope failure by PFC

3.2.1 Model generation

To assess the failure mechanism of slope, particularly the situation after the initiation of failure, the software PFC2D (Particle Flow Code in Two Dimensions) is used for the study of several slopes in this section. Model generation is quite complicated and crucial in PFC. Circle particle as ball in PFC2D is used to simulate the soil particles. The boundaries of the

model are defined by a series of walls that contain the particles. In general, the usual objective in creating an irregular packing is to fill some given space with particles at a given porosity and to ensure that the assembly is at equilibrium. In this study, particles are falling under self-weight gravity at random layer by layer lying on the bottom of the model, which represents the slope generation in nature. This kind of specimen generation technique is called “Rainy method”. Radius expansion which is called “Expand method” is also used in the particle generation, achieving in a trial-and-error manner to satisfy the requirement of porosity ratio. Thus two ways of specimen generation is combined and incorporated in this simulation model.

After the particle assembly is generated and compacted, boundary and initial conditions are applied to achieve the desired initial equilibrium state, which aims to define contact behavior and material properties, and to specify boundary and initial conditions. In parameter determination of the properties, normal and shear stiffnesses, density, frictions for ball to ball, and ball to wall, and bond strength are assigned to each soil particle. Calibration process is necessary to determine these micro parameters in PFC according to the macro parameters in laboratory parameters. Normally, triaxial test of the studied soil mass should be carried out both in physical lab test and PFC simulation. Calibration process is then conducted by reproducing the macrobehavior in PFC simulation to approach the results gained in physical test. And the micromaterial parameters will be varied over wide ranges until the two test behavior are matched, so that the micro-parameters will be determined, which will be introduced individually in the next section 3.22.

Excavation is applied after the whole assemble is generated. In order to bring the model to an initial stress state that is representative of the physical stress state for the problem, and also in equilibrium state, a long time running for cycles (approximately 1000 cycles for two-dimensional PFC model) is carried out with the PFC program. At last, the initial state of model is generated and is ready to perform the model calculations.

For the parameter determination, the friction coefficient μ at the contact for each ball in PFC is taken as the value of $\tan\phi$ (ϕ is the macro friction angle of soil). For the bond strength, the definition in PFC is relatively complicated. Particle flow code is based on contact constitutive law in theory. To simulate a medium with cohesion, optional bonding is defined in PFC. Unlike the friction coefficient, the bond cohesion in PFC cannot be compared with macro cohesive strength of soil. It is specified that bonded contacts may carry tension, and the bonds have finite strengths in tension and shear. The contact bonds which reproduce the effect of an adhesion acting over the vanishingly small area of the contact point are chosen to be used in this study, and the contact bond constitutes the tensile normal bond strength (n_bond) and shear bond strength (s_bond). Both bonds can be envisioned as a kind of glue joining the two particles. The contact-bond glue is of a vanishingly small size that acts only at the contact point.

3.2.2 Micro parameter calibration in model generation

In Particle Flow Code, individual particles act as linear-elastic springs in compression with cohesive contact bonding that acts in both shear and tension, and coulomb frictional

sliding that acts only along unbonded contacts illustrated in Figure 3.1. Model components include frictional, linear-elastic, spherical particles that act as springs in compression; frictional, elastic walls that are either fixed or velocity controlled; and contact bonds that resist tensional separation and shear displacement. Bonds are applied after the particles achieve static gravitational equilibrium, creating an initial solid that is capable of progressive fracture during loading. Particle size is determined by computational limitations and is varied about a mean radius of 50 m to prevent formation of hexagonal close-packed array. Kn and Ks are the particle and wall bulk and shear moduli, respectively. Particle and wall friction angle φ is simply a convenient representation of the critical ratio of shear to normal force required for a contact to slide.

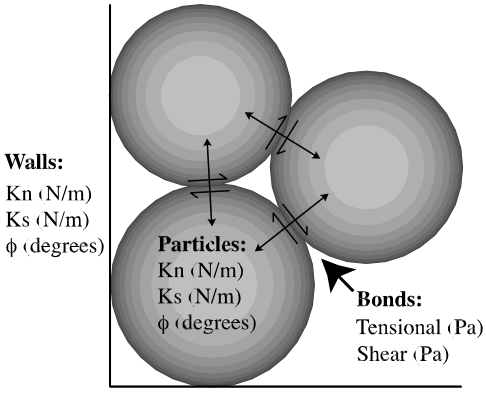

Figure 3.1 Microscopic elements of the particle flow code model

For a particle flow analysis, it is vital to choose the appropriate material parameters for the model in the analysis. Because of the discrete, particle-based nature of the model, specification of material properties and boundary conditions is more difficult than with available continuum methods. The material parameters for the particle flow analysis are however different from the macromaterial properties as they are controlled by the

microproperties such as the particle-size distribution, packing, particle and bond stiffnesses, particle friction coefficients, and bond strengths. The macrobehavior reflects the average behavior and is controlled by the micromaterial parameters, grading of the materials and state of packing. It is extremely difficult to determine the micromaterial parameters directly, so the micromaterial parameters will be varied over wide ranges until the macrobehavior are reproduced.

The user of PFC can specify micro-properties that control particle–particle interaction (e.g. particle shear and bulk modulus, coefficient of friction, and bond strength), but there is no direct way to prescribe the macro-properties of the model such as Young's modulus (E), unconfined compressive strength (UCS), cohesion (Co), Poisson's ratio (ν), coefficient of friction (μ), porosity, and the initial stress state. As a result, the process of generating an initial model with the appropriate material behavior and initial stress state is by trial-and-error, requiring the use of the numerical equivalent of a triaxial mechanics test shown in Figure 3.2 to derive the equivalent mechanical macro-properties. The specific steps are as follows: (a) To determine the macro-scale mechanical properties, a representative sample of the numerical model is subjected to both unconfined and confined biaxial compression tests. (b) Unconfined test results yield: (1) Young's modulus (E) from the slope of the linear or elastic portion of the curve; (2) unconfined compressive strength (UCS) from the peak of the curve; and (3) Poisson's ratio (ν) from lateral strains (not shown in Figure 3.2). (c) A linear regression through peak strength data plotted in shear-stress versus mean-stress space yields the angle of internal friction (φ) as the slope of the line and cohesion (Co) as the y-intercept.

Thus, this kind of calibration process is necessary to determine the micro parameters in DEM.

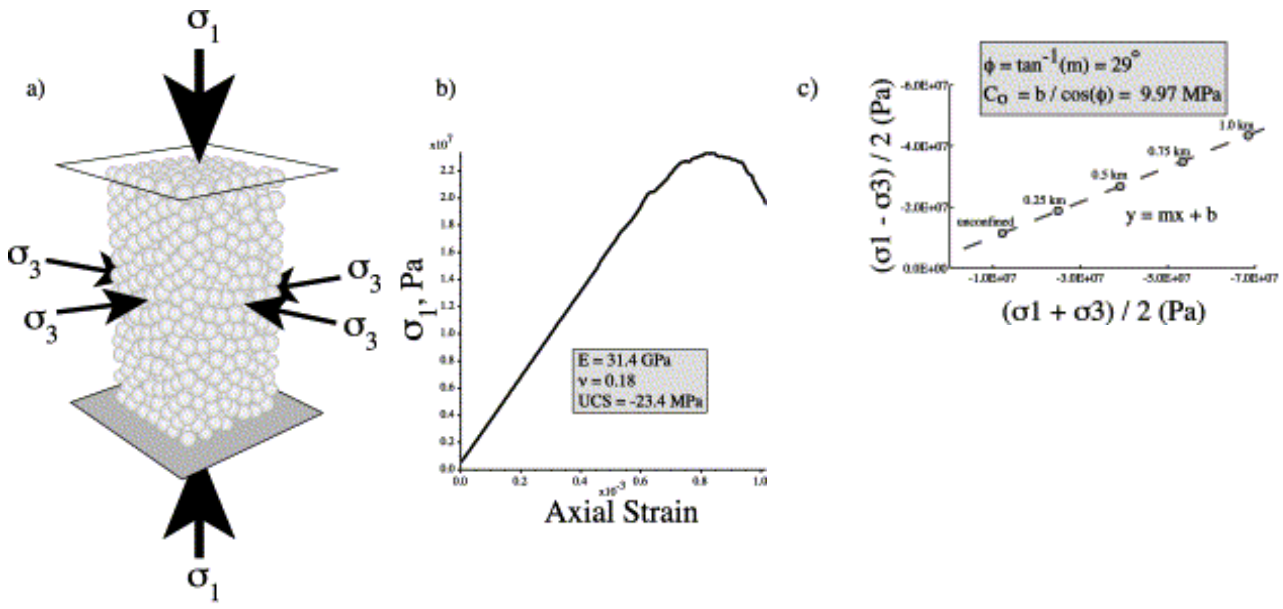

Figure 3.2 Numerical triaxial test

However, most of the discussions in relation to DEM modeling calibration in geomechanics to date consider the application of DEM to simulate the response of rock mass. For soil mass problem, there are not much previous research works available. Coetzee and Els (2009) have suggested a calibration of the microparameters for a silo flow, which is similar to the concept by Cheng et al. (2009), by performing biaxial tests and Brazilian tests in both physical test and numerical simulation. The parametric calibration in this research refers to the method mentioned above. For the present study, triaxial tests are performed before the numerical simulation so as to determine the appropriate microproperties for the particle flow analysis. It should also be pointed out that the geometric characteristic of the particles in the test samples must resemble that of the particles in the numerical model. Triaxial tests under different confining stresses on sand samples are performed and the

stress-strain relations are determined for the calibration of the microproperties required in the particle flow simulation. During the numerical tests, different combinations of the microproperties of the particles are considered until a stress-strain relation similar to that from the laboratory tests is obtained.

3.2.3 Failure pattern of simple slope

In this section, qualitative study about the failure mechanism of slope stability problems is carried out, and less rigorous micro parameter calibration is performed in model generation. Several slope models are generated with the approach mentioned above. The typical numerical model of a simple slope is shown in Figure 3.3. The height of the slope is set as 3m, and the base of both models is 14m long and 7m high. Friction coefficient is set to 0.4 (soil friction angle=21.8° less than the slope angle) and the density of the particle is set to 2000kg/m^3. Mohr-Coulomb criterion is adopted through the entire failure process. For simplicity, simple slopes with slope angles 45°and 60° are firstly considered. After model generation as mentioned above, further analysis is carried out. To study the progressive failure mechanism, cohesionless slope under gravity is considered at first to check massive eventual failure. In the microscopic study, contact bond strength, normal bond and shear bond, is set to zero to simulate a cohesionless slope like sandy slope.

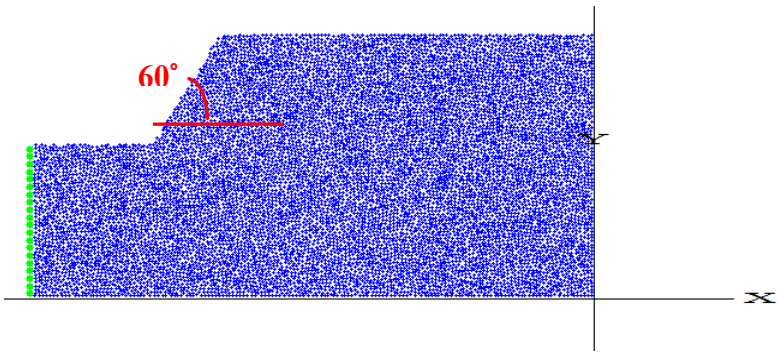

Figure 3.3 Basic numerical model & Initial state of slope

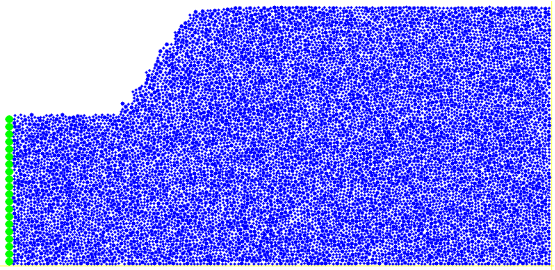

(a) $1x10^4$ step and corresponding

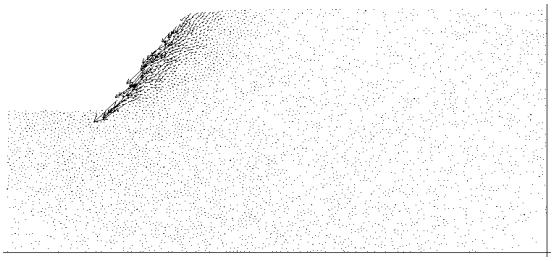

displacement vector

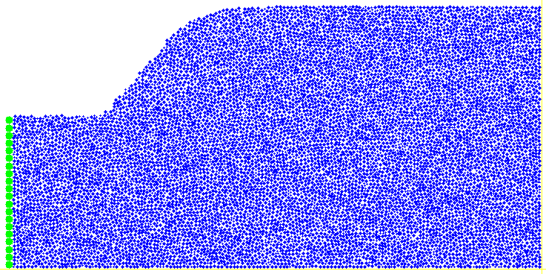

(b) $3x10^4$ step

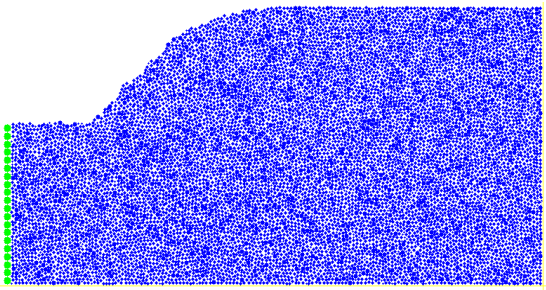

(c) $5x10^4$ step

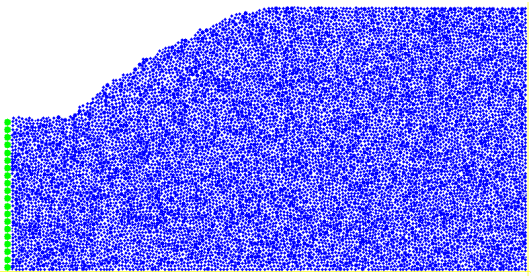

(d) $10x10^4$ step

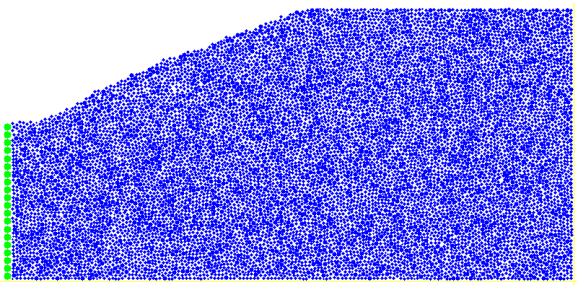

(e) $30x10^4$ step

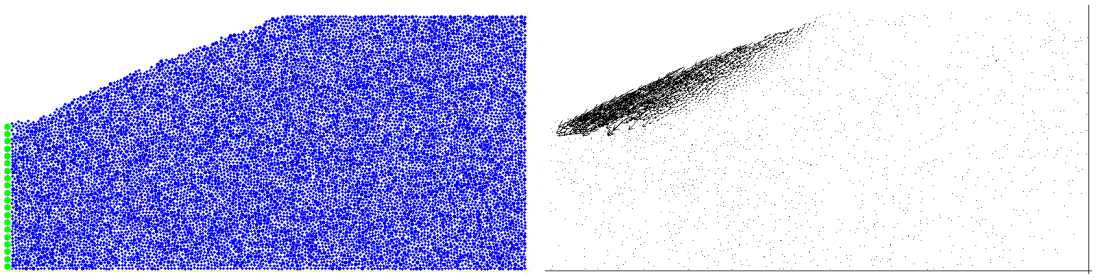

(f) $200x10^4$ step and corresponding displacement vector

Figure 3.4 Failure development of simple slope with n_bond=s_bond=0 and α=60°

The progressive failure of the slope, the post-failure mechanism and a critical failure surfaces are clearly shown in Figure 3.4. The failure mechanisms as shown in these figures are generally similar to that as predicted by LEM or SRM. Actually, by applying factor of safety to the micro-parameters, it is also possible to determine the factor of safety of such discontinuum system. It is noticed that failure seems to start from the crest of the slope while in practical cases, failures may initiate from the toe in Hong Kong (usually in rainy times). The displacements at different phases are therefore investigated in this study. From the parametric study (not shown here), it is found that the collapse is more sensitive to the contact bond strength than the slope angle, and the bond strength which can be regarded as the cohesive strength in macroscopic view is a controlling variable when the friction is constant. This result is actually well known among the engineers that cohesive strength is more important in the design in general. Actually, if the bond strength is large enough, the slope will be stable which is not shown in this paper.

The typical displacement of the simple slope with contact bond strength equals to 0 and slope angle α=60° is given in Figure 3.4. At the initial stage, basically only the particles around the slope face are mobilized. The grains at the crest slide down under the action of

gravity and hence large-scale deformation of the slope starts to initiate. The contact forces among the particles are re-distributed and further failure develops gradually. When the slope angle approaches the natural angle of repose, the slope has achieved a stable condition. The failure starts with tension failure firstly at the top of the slope, and accumulation of soil particles occurs at the toe at the later stages. Of course, the concept of one "safety of factor" on a "critical slip surface" normally accomplished in LEM and SRM cannot predict such "progressive" failure procedure with the presence of continuously modified large displacement movement. Nevertheless, rough "critical slip surface" can be determined at the later stage of failure based on the displacement vectors at the later stage of failure in Figure 3.4(f) which is the global failure.

For the simple slope where gravity (self-weight) is the sole factor in the failure, the toe of the slope is the exit end of the slip surface in classical slope stability theory. However, during the initial failure as shown in Figures 3.5 and 3.6, the horizontal and vertical displacements are only slightly changed at the toe, while more than 0.5m movement in both the horizontal and vertical directions can be found at the crest. The results indicate that failure occurs firstly at the crest of the slope which is a typical local failure while failure at toe is the initiation of the global failure. The rotation and sliding along the assumed slip surface in classical concept seem not to dominate the initial failure mechanism. This is a clear illustration of the progressive failure of slope which can be modeled by DEM but not by LEM or SRM. In PFC, the failure of the cohesionless slope initiates when the grains at the top firstly roll downwards with the resulted grains flow to the base of the slope. This flow

causes the accumulation of grains near to the toe and finally sliding out. When the resistance at the toe is fully mobilized, the extent of the collapse is enlarged which is a global failure. In reality, completely cohesionless soil is not commonly found in practice, and the actual slope failure is usually induced by ground water flow under raining. Actually, failures initiated at the crest of slopes are also found in Hong Kong. In general, the prediction by the PFC computations is acceptable, and DEM has the ability to assess the progressive failure which is not possible for the continuum based methods.

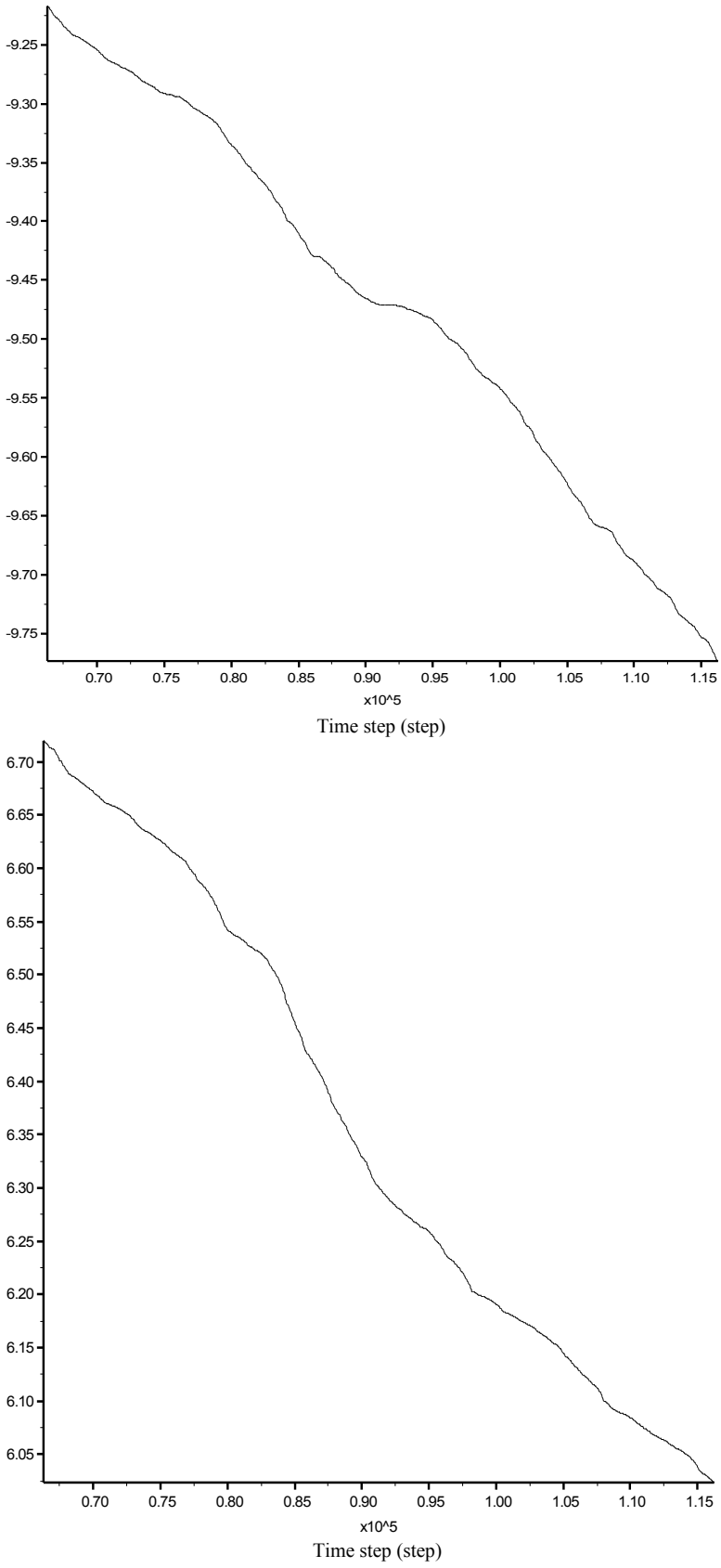

Figure 3.5 X & Y position history of ball 2673 at crest of slope (n_bond=s_bond=0, α=60°)

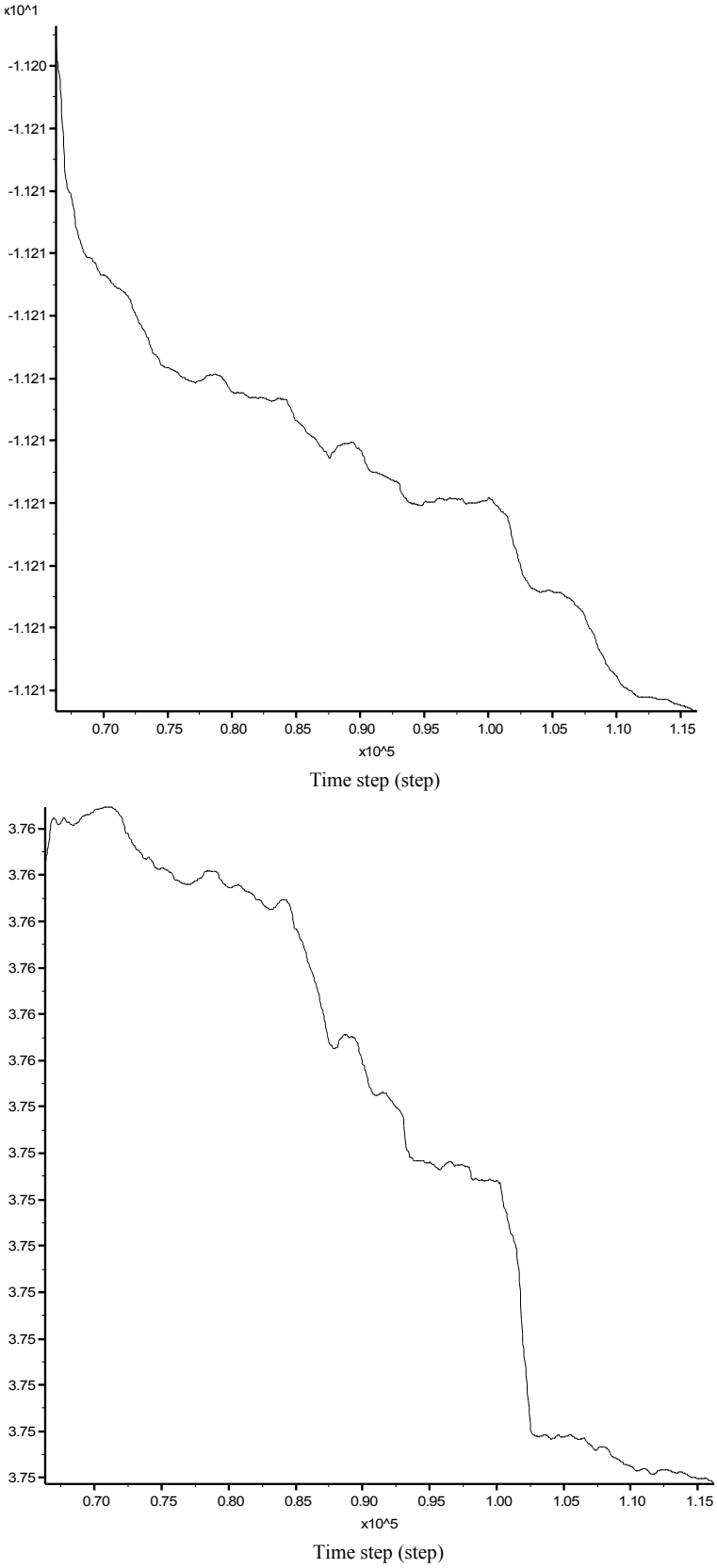

Figure 3.6 X & Y position history of ball 11870 at toe of slope (n_bond=s_bond=0, α=60°)

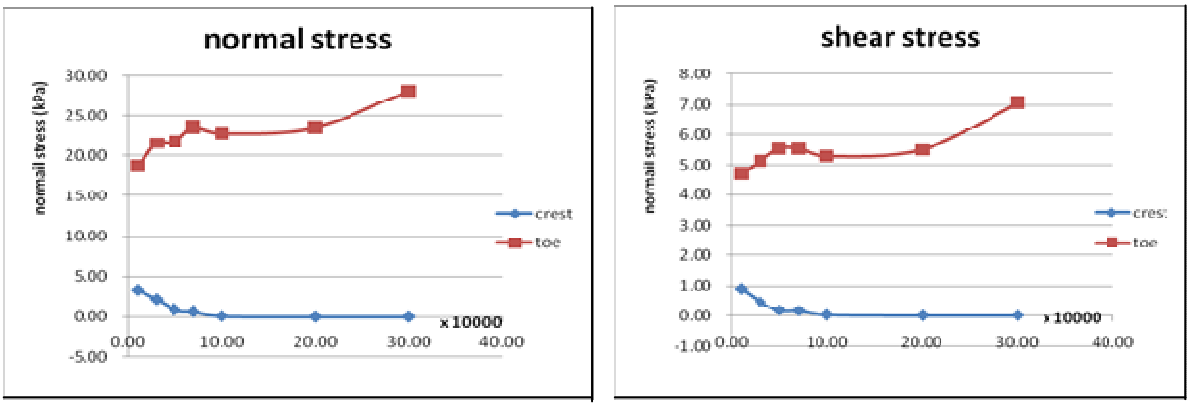

(a) Normal stress on failure surface vs. time-step (b) Shear stress vs. time-step

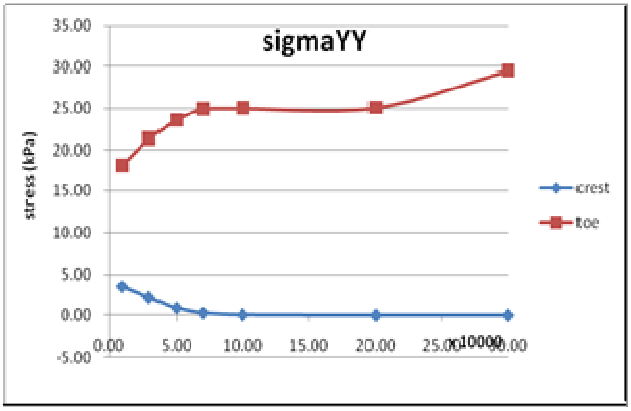

(c) Vertical normal stress vs. time-step

Figure 3.7 The stress state of simple sandy slope (n_bond=s_bond=0)

Stress state of unreinforced slope is analyzed in the study. The stress variation of the cohesionless slope at crest and toe of the slope is shown in Figure 3.7. It is well known that the stress is released and re-distributed during the collapse, so it can be noticed in Figure 3.7 that the majority of the changes take place at the initial stage of the failure. Along the development of slope failure, gradually increasing stress field can be found at the toe and decreasing stress field can be found at the crest. This result is reasonable as the stress descends at the crest under the unloading action. Due to limited small amount of confining

soil mass within this zone, the vertical stress dominates over the horizontal stress in the whole process. Both the vertical and horizontal stresses drop to zero at the later stage when the soil collapses at the crest. At the toe, the state of stress is more complicated because of the continuous accumulation of sliding soil mass from the upper part of the slope which is never modeled in LEM or SRM. The comparison of the stress on the slip surface as illustrated in Figure 3.7 shows that normal stress on the failure surface is nearly equal to the vertical normal stress and is much greater than the shear stress on the failure surface, which indicates that the vertical stress still dominates near to the slope face at the toe. Tension failure at the crest is not obvious from the stress analysis, and this may be due to the stress from the measure circle being the averaged value instead of the local value.

3.2.4 Influence of soil-nail on the slope failure

Soil nail is a common reinforcement used for slope stabilization. The essential concept of soil nailing is reinforcing the slope with closely spaced inclusions to increase the stability of the global soil mass. When soil movement is induced by excavation for cut slopes or by natural environment changes for existing slopes, resistant tension force is generated in the soil nail and is transferred to the soil by the friction mobilized at the soil-nail interface. Three models of soil-nailed slope with slope angle of 60°are conducted in this section: (1) n_bond=s_bond=0; (2) n_bond=s_bond=2000N and (3) n_bond=s_bond=5000N. Different contact bond strength is tested to explain its influence to slope stability. It is to be clear that the contact bond is defined as force acting at the contact point between particles in Particle

Flow Code (PFC) by the following two micro parameters: normal contact bond strength n_bond--Fn [force]; and shear contact bond strength s_bond--Fs [force], which can be envisioned as a pair of elastic springs (or a point of glue) with constant normal and shear stiffnesses. These two springs have specified shear and tensile normal strengths.

A set of two soil nails of density 2000kg/m^3, stiffness 10MN/m, friction=0.4 is introduced in the slope to study the effects of the soil nail on slope stability and failure mechanism. There is actually no soil nail or other structural material in DEM, as the basic formulation of DEM is discrete element with the stresses while axial force/bending moment for structural element never appear in discrete element formulation and cannot be modeled directly in the basic theory. To overcome this limitation, the soil nails are simulated by installing and clumping grains along the excavated hole in the original model. If the grains are clumped rigidly, then the action is practically equivalent to that of a soil nail. Moreover, the model is simplified in numerical analysis, no grouting material is considered, due to relatively minute void area between soil-nail and hole. Also qualitative study is carried on in this research, no need to focus on the complicated interface connection.

The use of soil nail head in continuum model has been demonstrated to be important by Cheng et al. (2007), and the effect of soil nail head is also studied in this section. From Figure 3.8 to 3.10, it is obvious that the stability of the slope is increased by the use of soil nails, especially for the region close to the soil nails, though falling and accumulation of soil particles still exist at the crest and around the toe of the slope respectively. Due to the resistance provided by the soil nails, global failure inside the slope is not formed, which is a

good illustration about the stabilizing effect of the soil nail. Furthermore, basically only local failure by tension and compression can be found in the soil mass. Local tension failure appears at the crest of the slope, while local compression failure exists at the toe of the slope. From Figure 3.8 where there is no nail head in the problem, it can be noticed that the stability of the soil mass near to the slope face between the soil nails seems not to be reinforced which is not surprising, and this is also the worry of many engineers in Hong Kong towards the use of soil nails in loose fill slope where the cohesive strength of soil is practically zero near to the slope surface. The stability of this local region has to be provided by the soil nail head and facing (if any), and this is a common understanding among the engineers in Hong Kong that a large soil nail head or even facing is required for a good slope stabilization work. There are also reported slope failure cases in Hong Kong for which the nail head is responsible for the local failures. Without the soil nail head, the confining action from the soil nail cannot be transferred to the slope surface for loose fill slope. For soil nailed slopes, failure initiates when the soil falls down by gravity at the upper part of the slope, and also the area between and beneath the soil nails to form tension failure. Similar to the situation without soil nail, the resulted accumulation of soil particles can later be found at the bottom of the slope. Therefore, in the view of geometry change, the progressive failure of soil-nailed slope in cohesionless slope without nail head is basically the same as that without nail, except that the region of shear failure is smaller and the movement is smaller than an unreinforced slope.

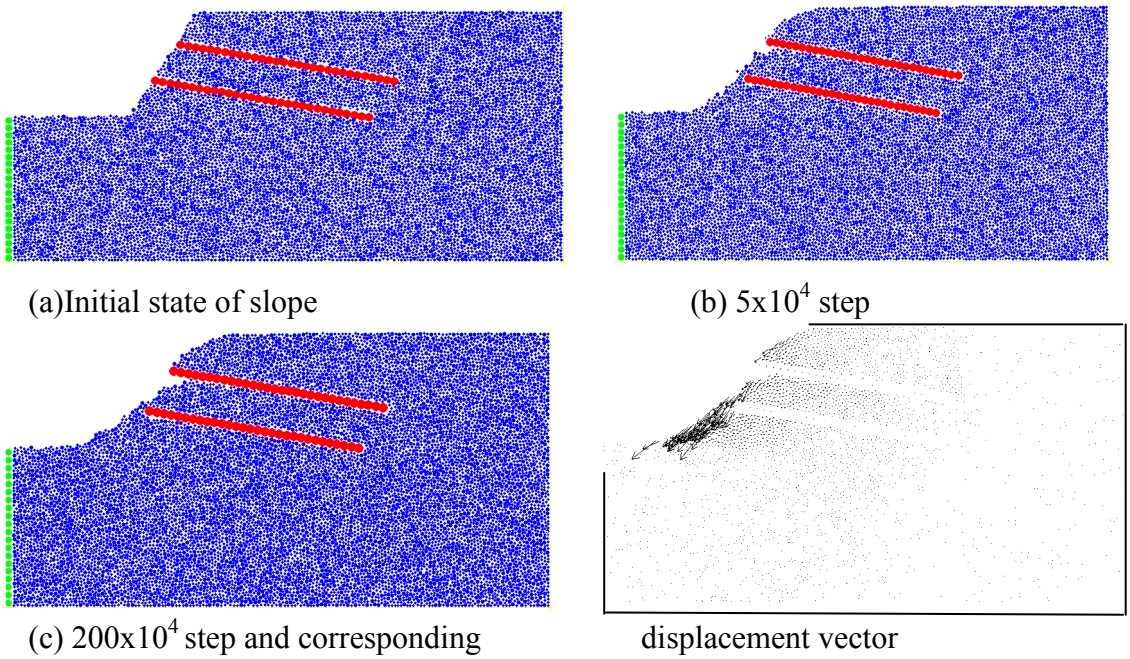

(a)Initial state of slope (b) $5x10^4$ step

(c) $200x10^4$ step and corresponding displacement vector

Figure 3.8 Failure development of nailed slope with n_bond=s_bond=0 and no nail head

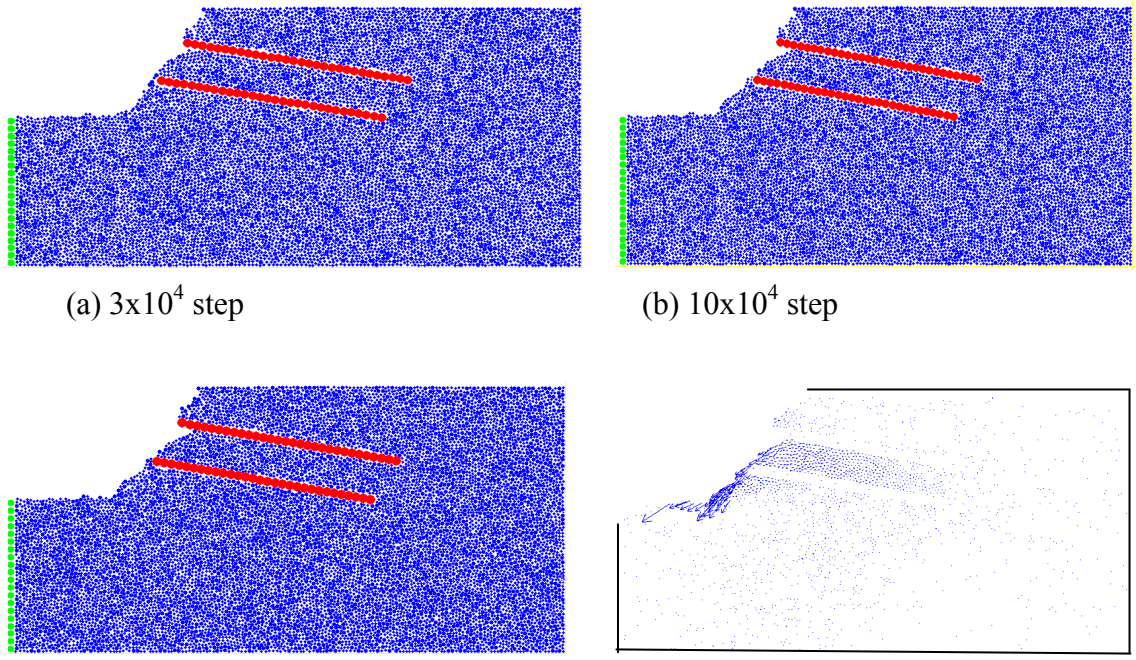

(a) $3x10^4$ step (b) $10x10^4$ step

(c) $200x10^4$ step and corresponding displacement vector

Figure 3.9 Failure development of simple slope with n_bond=s_bond=2000N and no nail head

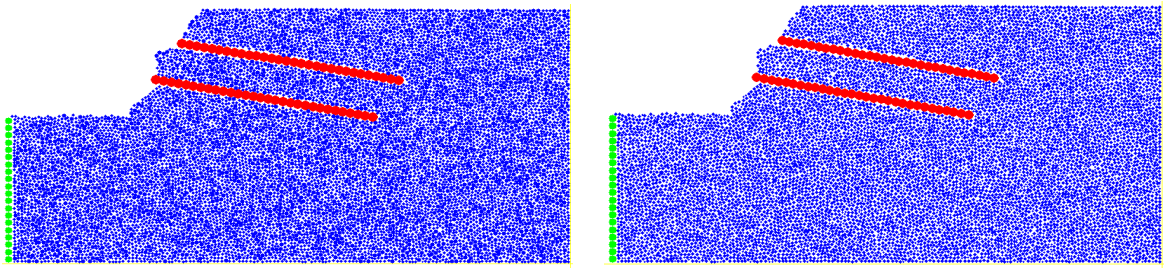

(a) $3x10^4$ step (b) $200x10^4$ step

Figure 3.10 Failure development of simple slope with n_bond=s_bond=5000N and no nail head

Soil nail head is generally used in construction and is an effective component to the local stability of the slope. If nail head is used in the analysis (by bonding the adjacent grains to the exit end of nail on the slope face together), the particles near to the slope face are well confined with increase local stability (Figures 3.11 to 3.13). For the slope failure, failure occurs only at the toe and crest and the stability after failure can be obtained. The effect of cohesive strength can also be summarized from the displacement graph. Higher cohesion of soil will give higher stability with less failure which is obvious. More importantly, in Figure 3.13, there is no obvious tension crack at the upper part of the slope and the rundown to the bottom is also less noticeable if c is high enough.

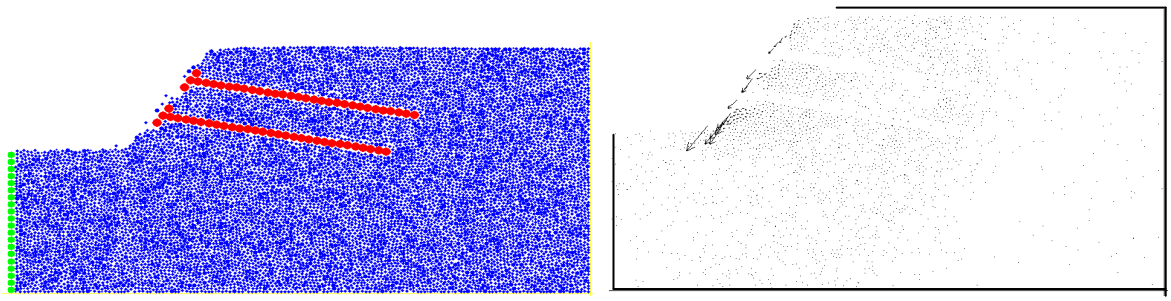

(a) $1x10^4$ step and corresponding displacement vector

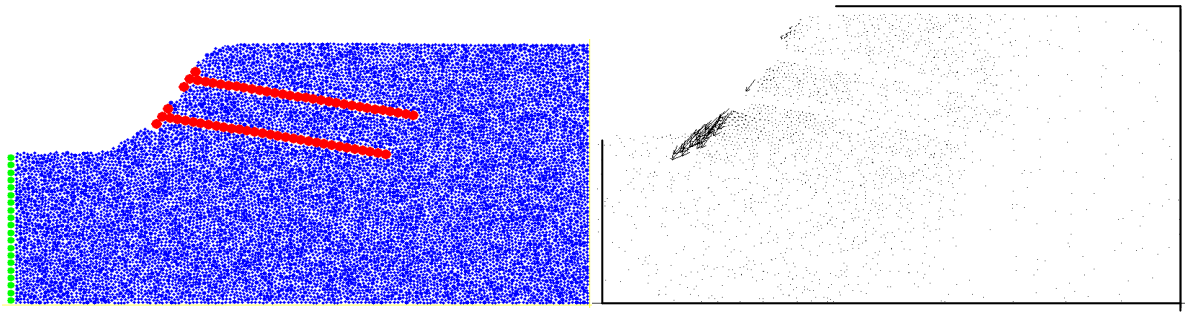

(b) $5x10^4$ step ~ $200x10^4$ step and corresponding displacement vector

Figure 3.11 Failure development of simple slope with n_bond=s_bond=0 and nail head

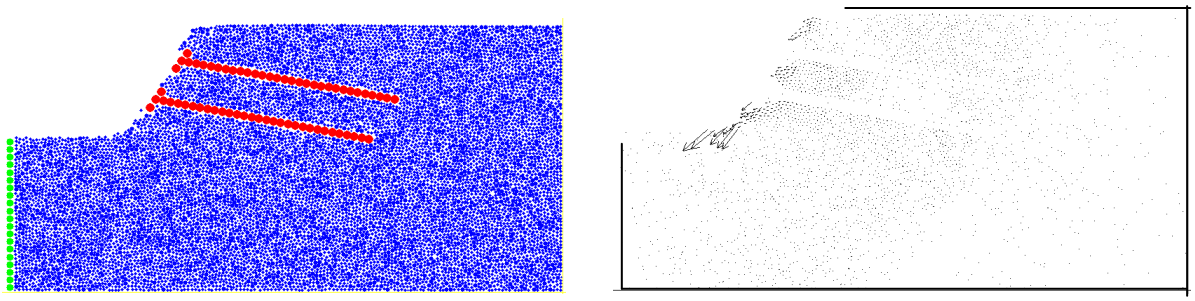

(a) $1x10^4$ step and corresponding displacement vector

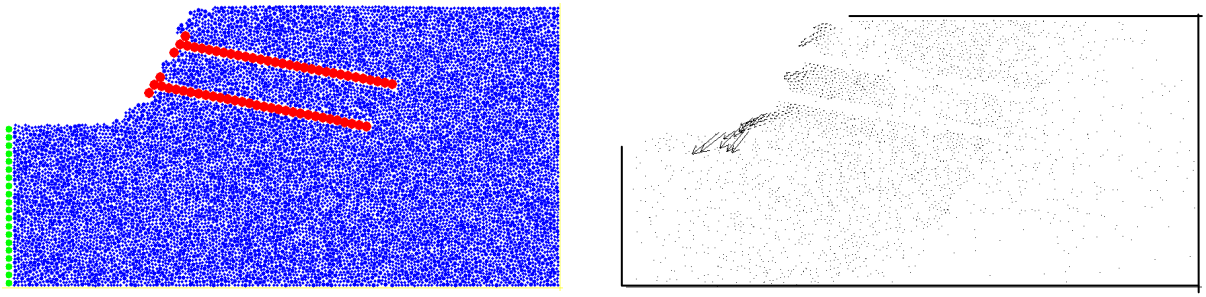

(b) $3x10^4$ step and ~ $200x10^4$ step and corresponding displacement vector

Figure 3.12 Failure development of simple slope with n_bond=s_bond=2000N and nail head

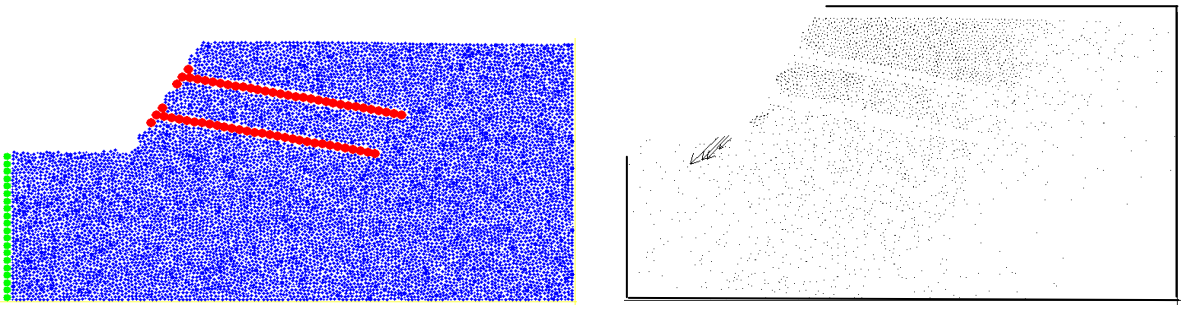

Figure 3.13 Failure development of simple slope with n_bond=s_bond=5000N and nail head (very stable)

Figures 3.14 and 3.15 illustrate the local failure at the toe and the crest in more details. By logging the displacement history of ball 2673 at the crest of the slope, it can be found that the particles around the top of the slope move downwards along the face and are restrained by the soil nail after a short displacement has occurred and the corresponding loading is taken by the soil nails. For the bottom part of the slope, the particles show the trend of moving out with upheaval. This failure is later controlled by the mobilized resistance of the soil nail. To sum up, soil nailing reinforces the global stability of the slope by resisting the formation of extended shear failure as well as limiting the local failure at the crest and toe.

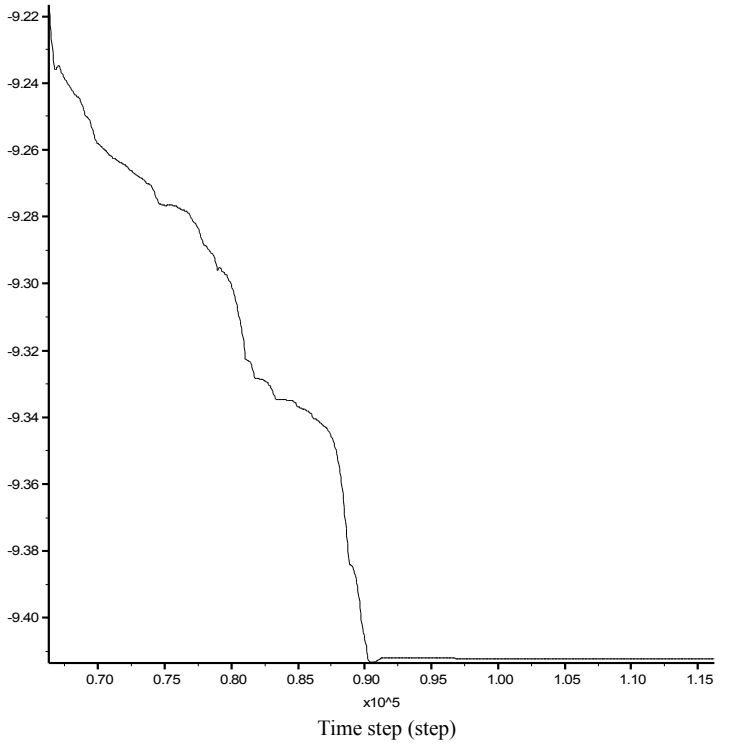

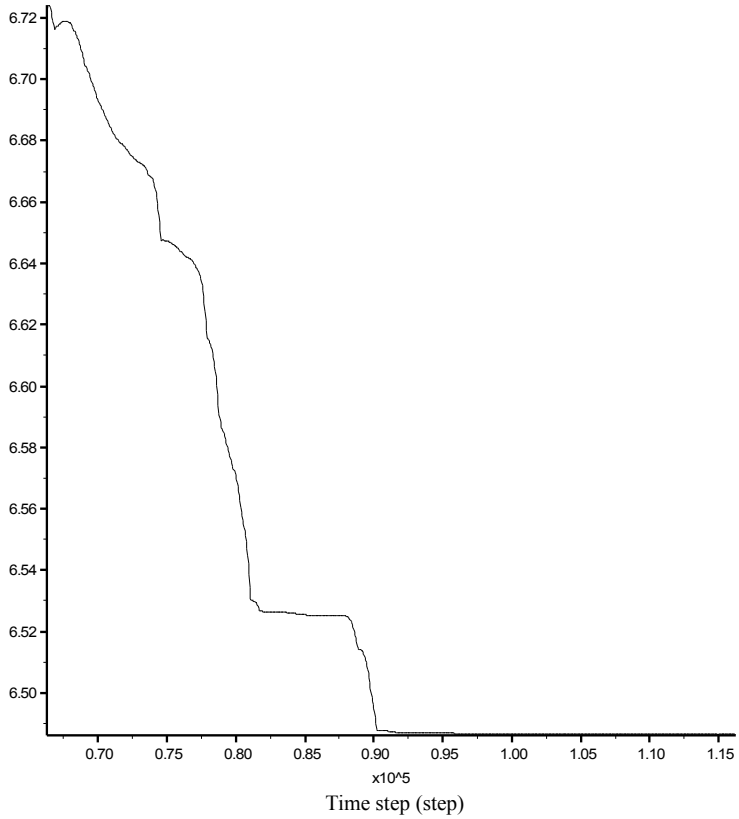

Figure 3.14 X & Y position history of ball 2673 at crest (n_bond=s_bond=0, soil nailed with head)

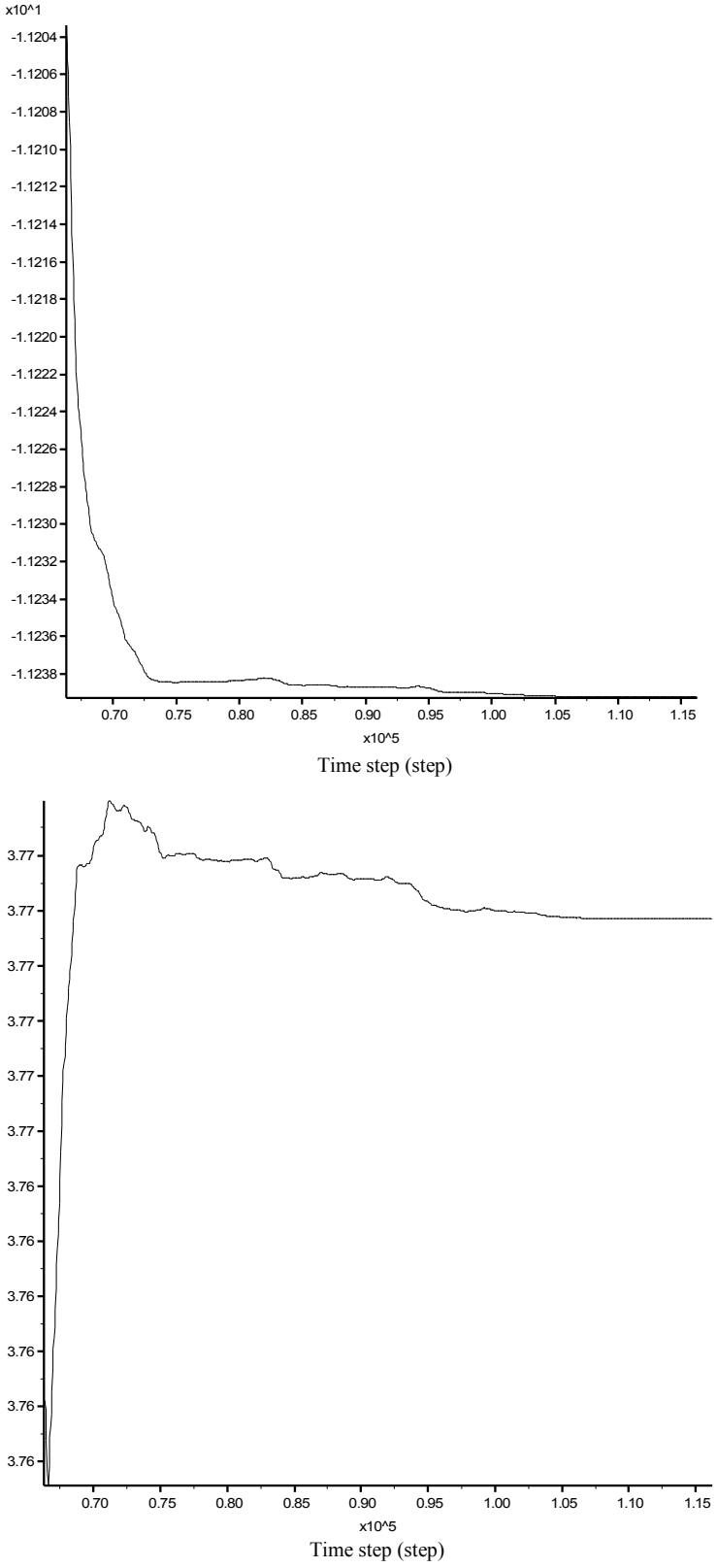

Figure 3.15 X & Y position history of ball 11870 at toe (n_bond=s_bond=0, soil nailed with head)

Soil nail is an efficient measure to reinforce the slope, as it mobilizes the shear strength on the contact surface to resist further failure. As shown in Figure 3.16, once there is slight displacement of soil, the tensile strength of the soil nails can be activated to take up the loading which will effectively reduce the instability of the stress field. The effect is particularly obvious for the soil mass below the nails, and the particles slide out at the toe only and are not influenced by the upper part of the slope which is well supported by the nails, so the normal and shear stresses are very stable as compared with the situation without the nails. The soil mass above the nails is also well stabilized against collapse. There is only slight collapse but no obvious loss at the crest (referring to Figure 3.11), and the stress maintains stable which is different from the slope without nails (referring to Figure 3.7). Overall speaking, the soil nails effectively help the slope to maintain a stable stress field.

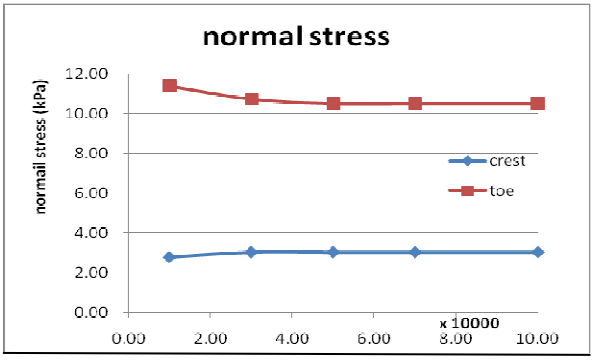

(a) Normal stress on failure surface vs. time-step

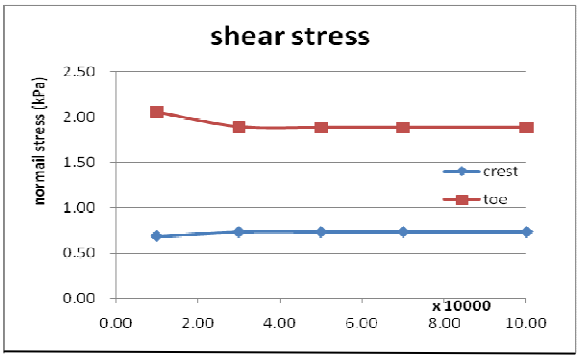

(b) Shear stress vs. time-step

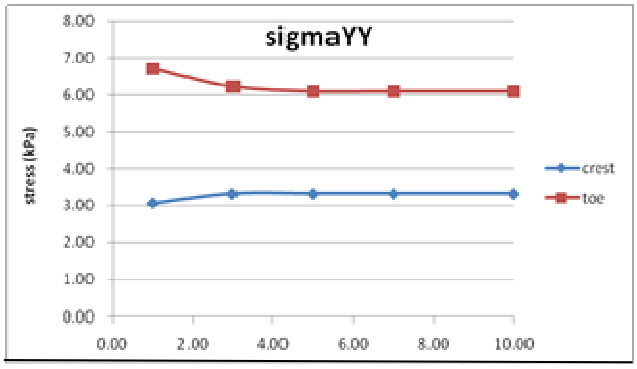

(c) Vertical normal stress vs. time-step

Figure 3.16 Stress state of soil-nailed sandy slope (n_bond=s_bond=0)

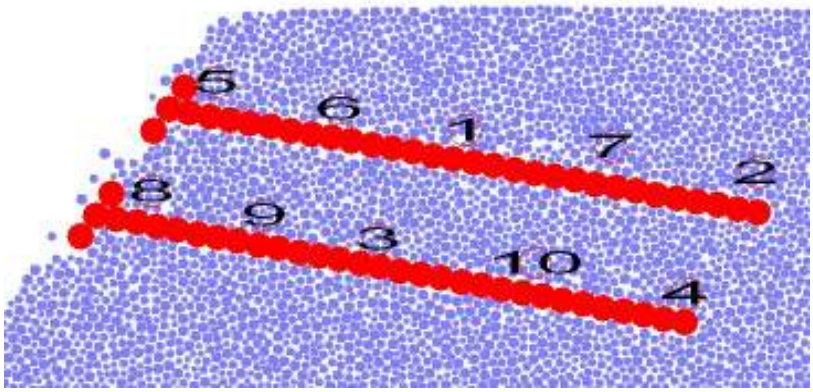

Figure 3.17 Measure circles next to the soil nails

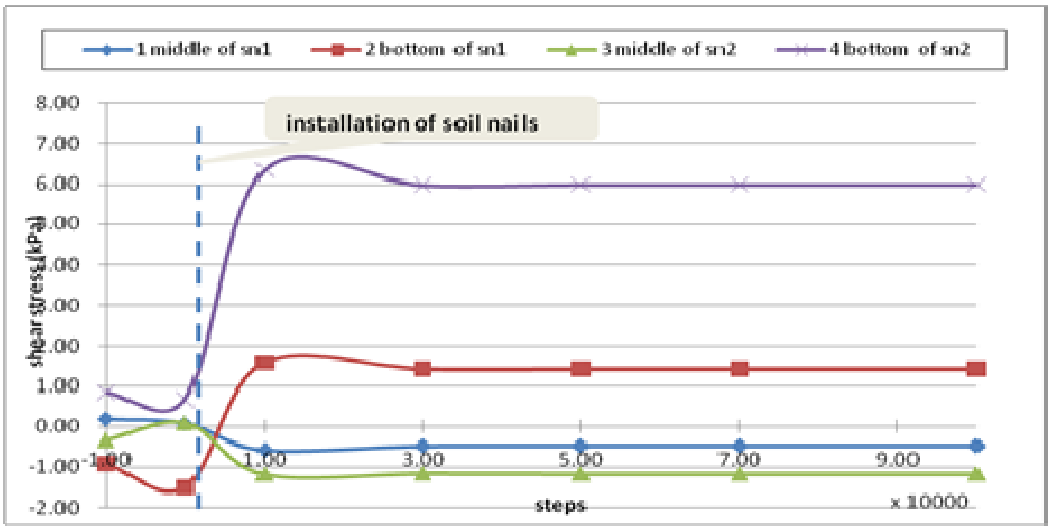

Figure 3.18 Stress analysis of soil nail during failure (n_bond=s_bond=0)

The shear stress along the soil nails is also checked by several measure circles (Figure 3.17). The action of the soil nails after the initiation of failure is clearly shown in Figure 3.18. When soil nail is inserted, there should be no stress on the soil nail. Equilibrium is reached when the slope is generated to the initial state in the beginning. When the slope begins to deform under gravity or external loading, soil nail enters to the working condition. The value of the shear stress on the nails firstly increases after the nails are installed and slight movement occurs. The tensile strength of the soil nail is therefore mobilized to resist further shear failure and maintain the reinforced soil mass at a stable stress. It is reasonable that the

lower soil nail has larger stress than the upper one as it bears more loading, while attention should be paid to the shear stress versus different positions of nails where there are large differences in the results. The shear stress at the bottom of the nail is much higher than that in the middle and the direction of the shear stress is even reversed. This indicates that the neutral point is approximately at the middle of the nails for the present problem, and the shear stress on the nails should be zero at the neutral point which is a well-known result and is supported by various laboratory and field tests. The results also demonstrate that the portions of nails outside the failure zone actually take up the stabilization action which is in accordance with the general understanding.

(a)

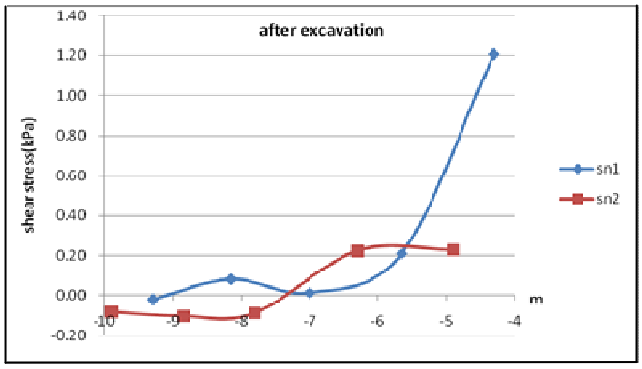

(b)

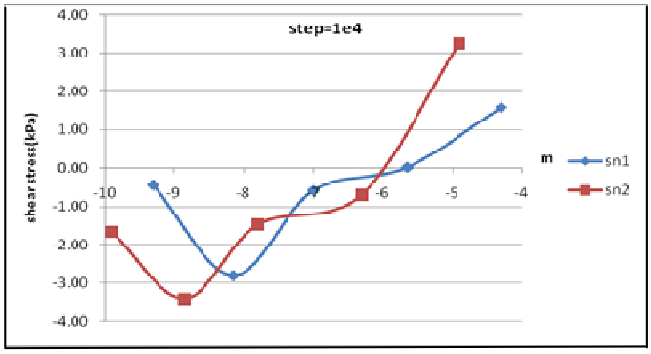

Figure 3.19 Stress analysis along soil nails at different steps (c=0): (a) the shear stress near the position of prescribed nails after the excavation of hole for soil nails; (b) Shear stress along soil nails at $1x10^4$ steps after soil nails installation

If the shear stress along the soil nails is investigated at different steps from the initial

condition to the reinforced state with the installed soil nails, the results can be found in Figure 3.17. The nail head moves with the surrounding soil so that the shear stress around the nail head is very small. At a distance away from the soil nail head, both shear and normal stress increase slightly but become smaller again near to the failure surface. Such finding convinces the reinforcement mechanism by soil nails.

3.3 Failure mode of slope influenced by rainfall induced water flow

Most of the slope failures in Hong Kong occur within May to September. Within this period, heavy rainfall which may last for many hours are not uncommon. Besides the saturation of the soil, the seepage of water can also create a major effect to the stability of slope which is however not considered in routine analysis and design in Hong Kong. The influence of underground water and water flow is always an important concern in slope stability problems. Infiltration from the watershed or runoff on the ground surface can even cause a thrust to the impacted area and accelerate the failure. After the initiation of the failure, water acts a lubricant and the soil will experience very large movement and finally debris flow will occur. PFC has the particular advantage over continuum based method in that very large scale soil movement or even debris flow can be modeled by distinct element analysis. The models selected in this section take the properties of contact bond strength =2000 N, density of soil particles equal to 2650kg/m^3 and ball to ball friction =0.5 which means soil friction angle=26.5°.

PFC can implement fluid coupling simulation by the fixed coarse-grid fluid scheme (CGFS). This code is available in 2D and 3D. It is part of the main PFC executable and does not require any additional programs. However, the geometry of the problem domain is limited to rectangular shapes with regular hexahedral elements in PFC. The fluid boundary conditions can only be applied to the faces of the rectangular domain. Due to the geometrical limitation, CGFS is not considered to be used in this study. Since the direct modeling of the effect of saturation and seepage is not possible, an approximate method is used in the present study. Four influencing factors are considered in this part as followings: (1) ground water effect; (2) seepage effect; (3) strength reduction; (4) persistent rainfall effect.

(1) Ground Water, which can reduce the effective density of soil mass and induce pore water pressure, is considered in the study. The submerged effect of underground water is modeled by applying negative body force γ_w layer by layer from bottom to simulate the rise of groundwater level, which means a decrease of soil density from 2650kg/m^3 to 1650kg/m^3, to take into account the buoyancy force. To examine the effectiveness of this approach, three cases are tried and compared as shown in Figure 3.20. For the standard model case in this research in Figure 3.20(a), the slope remains stable under gravity with no other external effect. For case (b), soil particle density is increased to 10000 kg/m^3 layer by layer from bottom. It is noticed in Figure 3.20(b) that the top of the slope has caved in obviously because large external force in form of body force on the soil mass is applied. The inclined surface of the slope collapsed dramatically. With the same contact bond strength of soil, soil mass with larger density appears to be more brittle than that in ordinary model case. For case (c), the

density of the soil is set to the same as water density 1650kg/m^3 layer by layer during modeling in order to take into account of the buoyancy force induced by ground water, so that zero effective weight is achieved. No obvious change of the slope geometry is seen in Figure 3.20(c), but there is minor upheaval at the bottom of the slope. It can represent that small lifting force is imposed on soil mass by the buoyance force, so the effect of ground water can be simulated in this way.

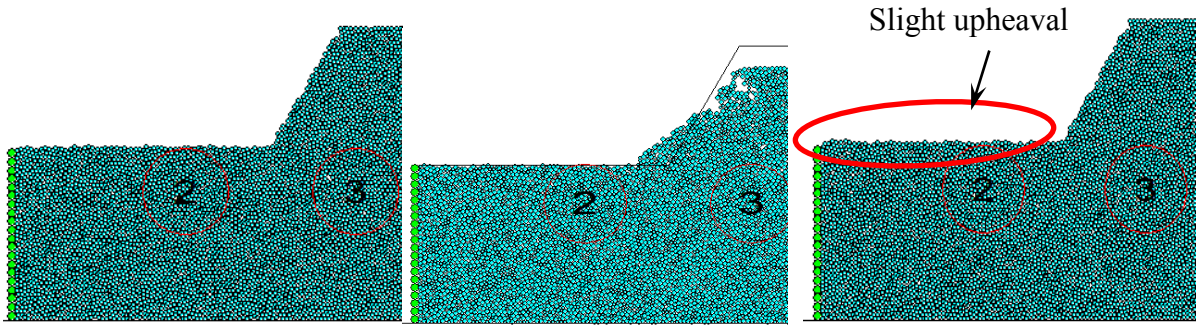

(a) Soil particle density = 2650 (b) density = 10000 (c) density = 1650

Figure 3.20 Eventual state of cut slope with different soil particle density (kg/m^3)

(2) Seepage effect due to water flow generates a thrust on soil mass(seepage force), and this seepage force will push the soil mass above the water table outwards with an obvious decrease in the stability of the slope. The real seepage flow discussed in this section is under fully saturated condition illustrated in Figure 3.21(a). It is imitated from classical theory of seepage that an approximate set of flow lines is introduced in the numerical model shown in Figure 3.21(b), and body velocity is added to simulate rainfall induced seepage force to the unsaturated slope from crest upper top at right hand side to slope bottom at left hand side. The body force of each soil particle under water flowing interface should be changing at different location which is very difficult to be modelled by PFC. In the present study, seven curved flow

regions with gradually changing flow rate from top down (from 0.01m/s to 0.002m/s on the upstream side, from 0.005m/s to 0.002m/s on the downstream side) are used for the approximation of the seepage force which can be noticed in Figure 3.21(b). Flow rate near the water table is the largest one, and the value on the left hand side is about half of that on the right hand side which will be similar to the real seepage effect.

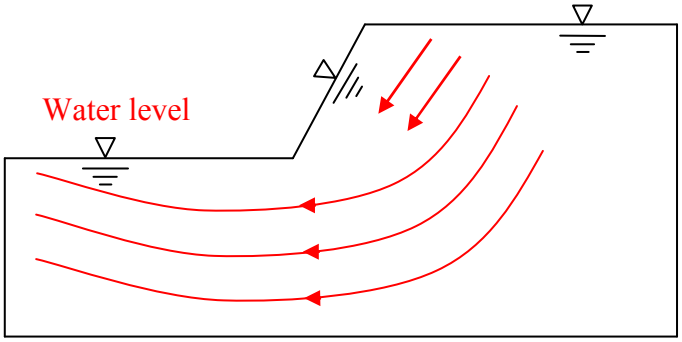

(a) Real seepage flow in fully saturated slope

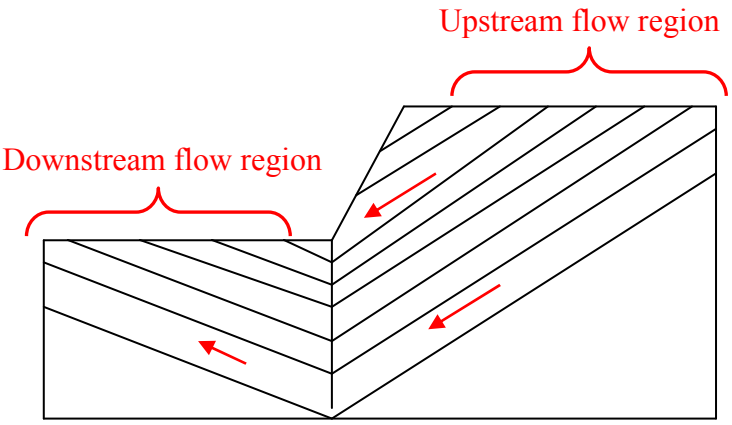

(b) Approximate seepage effect in numerical model case

Figure 3.21 Seepage effect illustration in fully saturated slope & numerical model

(3) Strength reduction occurs after stress redistribution induced by cracking of structural element and soil mass. It should be considered in numerical simulation by decreasing the bond strength gradually during failure process. Once crack appears, contact bond is broken

between those affected soil particles, and stress around cracking area will redistribute. Bond strength is no longer the same as that in the initial state. In DEM simulation, contact bond strength is reduced step by step, thus new normal and shear bonds in each contact point are generated between particles.

(4) Persistent rainfall often happens in Hong Kong. The rainfall duration could always be several hours. Much deeper and serious slope failure would take place after or even during sustained rainfall. In order to simulate this phenomenon, several times of seepage flows are imposed to the slope intermittently in the numerical simulation process. In each time, like mentioned in the above influencing factor (2), different velocity is added to several inclined layers illustrated in Figure 3.21(b) to simulate the impact of seepage force. Velocity is increasing layer by layer from bottom to top, and the flow rate near the slope crest is the largest. Due to instantaneity of the method, it takes time to digest the momentary action of seepage flow. After that the second time of seepage flows is imposed to soil mass. The number of impact time makes obvious influence on eventual failure mode, the larger the number is, more smooth the failure profile is. In reality, impact force accumulated among soil mass is increasing by the persistent rainfall, meanwhile, soil is developing from unsaturated state to subsaturated state and finally to saturated state. Rainfall is scouring the soil mass continuously untill the slope is subjected to eventual failure.

The case considering all the above four influencing factors is modeled to simulate the slope impacted by ground water effect, curved seepage flow and persistent rainfall effect with strength reduction. Progressive failure process of slope is illustrated in Figure 3.22. The

noticeable slipping zone is shown in Figure 3.22(a) from the beginning of the rainfall seepage force, accompanying with an increasing settlements at the top of the slope and incremental upheaval at the toe step by step. After the first rainfall seepage force is applied from the right top side of the slope, ground water level begins to rise from bottom. The effective density of soil mass is hence reduced layer by layer. The affected area then develops larger and larger gradually. Meanwhile, seepage flow region grows and is clearly visualized after four-time the seepage force is applied. Eventually, a smooth failure profile is formed under streaming water washing as shown in Figure 3.22(f).

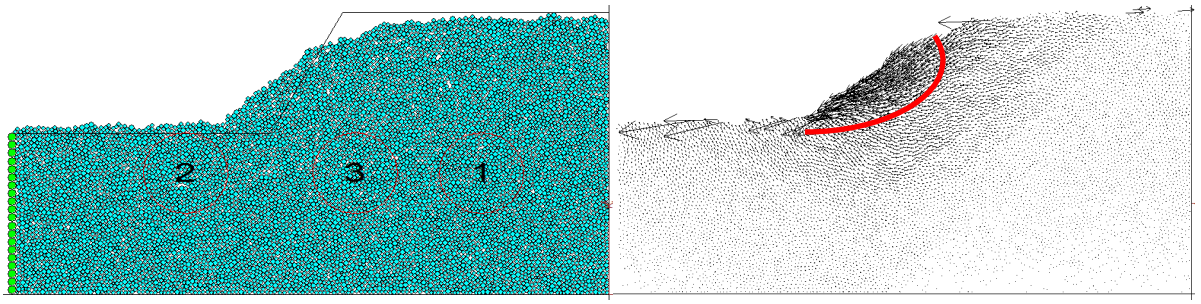

(a) $2x10^4$ step after 1st seepage force impact Displacement vector graph

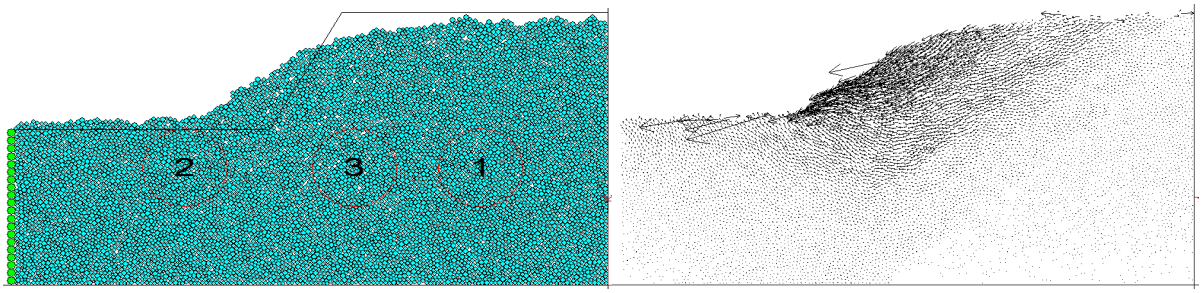

(b) $4x10^4$ step after 2nd seepage force impact & ground water effect Displacement vector

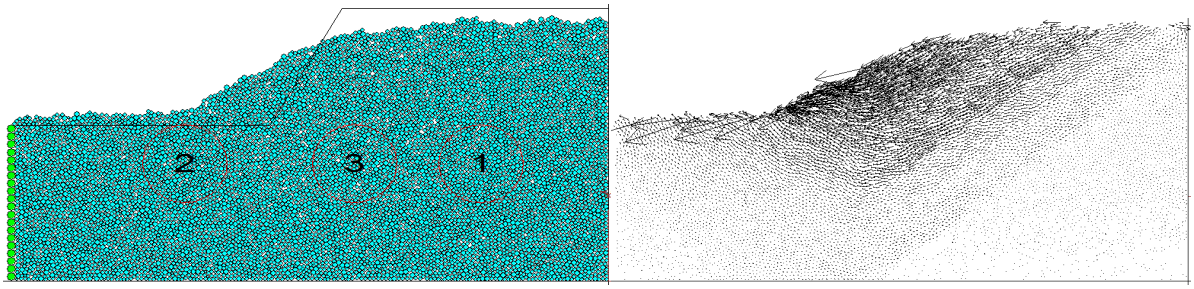

(c) $6x10^4$ step after 3rd seepage force impact Displacement vector graph

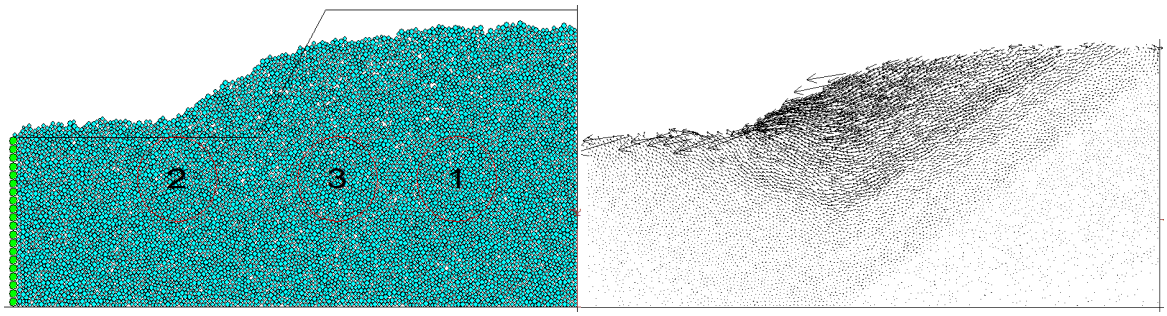

(d) $8x10^4$ step after 4th seepage force impact Displacement vector graph

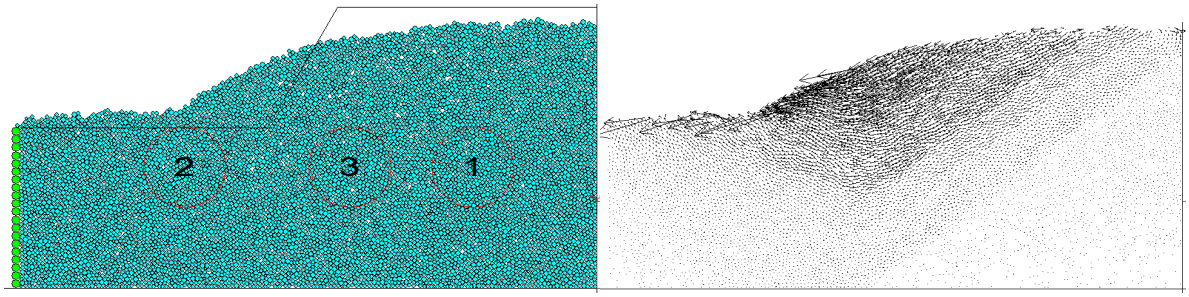

(e)$20x10^4$step Displacement vector graph

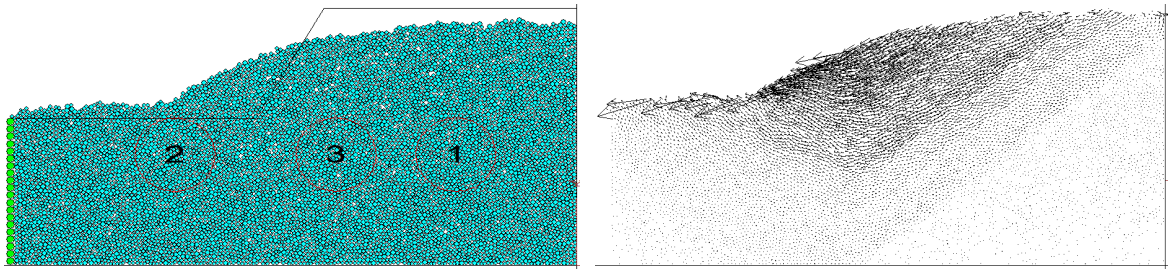

(f)$50x10^4$step Displacement vector graph

Figure 3.22 Progressive Failure Development of slope induced by ground water effect, curved seepage flow and persistent rainfall effect with strength reduction

Another seepage flow pattern which can simplify the model is also proposed as follows. It is a linear seepage flow region illustrated in Figure 3.23 to simulate the seepage effect due to water flow. This inclined flow region constitutes 7 gradually changing flow rates (from

0.01m/s to 0.001m/s) oriented from the upper crest corner of slope to middle part of the slope body. In this new case, the basic parameters of the soil mass remain the same, which are bond strength equal to 2000N and friction coefficient equal to 0.5. Other than different flow pattern, strength reduction and persistent rainfall effect are also taken into account.

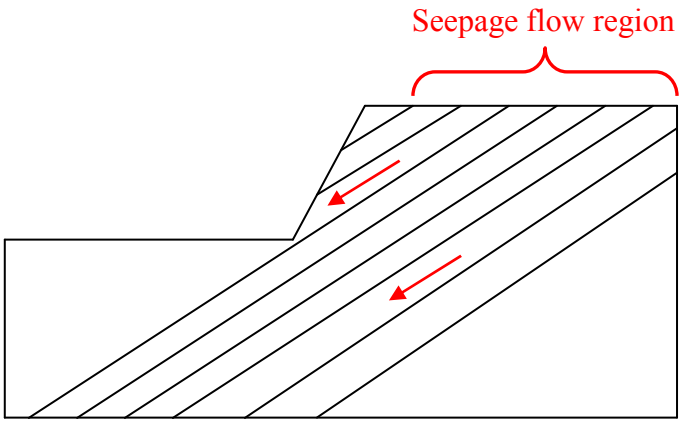

Figure 3.23 Simplified case with eight linear seepage flow lines

Figure 3.24 shows the progressive failure development of the slope under linear seepage flow. After the first application of rainfall induced seepage force as shown in Figure 3.24(a), slope crest is scoured smoothly by the soil particles moving forward. Small settlement appears on the top of the slope, while bottom of the slope is pushed with slight upheaval. Under the continuous seepage effect, the soil mass is pushed further forward and slope crest becomes a smooth surface, while upheaval becomes increasingly evident at the bottom of the slope. Relatively obvious soil movement arising from seepage can be noticed, especially for the results in Figure 3.24(c). At last, completed failure is triggered to the slope with an obvious settlement at the top, extended failure zone and noticeable upheaval at the toe in Figure 3.24(f).

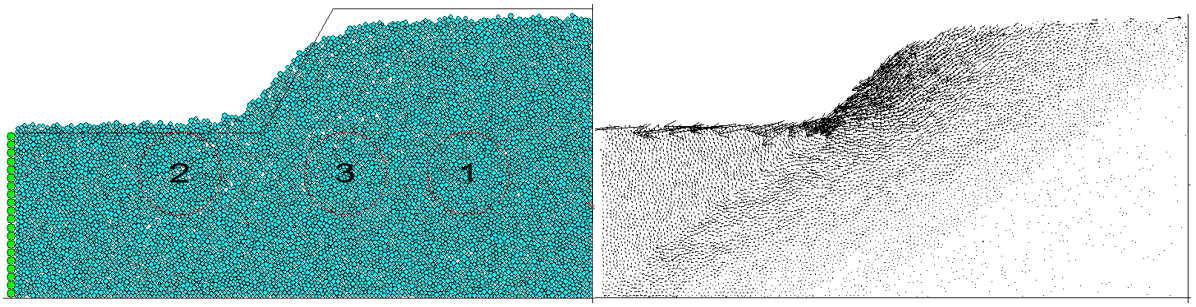

(a) $2x10^4$ step after 1st seepage force impact Displacement vector graph

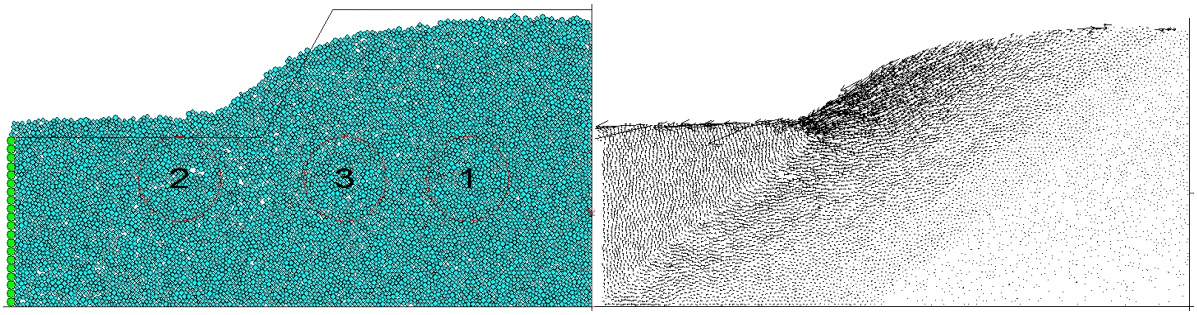

(b) 4x104 step after 2nd seepage force impact & ground water effect Displacement vector graph

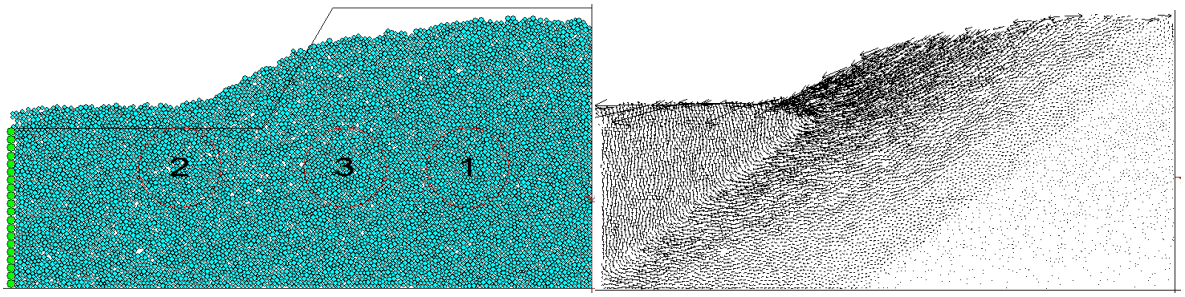

(c) $6x10^4$ step after 3rd seepage force impact Displacement vector graph

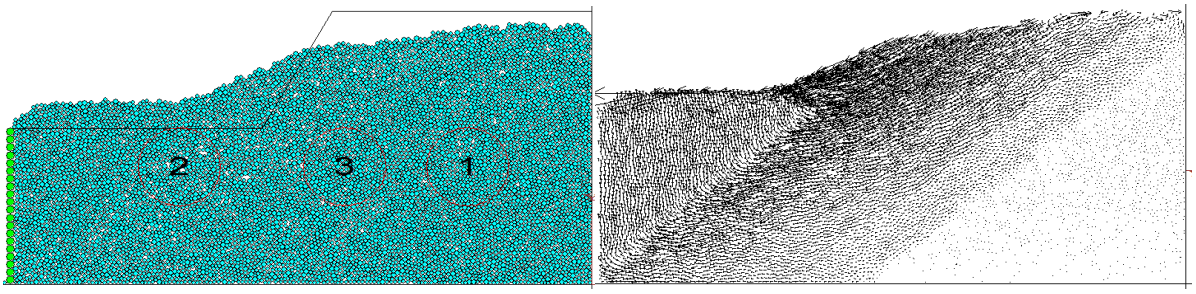

(d) $8x10^4$ step after 4th seepage force impact Displacement vector graph

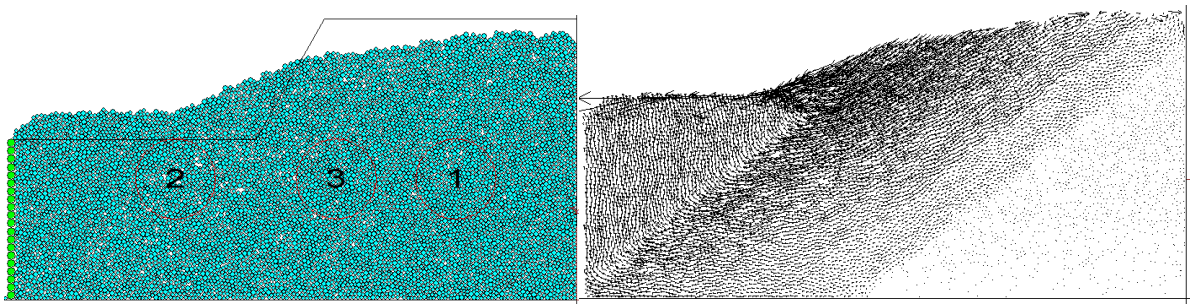

(e) $20x10^4$ step Displacement vector graph

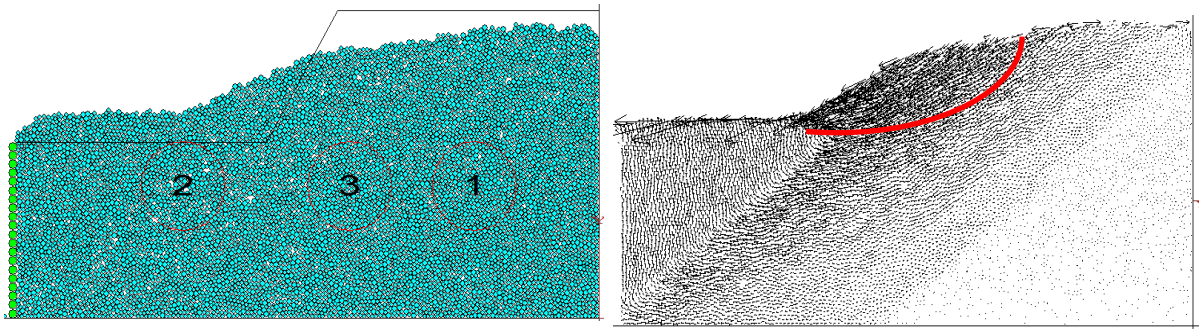

(f) $50x10^4$ step Displacement vector graph

Figure 3.24 Failure process of slope under linear seepage flow impact

For soil particles with lower bond strength, rainfall greatly enhances the rate of failure and finally induces more thorough collapse. Several model cases are tried to carry out the comparison, and the selected results are shown in Figures 3.25&3.26 with bond strength 650N while the density and friction remain unchanged. The approximate water table is imposed in these cases, assuming it to be a polygonal line as shown in Figures 3.25&3.26, as a smooth water table is not easily defined due to the limitation of particle flow code.

The progressive failure mechanism due to underground water flow in Figure 3.25 shows that slope failure is accelerated by the water as compared with a simple slope. Unlike the failure (both sliding at the crest and the accumulation at the toe) in simple slope which are influenced only by gravity, the pore water pressure induces a continuous sliding failure on the

slope face. The failure zone develops towards the inside of the slope and results in obvious loss of soil grains as shown in Figure 3.25(c) and (d). At the later stage of failure, the driving force tends to be gentle with a change of the geometry and reduced slope angle and the development of failure becomes slower.

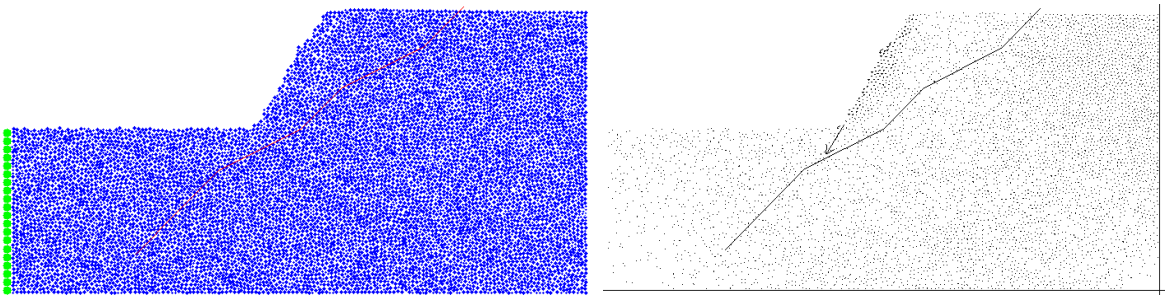

(a) $1x10^4$ step Displacement vector graph

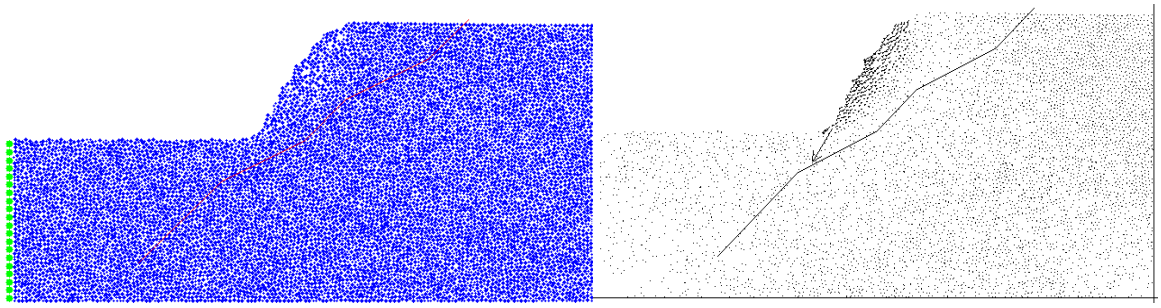

(b) $3x10^4$ step Displacement vector graph

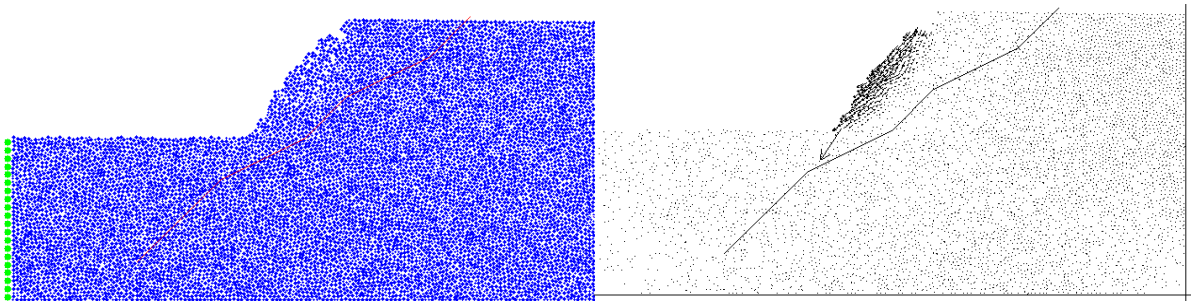

(c) $5x10^4$ step Displacement vector graph

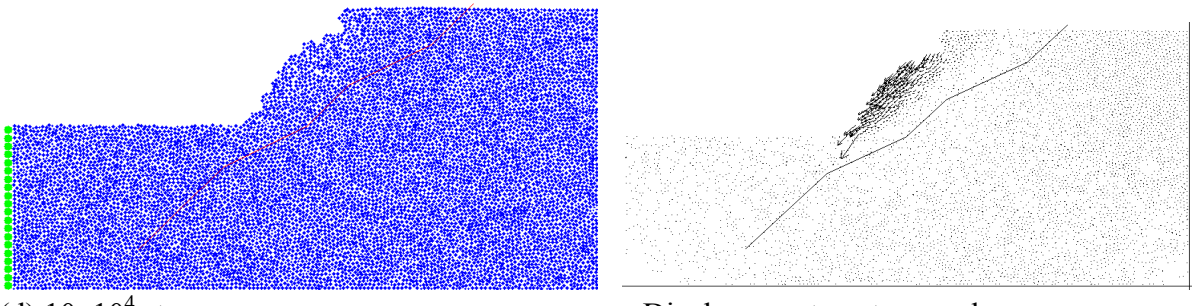

(d) $10x10^4$ step Displacement vector graph

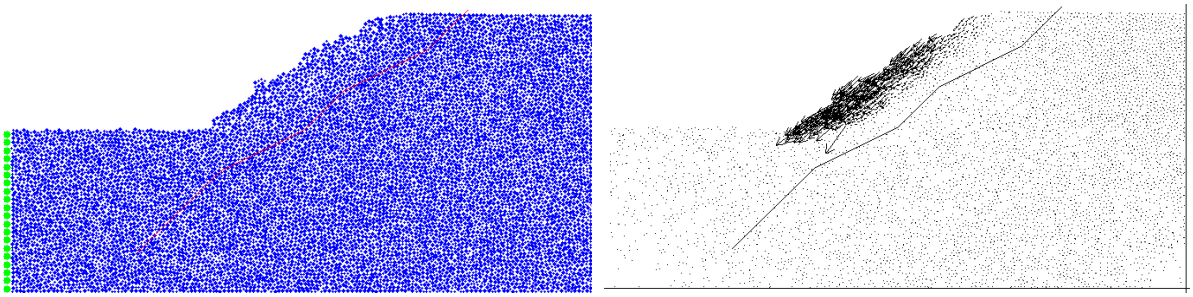

(e) $30x10^4$ step Displacement vector graph

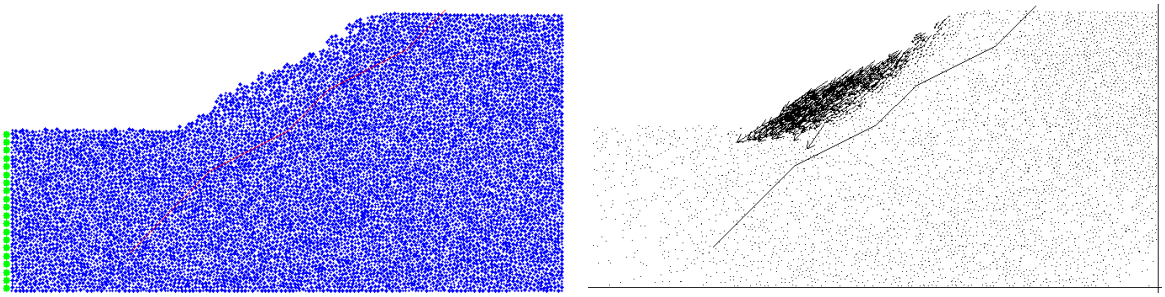

(f) $100x10^4$ step Displacement vector graph

Figure 3.25 Failure development of slope under lower bond strength impacted by Underground Water

If both the effect of underground water (reduce the effective density only) and water flow (including the seepage force) are taken into consideration, the failure becomes more complicated. Linear flow pattern is used in this case including only 5 flow zones with gradually changing flow rate (from 0.01m/s to 0.001m/s). The forward movement and upheaval at the toe for the combined effect are quite considerable as shown in Figure 3.26. The seepage force reduces the stability accompanying with an obvious settlements at the top of the slope. For the groundwater, the combined effects of buoyant force and water seepage induce deeper failure, and obvious zone of shear failure can be found in Figure 3.26(g).

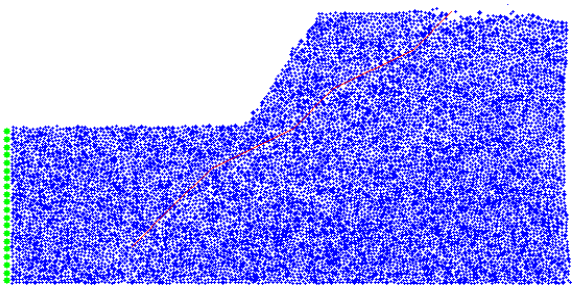
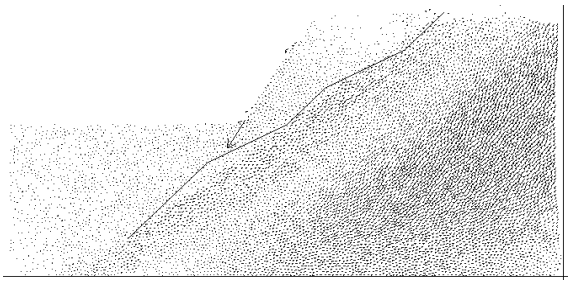

(a) Initial state after adding velocity to 5 inclined layers Displacement vector graph

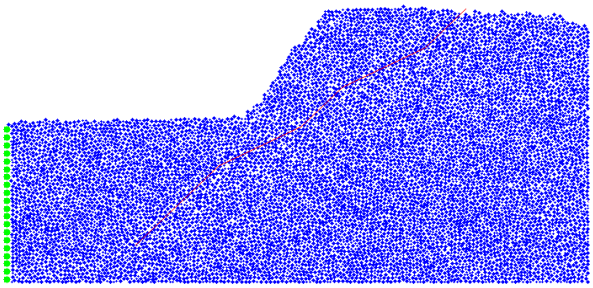
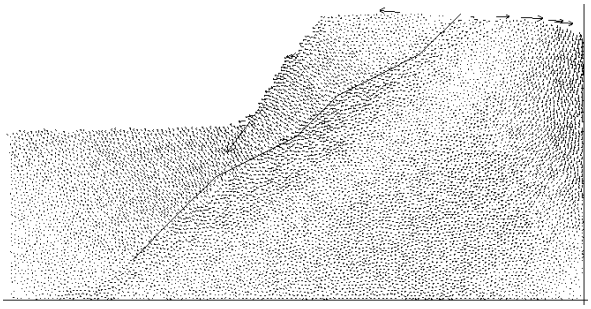

(b) $1x10^4$step Displacement vector graph

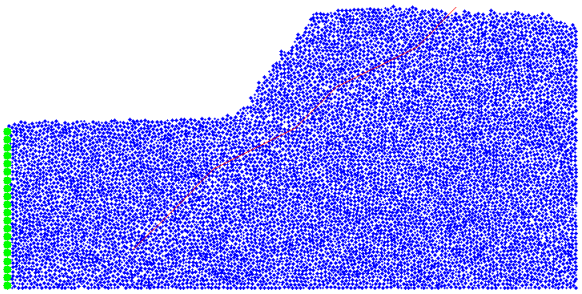
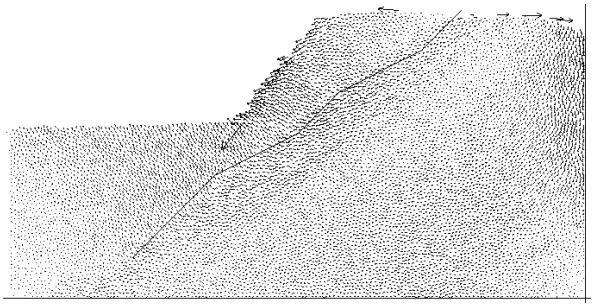

(c) $3x10^4$step Displacement vector graph

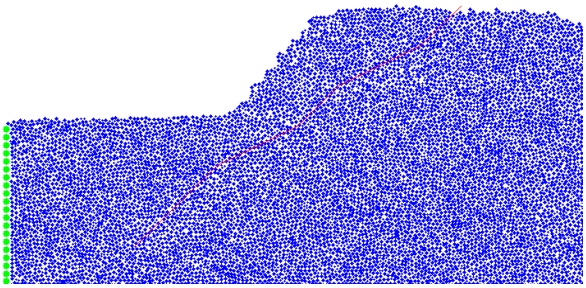
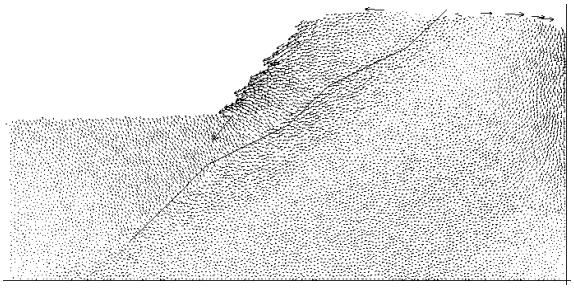

(d) $5x10^4$step Displacement vector graph

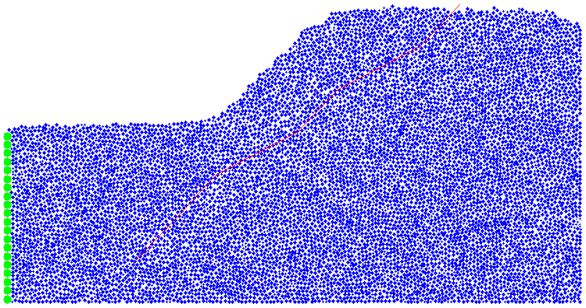
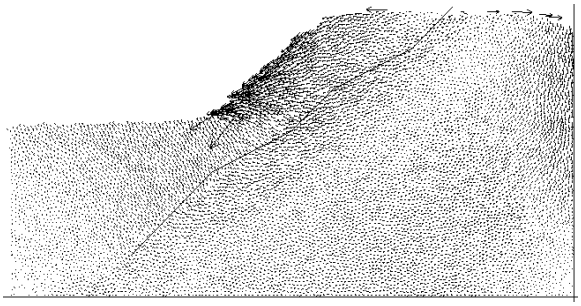

(e) $10x10^4$step Displacement vector graph

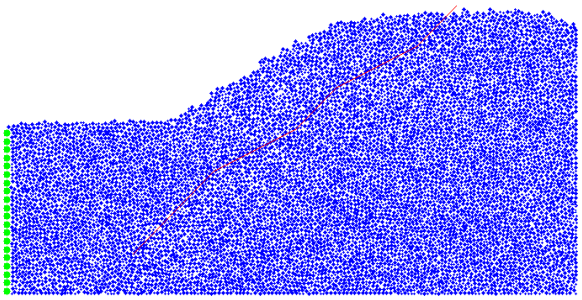

(f) 30x10^{4}step

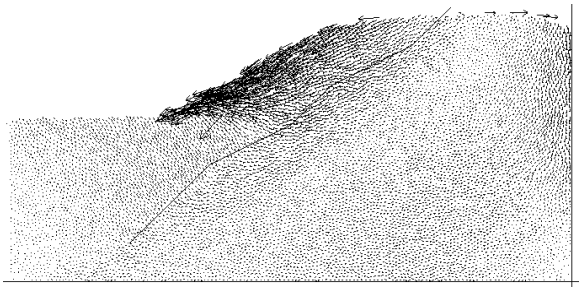

Displacement vector graph

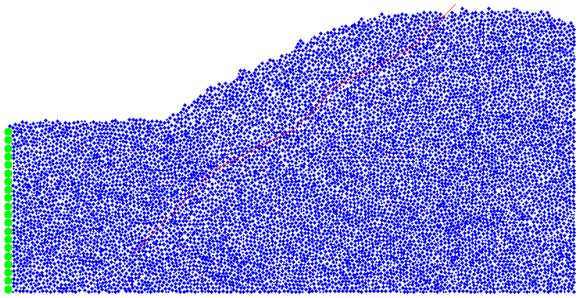

(g) 100x10^{4}step

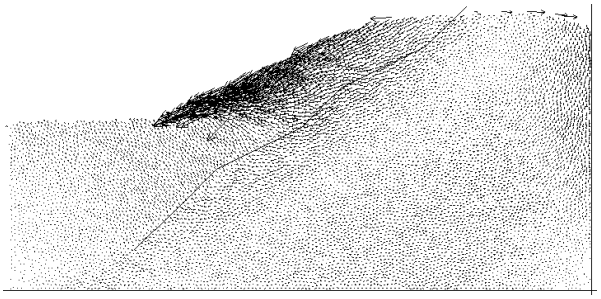

Displacement vector graph

Figure 3.26 Failure development of slope under lower bond strength impacted by Underground Water and Water Flow

For the effective stress on the failure surface, smooth and relatively stable normal and shear stresses at the crest and decreasing normal and shear stresses at the toe can be found as shown in Figure 3.27. The seepage force from the water flow and ground water induce buoyant force to the soil and reduces the effective stress, so the stress decreases during failure process. Such phenomenon demonstrates that the water does not simply reduce the strength by reducing the effective stress, but the seepage force can also greatly magnify the instability of the whole slope.

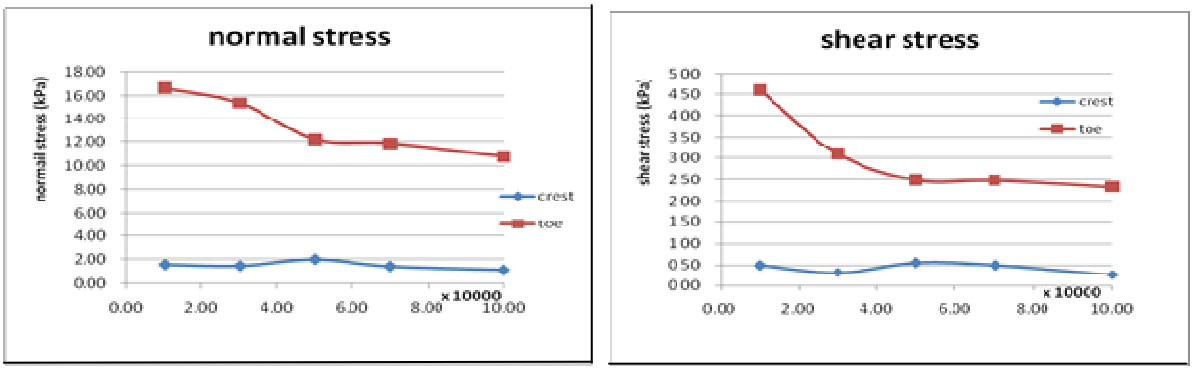

(a) Normal stress on failure surface (b) Shear stress on failure surface

Figure 3.27 The stress state of slope influenced by water flow

3.4 Conclusion and discussion

This chapter is mainly focused on the failure mechanism of slope under the action of self-weight, soil nail and rainfall induced water flow. Two-dimensional DEM analysis is carried out in the above sections. Although two-dimensional analysis is a simplified picture of the actual picture of the failure, it is not a bad approximation, and many of the important processes about the soil movement and development of the failure mechanism can be studied by the simplified two-dimensional analysis with relatively acceptable computer time (may also take 1 week for the complete analysis). Three-dimensional analysis which is considered in the next chapter is much more time-consuming in the analysis and is more suitable for fundamental micromechanics study of the failure process.

From the large displacement simulation of slope failure, it is found that for a slope with cohesionless soil, failure firstly occurs at the crest of the slope, and the failure gradually extends to the base of the slope until failure where the slope angle is equal to the friction angle of soil. The failure is generally caused by soil sliding where a precise slip surface cannot be found, and this is a typical surface slope failure which is well known in the basic

soil mechanics. Considering the overall particles flow will reveal that the downward movement of the particles at the crest induces tensile failure, and tension crack can be found at the crest of slope. The deposition of the particles at the toe causes the failure in the forms of sliding out and upheaval; and the area in the middle of the slope actually turns into a shear failure zone due to the continuous sliding of soil. When the bond strength is relatively high, the whole instability can be reduced and the displacement is limited. The bond strength can be regarded as cohesive strength in macroscopic view, so that the cohesive strength is hence an important factor in slope stability which is actually a well-known fact among the engineers. In Hong Kong, the soil cohesive strength is usually controlled to a threshold limit even the soil tests may indicate a very high cohesive value. This practice is adopted because of the doubt on the long term cohesive strength of soil and the factor of safety is rather sensitive to the cohesive strength of soil. From this study, it seems that this practice is reasonable for Hong Kong where there are many slope failures each year.

Soil nails can effectively reinforce the slope stability, especially when nail head is used in the numerical analysis, and the overall stability is greatly enhanced. Soil nail provides the resistance to soil movement by mobilizing the shear strength along the nail and massive movement of soil is restrained and limited. The stress field is also more stable under the action of soil nails. Failure for soil nailed slope is hence generally comprised of the tensile failure at the crest and the shear failure at the base.

The effect of water flow in slope stability problem by PFC is more complicated in nature. Four influencing factors are taken into account in this part, including ground water effect,

seepage effect, strength reduction and persistent rainfall effect. Also, different seepage flow patterns are tried and illustrated. The simulation results show that the slope crest is scoured smoothly under continuous effect of rainfall induced water flow. More obvious settlements at the top, extended failure zone and noticeable upheaval at the toe are developed compared with normal failure. Thus rainfall induced water flow not only accelerates slope failure and results in an obvious decrease in the stability of the slope, but also causes further thorough collapse at the end. That is to say, rainfall is the most important issue requiring the attention from the engineers.

To sum up, by the use of the distinct element method in the qualitative study of this section, it is found that slope failure occurs firstly at the crest because of insufficient resistance to driving forces like gravity or combined influence of gravity and water. The soil particles slide continuously and enlarge the extent of failure to the lower part of slope and eventually sliding out at the toe. Sliding out can further decrease the support to the upper soil mass and promote the global failure, especially in the cases where water takes effect. The stability of the toe is hence also an important factor in maintaining the overall stability of a slope.

CHAPTER 4 PHYSICAL MODELING AND THREE-DIMENSIONAL NUMERICAL SIMULATION OF SLOPE UNDER EXTERNAL SURCHARGE

4.1 Introduction

Bridge foundation is often built on slope, especially in the hilly terrain like Hong Kong and many other countries. The slope stability analysis and foundation design are crucial topics for the engineers, and actually the French engineers define the factor of safety of a slope in terms of the ultimate bridge abutment loading against the applied load. For the study on the failure mechanism of slope under surcharge loading, both macroscopic and microscopic aspects should be taken into account and considered in details with comparisons. Qualitative study on the failure mechanism of two-dimensional slope stability problems has already been carried out in the previous chapter using the discrete element method. It gives decent results to illustrate the phenomenon and demonstrate the problems. On the other hand, quantitative study is also required to testify the accuracy of the discrete element analysis. In general, it is difficult to carry out quantitative study on DEM analysis, and qualitative study is the main application of the DEM analysis at present.

Many previous studies using the discrete element method to consider the discrete nature of soils provide insight into the constitutive behavior of soil mass. The DEM starting with the behavior at the scale of a grain can help understanding the constitutive relation without the need for contractive/dilative assumption, flow rule or hardening rule which are merely curve

fitting by nature. Moreover, it is also widely used to simulate the behavior of a large range of geomaterials for mainly qualitative analysis. It should be noted that there are only limited applications of the Distinct Element Method for slope stability analysis, especially about the progressive failure mechanism of slope. DEM is also more suitable for qualitative instead of quantitative assessment of the stability of slope, as there is a difficulty to define precisely the microscopic parameters, and most of the DEM models cannot reflect completely the grain distribution, initial stress or drainage condition.

Also, there are many advances in distinct element method over the last twenty years, and complex mechanical interactions of a discontinuous system can now be analyzed in three dimensions (though still very tedious and time-consuming at present). However, there are only limited previous three-dimensional particle flow modeling on real problems (most works are devoted to fundamental study of soil behavior) due to the various constraints in image capturing, model generation in three dimension and large volume of data for manipulation. Traditional approaches in DEM have modeled soil samples as an assembly of two dimensional discs or three-dimensional spheres. PFC3D is the exclusively commercial 3D DEM program considering assembly as spheres. It simulates the movement and interaction of spherical particles using distinct element method (DEM), described by Cundall and Strack (1979). PFC3D is designed to be an efficient tool to model complicated problems in solid mechanics and granular flow, but it still takes great effort to develop the desired model and a very long computation times in terms of days or weeks are necessary for a typical problem.

In this chapter, the progressive failure mechanism of the model slope under local

surcharge is determined both from the laboratory model test and numerical analysis for comparison, and the procedures to set up an appropriate three-dimensional distinct element model is discussed. In the present work, a tedious and very time-consuming three-dimensional DEM analysis has been managed to carry out together with laboratory test aiming at quantitative slope failure analysis which is an important work in distinct element analysis of the complete failure process of a slope. Furthermore, both qualitative and quantitative studies have been carried out in the present study which is difficult to be found in literature.

4.2 Physical modeling of slope under external surcharge

Physical test were carried out in laboratory of department of civil and environmental engineering, Hong Kong Polytechnic University in 2008. The slope physical models were constructed to investigate the failure process of slope under external local loading. A physical soil tank was built with a layout as shown in Figure 4.1, and the tank is about 1.5m depth x 1.84m wide x 1.2m high. The height of the model slope was 0.7m with a slope angle of 45°. The section view of the soil slope model was illustrated in Figure 4.4. Sandy soil with 5% moisture content and particle size distribution shown in Fig.4.3 was compacted to form a slope model in 7 layers using an electric vibrator. The average bulk density of the soil model was determined as 1672kg/m^3. Direct shear test was conducted to determine the shear strength parameters of the river sand used in the laboratory test, and the shear-normal stresses relation was illustrated in Figure 4.2 which gave a friction angle of 58.6° to the compacted sand with a cohesion of 0.6 kPa. The parameters of the river sand used for the physical model were given in Table 4.1.

Figure 4.1 Outlook of soil physical slope

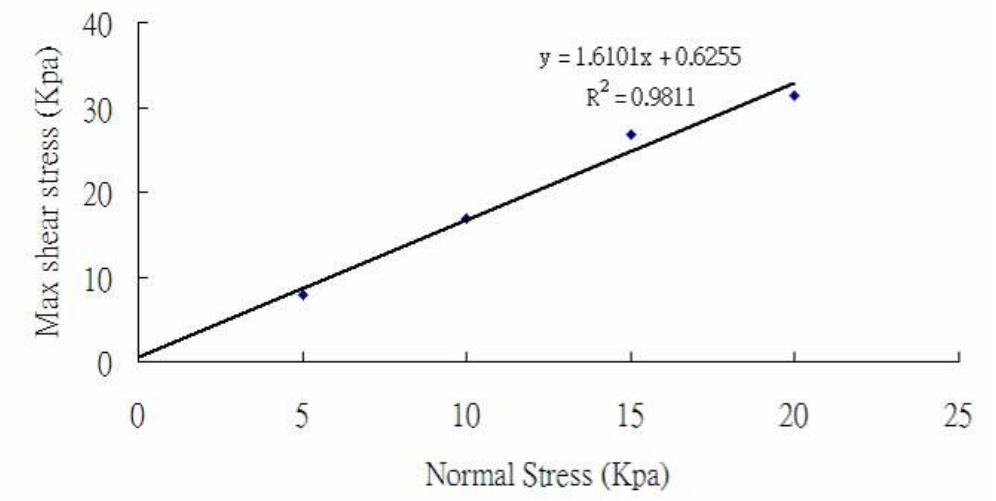

Figure 4.2 Shear-Normal stress curve

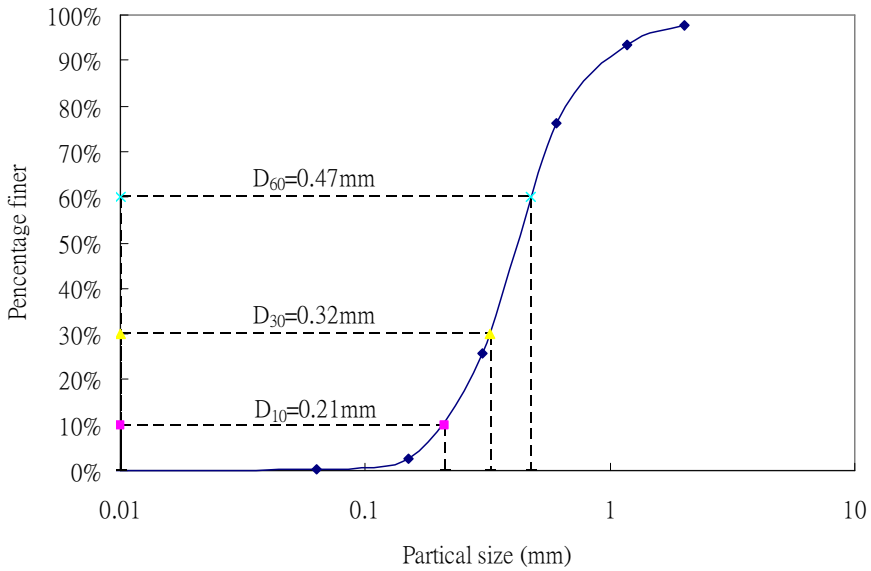

Figure 4.3 Particle size distribution

Table 4-1 Shear strength parameters of the river sand

Cohesion Value (kPa)	Friction angle (degree)	Moisture content (%)	Average bulk density (kg/m^3)
0.6255	**58.61**	**5.2**	**1672**

In this test, the surcharge loading was applied from the hydraulic jack, and the loading was transferred to the steel plate to simulate a local distributed load as shown in Figure 4.4. The loading plate was placed at the center of the slope with 100mm offset away from the slope crest and the back of the frame to reduce the end effect. The loading was applied slowly and the test lasted for about 4 hours with a maximum applied load of 35 kN.

Five Linear Variable Differential Transducers (LVDT), shown in Figures 4.4 and 4.6, were set up to measure the displacement of soil at different locations which included the upper right (RHS), upper left (LHS), lower right (RHS) and lower left (LHS) on the slope face and at the loading plate on top of the slope. The displacements at different vertical loads are monitored up to failure as shown in Figure 4.8. The 2 pairs of transducers on the slope surface are placed symmetrically with a horizontal spacing of 300 mm. The first and second pairs of transducers are placed at vertical distances of 150 mm and 450 mm from the top of the slope respectively.

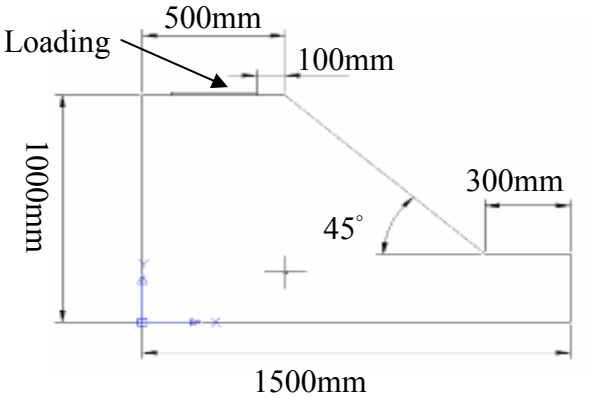

Figure 4.4 Section view of soil slope model

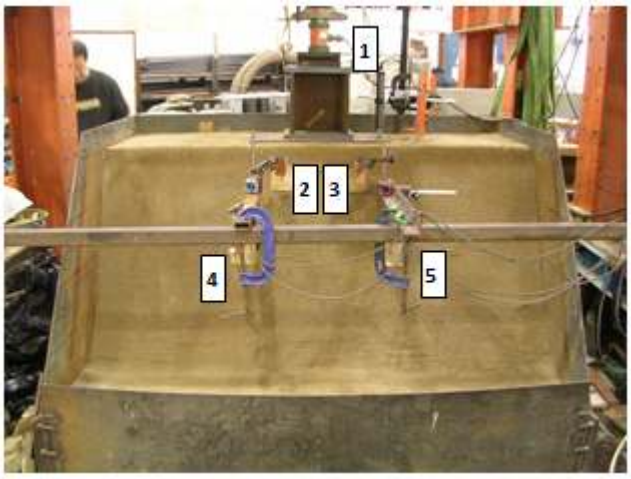

Figure 4.5 Locations of transducers

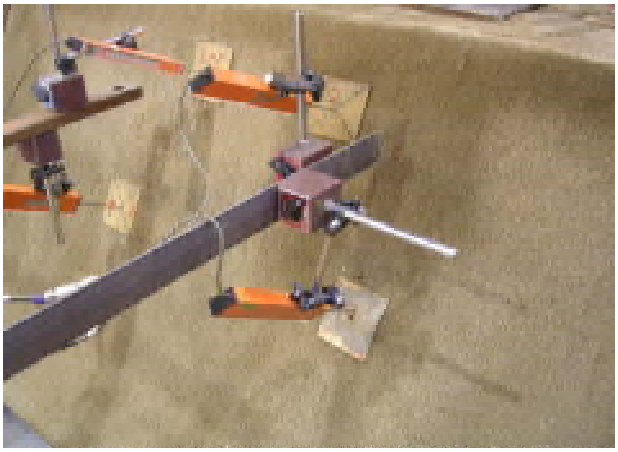

Figure 4.6 LVDT at top and sloping face of the model test

(a) intermediate process state

(b) sideview of intermediate process state

(c) Final failure state after failure mass

(d) global failure surface after failure mass is removed

(e) Cracks developed at slope surface and crest originated from the loading plate

Figure 4.7 Failure process of soil slope under increasing loading

The intermediate and final failure states of the model slope were illustrated in Figure 4.7, and the results from the five transducer were given in Figure 4.8. From Figure 4.7(a) and 4.7(e), we could see that cracks developed firstly around the steel loading plate and extended towards each corner side of the slope crest with an angle 45° which were basically in accordance with the classical theory. During the test, flags with different colors were used to locate the time of appearance and the location of cracks during loading which could also be seen in Figure 4.7. From Figure 4.7(d), it was noticed that the failure surface was approximately a triangular zone at top plus a log-spiral zone similar to the Prandtl mechanism for a bearing capacity problem with an inclined surface below the top triangular zone (Cheng and Au 2005). The inclination of the failure surface to the horizontal direction in Figure 4.7(d) was also close to 74.3° (45°+ϕ/2) which was a good illustration of the general shear failure for the present test. The soil mass actually failed gradually instead of a sudden failure in the loading process. As the steel plate kept going down, the inclined slope face was covered with vertical cracks and diagonal cracks which were directed towards the steel plate (see Figure 4.7e). The soil mass at the slope surface was drawn down layer by layer to the slope toe by the action of the loading steel plate, and this was the typical face failure phenomenon for cohesionless soil. After four-hours of loading, the sand at the middle top of the slope was highly compressed and a cavity was formed underneath the steel plate which could be noticed after the removal of the steel plate, while the largest cracks were generated at the critical failure surface within the slope body for the global failure (Figure 4.7d). The global soil mass was pushed down to the toe of the slope gradually, and the complete physical slope model collapsed eventually which was shown in Figure 4.7.

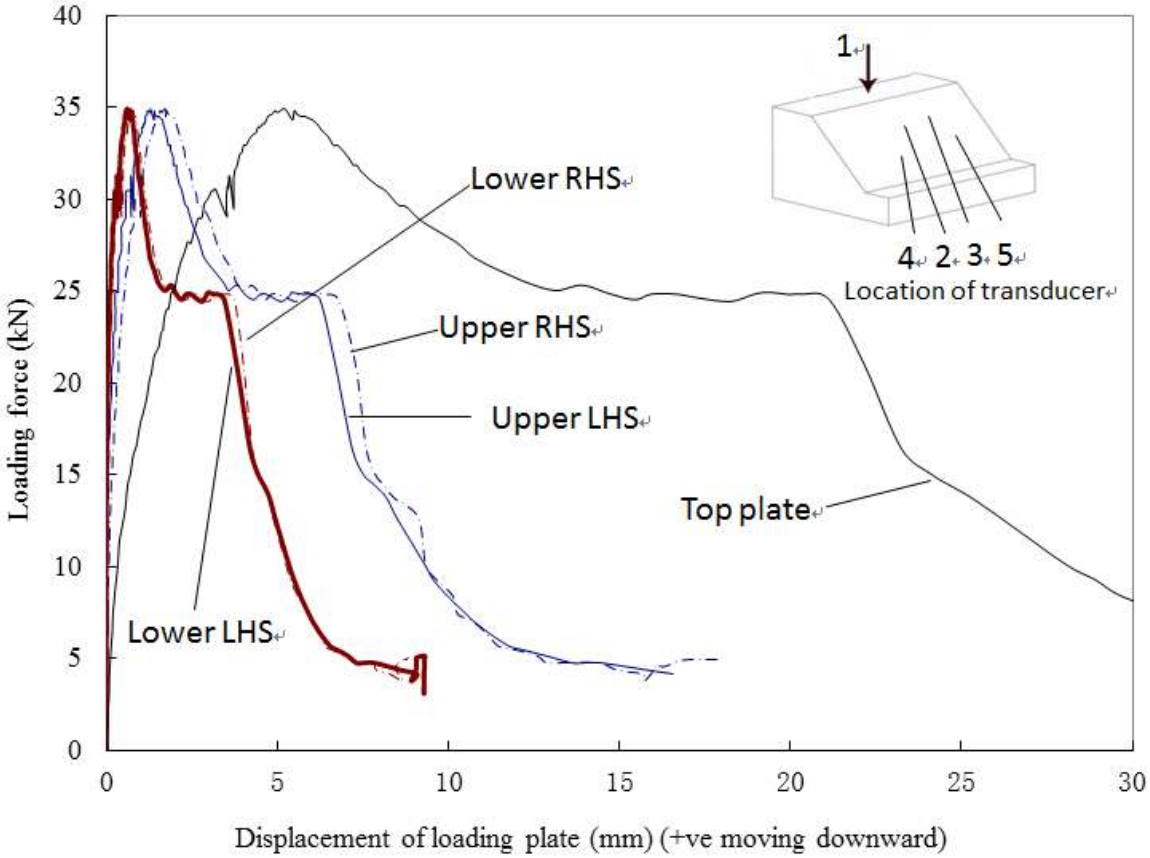

Figure 4.8 Loading force against the displacement of slope surface

An ultimate load of 35 kN has been attained at the displacement of about 6 mm as shown in Figure 4.8. For the slope surface, the corresponding displacement at the maximum pressure was about 2 mm and 1 mm at top and bottom of the slope respectively as shown in Figure 4.8, which were much lower than the corresponding displacement at the loading plate. Beyond the peak load, the applied load decreased with increasing jack displacement. From the displacements for the left and right LDTV at upper and lower level, it was clear that the displacements of the slope were basically symmetrical. In Figure 4.8, after the maximum load has been achieved, the loading force decreased with increasing displacement until a

displacement of about 13mm for which the load maintained constant for about 9mm. At the beginning of this constant load stage, the local triangular failure zone was fully developed while the failure zones at the two ends of the plate were still not clearly formed. At the end of this constant load stage, the failure zones at the two ends became visually apparent. When the displacements were further increased, the applied load decreased further and the failure zone propagated towards the slope surface until the failure surface as shown in Figure 4.7(c) and (d) is obtained. At last, the residual load of the test was around 5 kN.

For this test, there were several interesting phenomena worth discussing. The failure profile and cracks first initiated beneath the footing as shown in Figure 4.7(e), which was a typical bearing capacity failure with a triangular failure zone. This could also be observed from the upper part of the failure profile as shown in Figure 4.7(c) and 4.7(d). As the load increased, the failure zone extended and propagated towards the toe of the slope and the final failure surface was shown in Figure 4.7(d). It was observed that the failure mechanism of the physical model test is hence a local triangular failure beneath the bearing plate, and the failure surface propagates towards the slope surface with a curved surface similar to a logspiral curve until a failure mechanism is formed. This type of problem could be considered as a bearing capacity problem as well as a slope stability problem, which was demonstrated to be equivalent by Cheng et al. (2013).

4.3 Three-dimensional numerical modeling of slope under local surcharge

To further assess the laboratory test results, the authors have adopted the DEM in the numerical analysis because the development of cracks, face failure and the final collapse are difficult to be assessed by finite element analysis. In DEM, there are several methods of model generation. For the present problem which is relatively simple in geometry and layout, the desired porosity is obtained by the radius expansion method. By using numerical biaxial tests, the micro-mechanical properties of the assembled material in the numerical models are calibrated in order to match with the macroscopic response of the real material in the physical test. Numerical simulations to reproduce the stress-strain and the normal/shear stress relations (Figure 4.2) similar to that by Cheng et al. (2009) and Cheng et al. (2010) are carried out under the same conditions as the physical experiments such as porosity, boundary conditions and loading. The micro-properties of the river sand as shown in Table 4.2 are determined by varying the micro-properties until the macro-properties obtained numerically match with the experimental results (angle of repose and stress-strain relation). The diameters of the particles in the DEM model is kept to be the same as those as given in Figure 4.3. The frictional coefficient of sands is set to 1.638 (corresponding to a friction angle of 58.61° in Table 4.1). The bond strength is fixed at a value of 6N as referred to Cheng et al. (2003). The particle density of the sandy soil is 2650 kg/m^3, while the bulk density for the sand soil is 1650 kg/m^3.

Table 4-2 Microscopic Parameters of the Sands for Particle Flow Analysis

Sand	Diameter (mm)	Density of sphere (kg/m^3)	Friction coefficient	Normal & Shear stiffness (N/m^2)	Normal & Shear bond strength (N)	Friction coefficient of the wall
Tested sand	0.2~0.5	2650	1.638	1e6	4	0

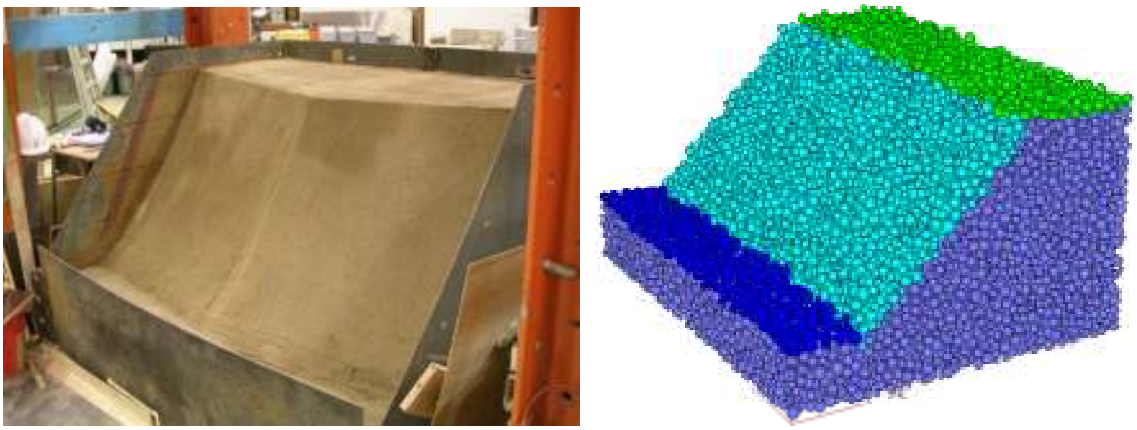

Figure 4.9 The Outlook of formed physical & numerical slope model

For the three-dimensional DEM numerical simulation as shown in Figure 4.9, the dimensions of the numerical model in the particle flow simulation are exactly the same as the physical model. A full scale distinct element analysis is seldom carried out in literature due to the great computer resources requirement, and significant amount of computer time has been used for the analysis in the present work. In this study, two different loading patterns are modeled in order to assess the results of analysis using PFC3D: (1) applying the force on the raft footing, (2) adding velocity on the loading wall, which are illustrated in Figure 4.10.

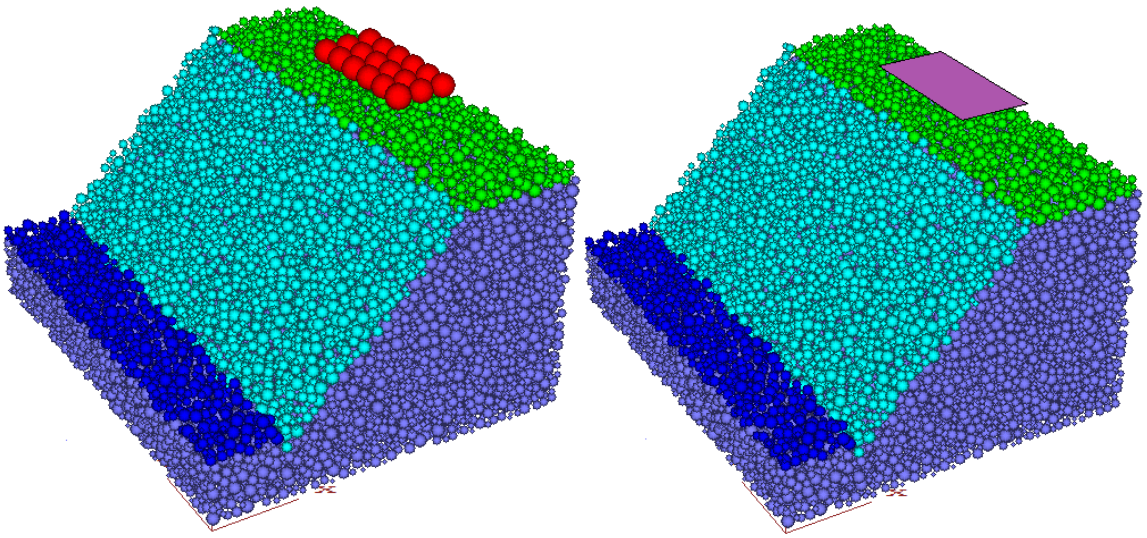

(a) (b)

Figure 4.10 Two loading patterns of simulation models: (a) applying the force on the raft footing; (b) adding velocity on the loading wall.

4.3.1 Raft footing loading pattern

In this loading pattern, the footing raft of balls is created by bonding the particle with larger contact bonds, fixing velocity constraints on the balls and modifying their stiffness and friction properties. The raft footing is added to the top of the model, and the footing load is applied in the vertical direction (x-direction) with a magnitude of 2.0 x 10^4N as shown in Figure 4.10(a). The parameters of the sands are the same as that in Table 4.2, where both normal and shear contact bond strength (n_bond, s_bond) of the particles are 6N. The failure process development under loading is illustrated in Figure 4.11 and 4.12. It is noticed that on top of the slope crest, the region below the loaded surface has deformed to form a depression zone from the DEM modeling which is also observed from the test as shown in Figure 4.11(e). Sand particles are triggered to move down the slope, dragging more and more sands

downward. The depression zone develops larger and deeper, accompanying with considerable settlement at the top of the slope, and the inclined slope face moves forward with an upheaval at the slope toe as shown from the XY direction view in Figure 4.12(d).

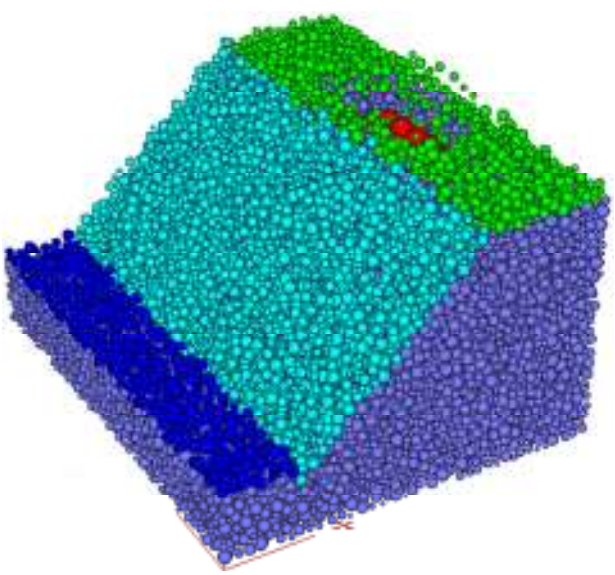

(a) 300 step

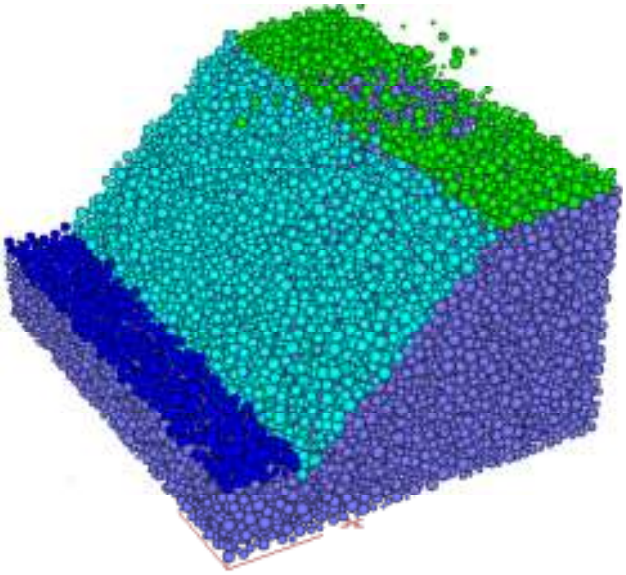

(b) 1000 step

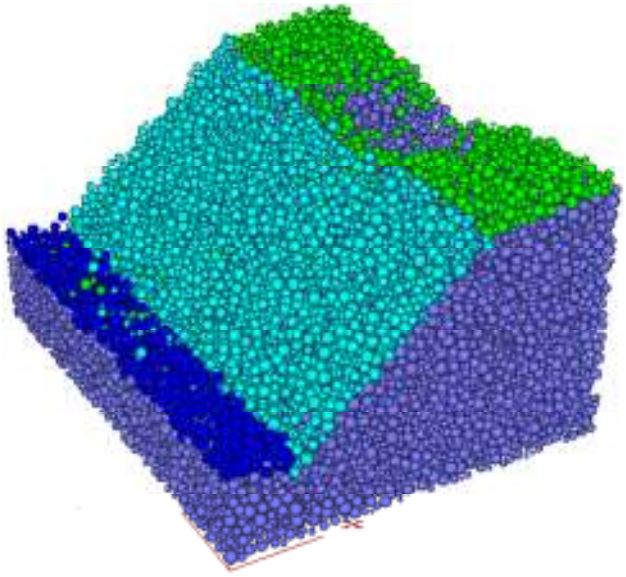

(c) 1.0 x 10^4 step

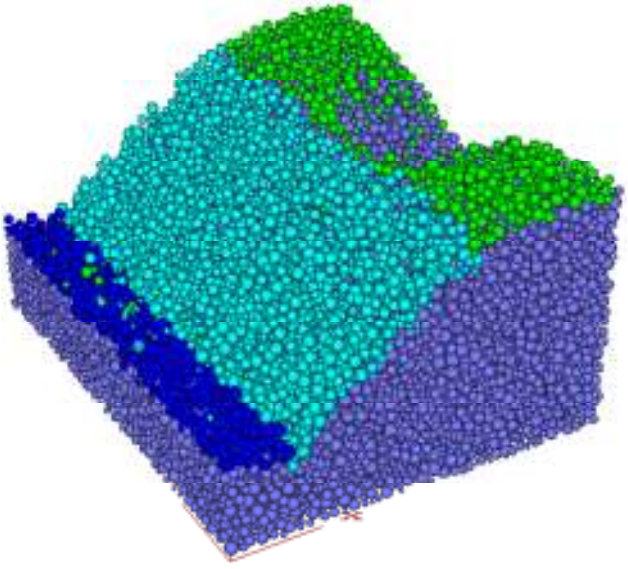

(d) 12 x 10^4 step

(e) Penetration of base plate into the soil

Figure 4.11 Failure process of numerical slope model under Loading Raft

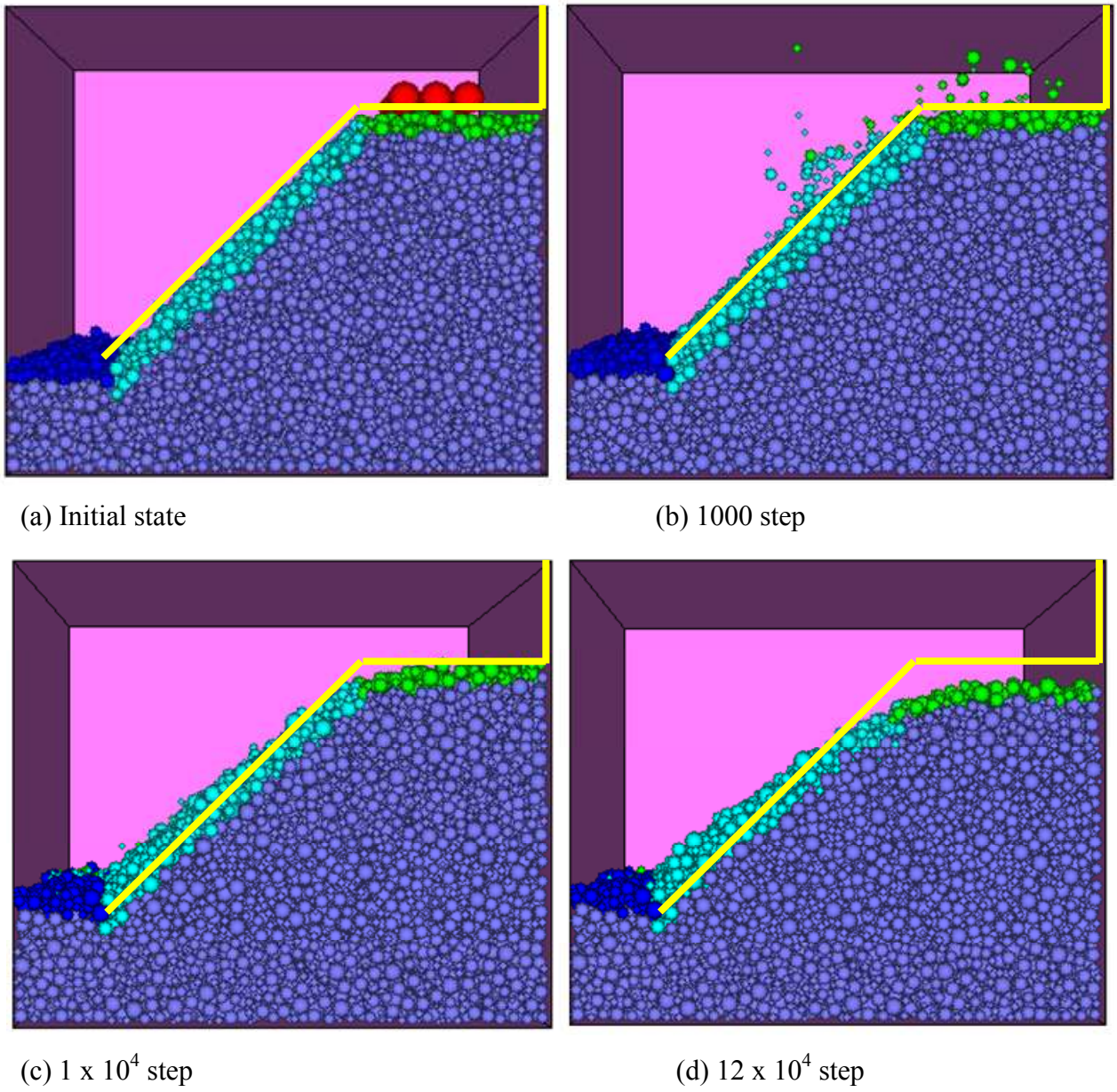

(a) Initial state (b) 1000 step

(c) 1 x 10^4 step (d) 12 x 10^4 step

Figure 4.12 Failure process of numerical model under loading raft in XY direction

Slope with soil particles under higher bond strength is also simulated, where the normal and shear contact bond strength of particles value are increased to 60N, which is ten times larger than that in the former case. The results of the comparison are shown in Figure 4.13. It is observed that noticeable collapse has taken place in Case 1 with forward movement of slope body and extruding slope toe. On the contrary, the soil movement in Case 2 is not

major and the slope is actually stable under the loading as shown in Figure 4.13(b). It is demonstrated that larger bond strength between soils is followed by slower and smaller failure, or the soil is more stable under the external load.

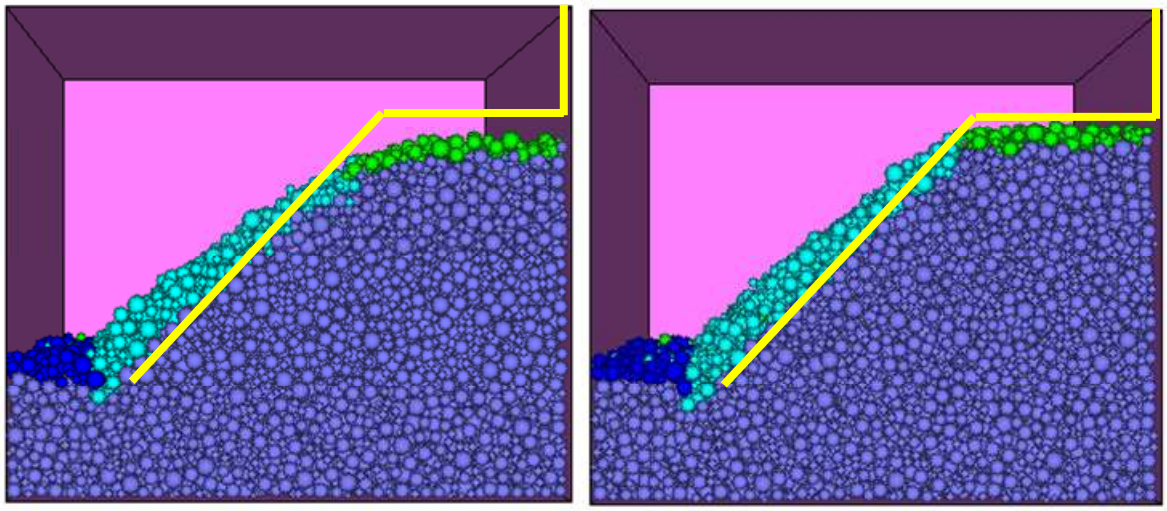

(a) Case 1: bond strength = 6N (b) Case 2: bond strength = 60N

Figure 4.13 Eventual failure of two modeling cases under loading raft in XY direction

4.3.2 Loading wall pattern

The second loading pattern is considered by applying velocity on the loading wall as shown in Figure 4.10(b). Velocity is applied on the footing wall with a value $0.5x10^{-5}$ m/step in z-direction. The force that develops along the footing as it is being pushed into the balls is monitored. The failure process of particle flow numerical slope model is shown in Figure 4.14. Slope crest experiences an obvious collapse in the middle where loading plate falls down. Sand particles on the top, as well as soils in the slope surface, run down along the inclined plane to the slope toe, which can be noticed in Figure 4.15. From the XY direction

view, the initial slope profile is illustrated by yellow line, and the top of the slope is pressed downward while the main body of the slope moves forward gradually, and the accumulation of soil occurs at the toe of slope forming an apparent upheaval which is clearly shown in Figure 4.15(4).

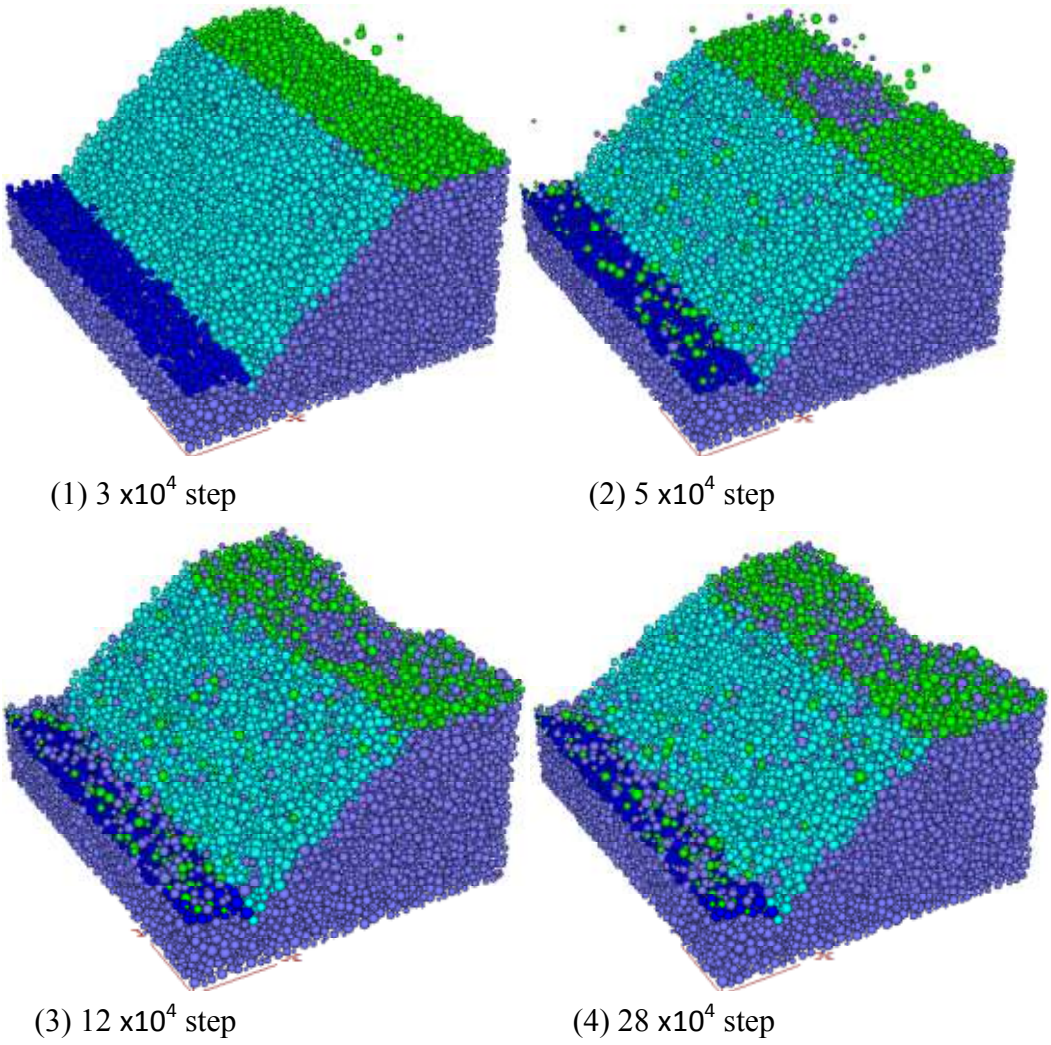

(1) 3 x10^4 step (2) 5 x10^4 step

(3) 12 x10^4 step (4) 28 x10^4 step

Figure 4.14 Failure process of numerical slope model under local loading wall

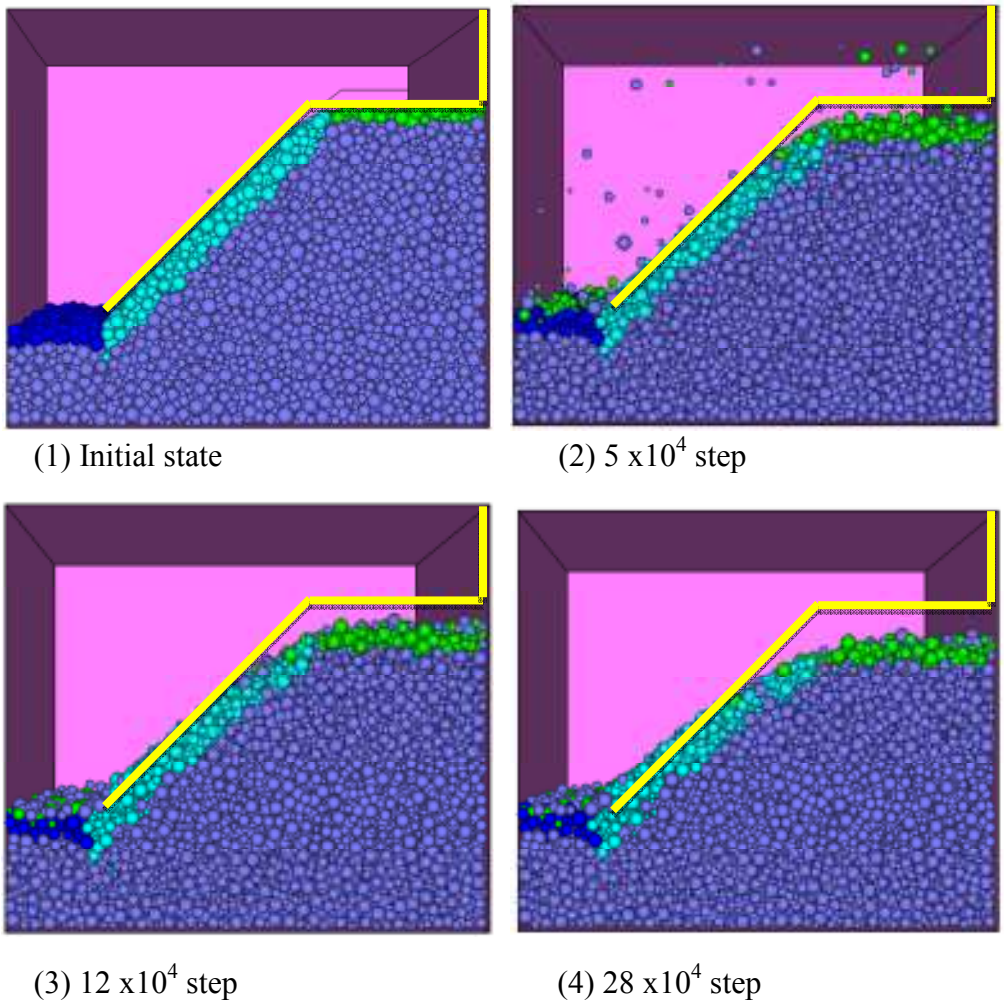

(1) Initial state (2) 5 x10^4 step

(3) 12 x10^4 step (4) 28 x10^4 step

Figure 4.15 Failure process of slope under local loading wall in XY direction

Soil particles at the left corner, right corner and middle part of the slope crest are selected to monitor the position and velocity change in z-direction (vertical direction) respectively, which are illustrated in Figures 4.16-4.19.

For the left corner of the slope crest as shown in Figures 4.16 and 4.17, the sand at the crest moved down with a high velocity at the beginning, so the displacement increased at a rapid rate within 2x10^5 time steps. Such a high initial velocity is normal even for laboratory test as the plate is not fully in contact with the soil at the beginning of the test. A small

amount of plate movement is required so that the plate is in full contact with all the soil particles at the top of the slope. The increase of the vertical displacement became smooth afterwards with several fluctuations points (typical phenomenon from DEM calculation). For the right corner of the slope crest as shown in Figure 4.18, the sand also moved down quickly at the beginning and also experienced a rapid rate within $2.1x10^5$ time steps. After that, both the displacement and velocity did not vary much in the subsequent loading process. Equilibrium is reached slightly earlier at the right corner than at the left corner. In theory, the problem is symmetric as the loading plate is located at the center. In microscopic view, there will be minor deviation from symmetric as it is virtually impossible to keep all the soil particles to be truly symmetry in the generation of the model or for actual physical model. Such minor deviation from symmetry will however become negligible as the movement of the plate increases.

For the slope crest corner as shown in Figures 4.16-4.18, it can be noticed that the particle moved down firstly at the corner of the crest where crack is generated at the very beginning of the slope failure process. With further increase in the displacement of the loading plate and when a critical failure surface is generated, an instant collapse is observed from the great fluctuation of these history records.

At the middle of the crest of the concave slope as shown in Figure 4.19, the situation is different in that a more rapid and less moderate trend can be noticed. The displacement reaches to more than 0.2m at the middle of the crest compared with a displacement of almost 0.17m at the crest corner. However, the particles at the corners move faster than those in the

middle in the beginning, which are demonstrated by the sharp increase of the settlement in Figure 4.16 and 4.18. Figure 4.19 shows that the loading at the middle the slope top has pushed the sands at the middle of the slope crest downward and accumulated at the toe of the slope.

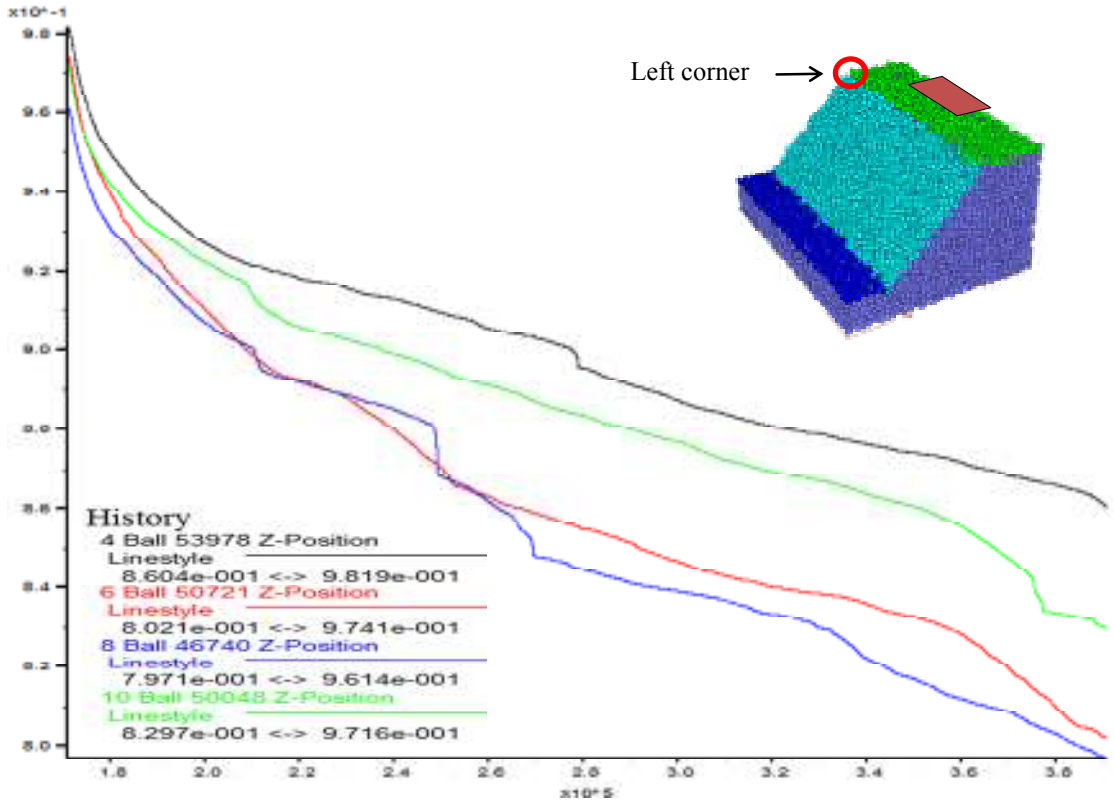

Figure 4.16 z-position history for balls in the Left corner of crest

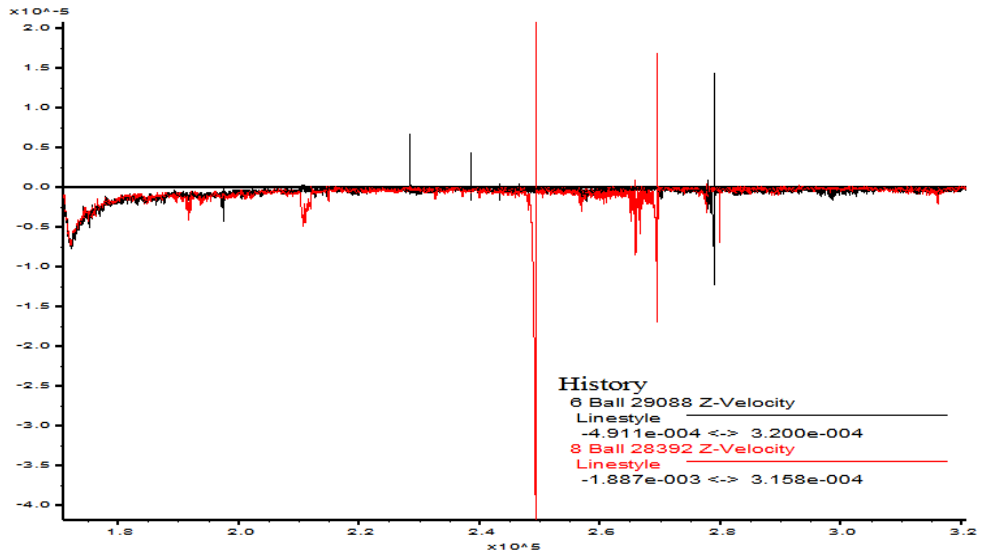

Figure 4.17 z- velocity history for balls in the left corner of crest

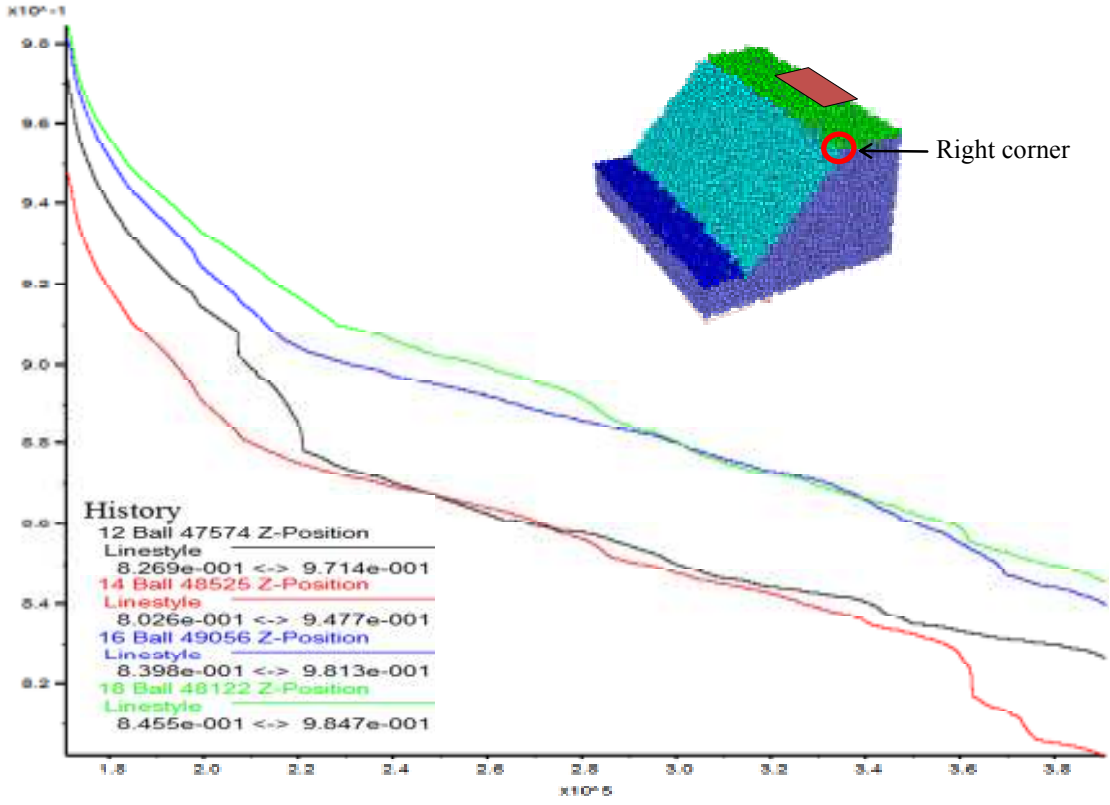

Figure 4.18 z-position history for balls in the Right corner of crest

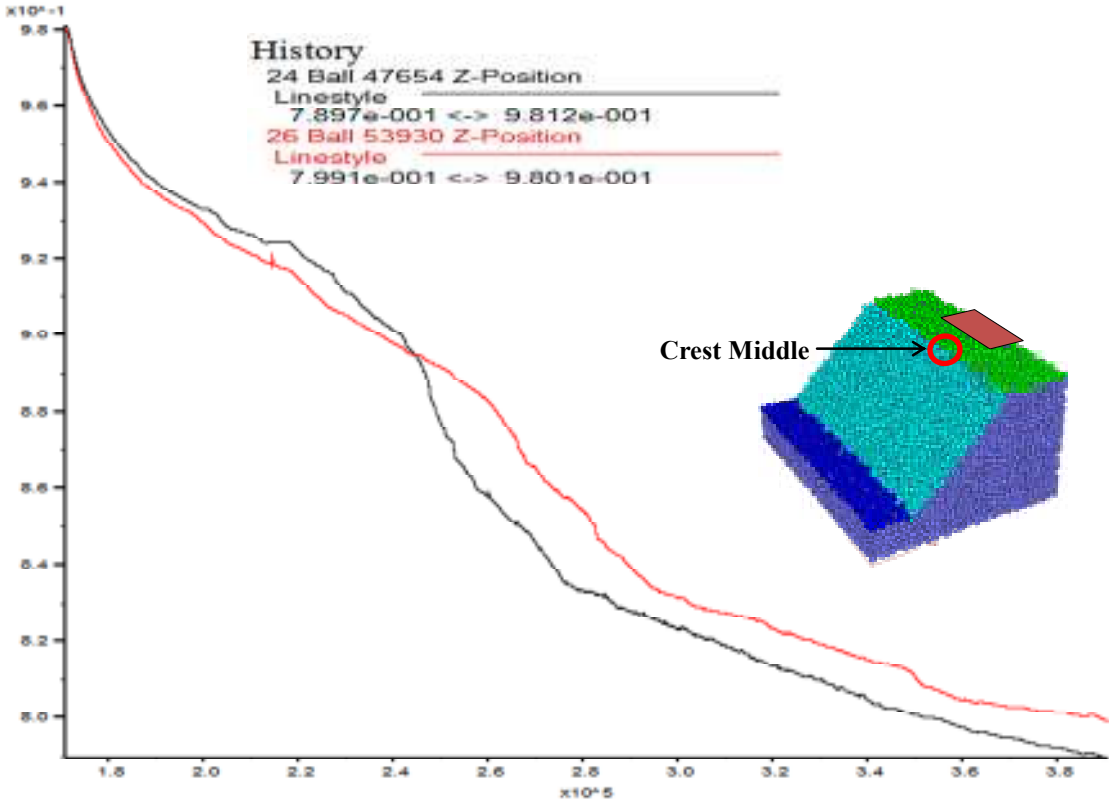

Figure 4.19 z-position history for balls in the crest middle

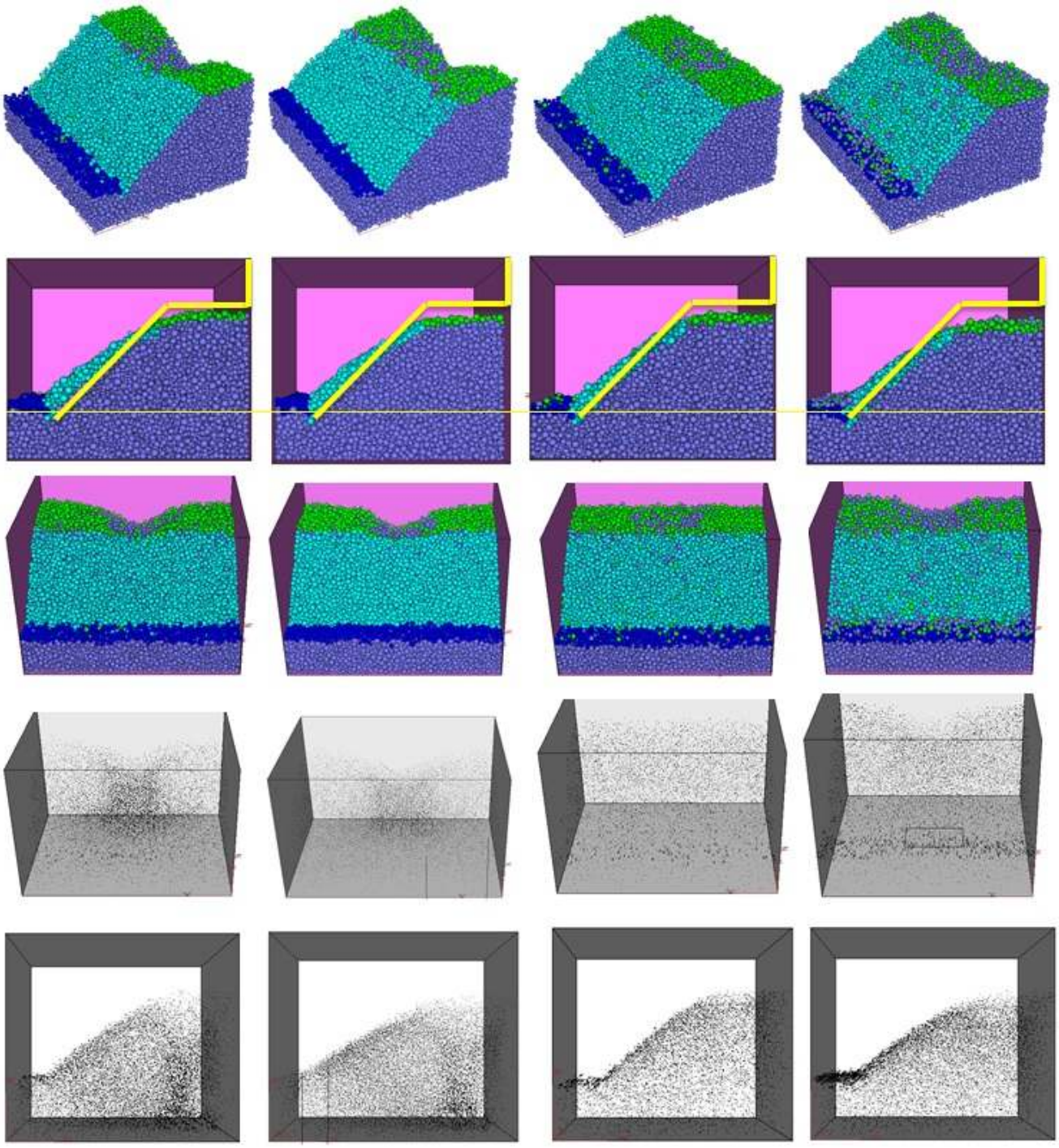

Figure 4.20 Comparison between Loading Wall and Loading Raft of final failure state

The two loading pattern cases are compared with their eventual failure profiles and displacement vector graphs in Figure 4.20. For the two loading raft cases, relevant results show that an obvious hollow zone can be seen while forward displacement of slope body and extruded upheaval at slope are noticed in Figure 4.20(a) & (b) (deeper hollow zone occurs in (b) than that of (a)). On the other hand, there are some minor differences as evaluated from the two loading cases. For loading wall with velocity $0.5x10^{-3}$ m/step, the results for final stage in Figure 4.20(c) demonstrates that the larger vertical collapse on the top occurs while there is no apparent change for slope inclined surface and toe bottom. It can be explained by the reasoning that due to the applied loading being applied within a very short time, there is no enough time for moving wall to transfer the load to the soil particles in DEM calculation. Short-time disturbance is induced in the soil mass close to the loading which is followed by direct settlement downward with an eventual failure with no evident hollow zone on the top of the slope. For loading wall with a smaller velocity $0.5x10^{-5}$ m/step, there is sufficient time for the force to propagate and the final failure profile develops more thorough than that for the former three cases accompanying with pit in top middle part of the slope and accumulation of soil at toe generated by soils mass slipping down. This completed failure reveals that sufficient time is required to spread and distribute the loading force to surrounding soil mass by applying loading wall in a relatively low speed in DEM analysis. A time-step which is large in magnitude can give unreasonable result as the force/signal has not sufficient time to spread through the whole soil mass which is different from the continuum analysis where there is not a concept of time-step. The result from the use of a small time-step also match well with that from the physical test which takes four hours to reach the

slope failure under pressure valve, which is a low-speed loading mode to trigger the progressive failure process.

4.4 Physical modeling versus three-dimensional DEM simulation

Two ways of loading patterns in three-dimensional DEM simulation are discussed and compared above, which is then compared with the physical model test. For geotechnical material such as sand soil, material stiffness is far smaller than the equipment stiffness. In the physical test, surcharge applied by hydraulic jack is controlled by velocity instead of the load. That is to say, velocity of the loading plate remains constant while the applied load is varied to maintain the applied velocity. Therefore, loading wall pattern is selected in numerical modeling corresponding to loading mode in laboratory test for comparison purpose.

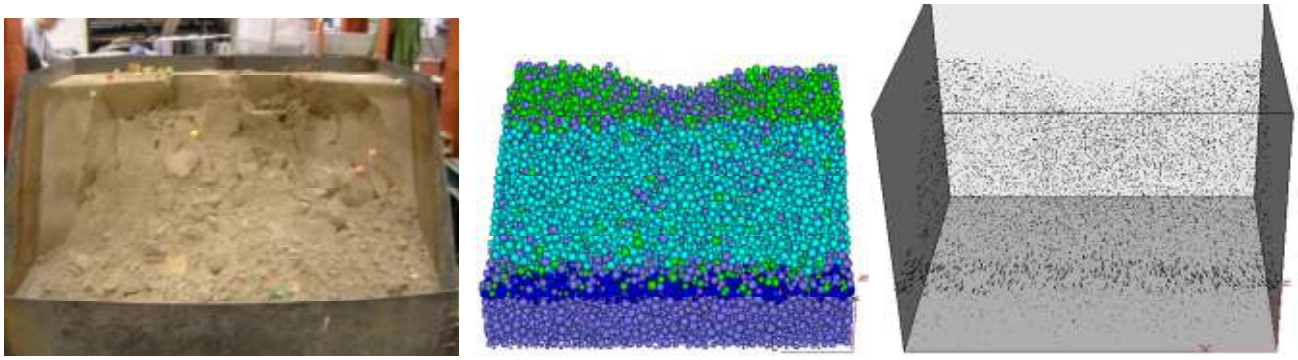

(1) Lab test - slope without soil-nail (2) DEM Case1 - bond strength = 6N (3) DEM displacement

Figure 4.21 Eventual failure of laboratory test and DEM modelling

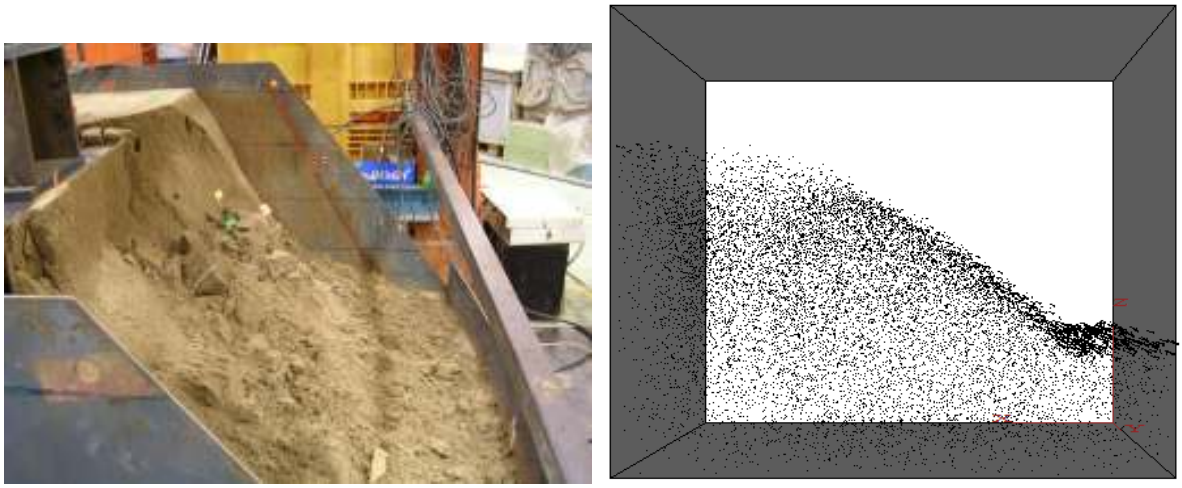

(1) Lab test of slope without soil nail (2) DEM displacement vector

Figure 4.22 Side view for the eventual failure of laboratory test displacement from DEM modelling

Figure 4.21 shows the eventual failure state of the physical test and the numerical modeling. In the beginning, crack firstly appears along each crest corner in the laboratory test which is the side effect. This result can be deduced from Figures 4.16, 4.18 and 4.21 of the z-position history in that initial gradient of displacement curves at slope crest corner is larger than that at the crest middle. In the particle flow simulation, the loading plate is applied with a small velocity of 0.5×10^{-5} m/step. There is sufficient time to deliver the applied force to the soil mass around so that in the failure process, the sand mass is driven to move downward with the largest displacement at the slope toe as shown in Figure 4.22. It takes four hours to continuously apply the loading with hydraulic jack to cause the gradual slope failure. Furthermore, there is an obvious failure zone in the middle of the slope top and the soil moved downward and accumulated at the bottom of the slope which was also observed from the physical test. Based on the observation and comparison above, it can be concluded that

DEM can give a very good qualitative description about the complete failure process which was not possible with Strength Reduction Method (SRM) or LEM.

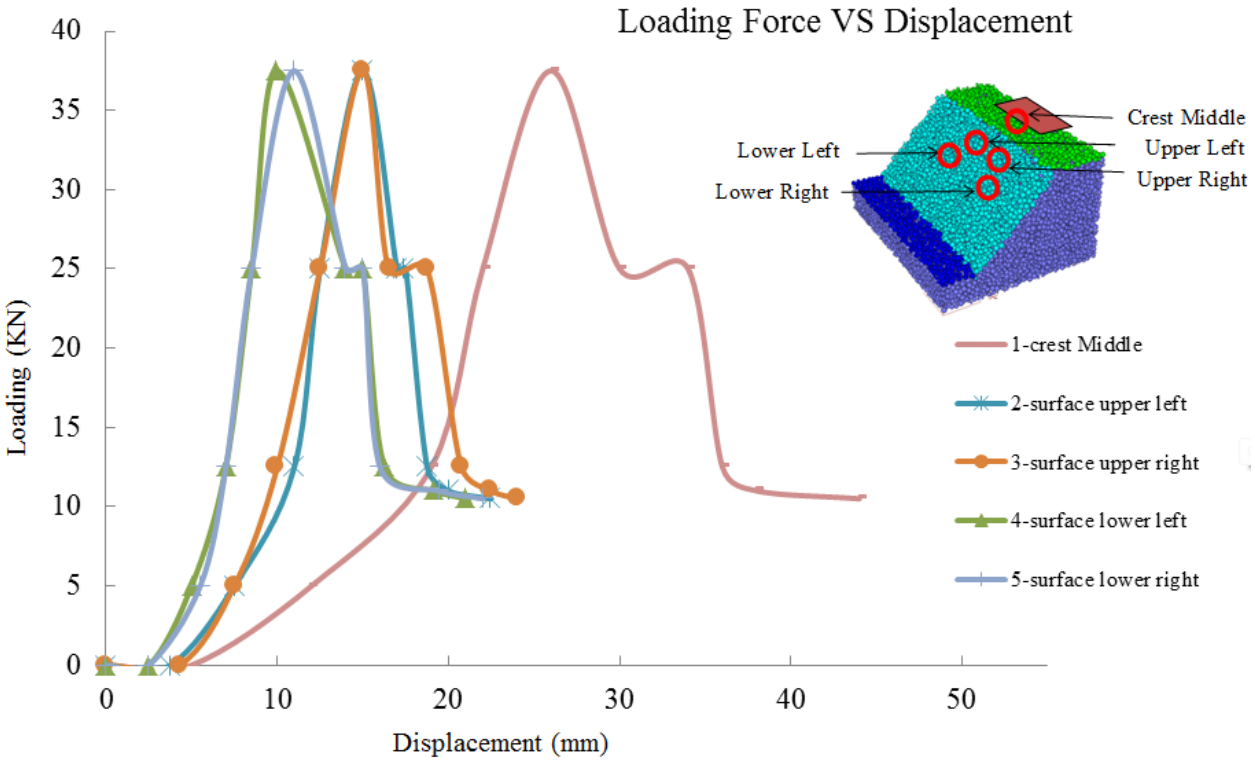

Figure 4.23 Loading force against displacement curves of the slope at different measuring points

The relation between the applied load and the displacement of the loading plate from DEM is illustrated in Figure 4.23. Three groups of curves were generated from the measuring points of lower position, upper position of slope surface and middle crest respectively. For the soils at the lower position of the slope surface, there is a rapid increase in the loading applied before the displacement has reached 10mm, which can be noticed in green and light blue curves in the figure. The applied load reaches the peak value of 37kN at about 10mm

settlement, and then the loading firstly drops to around 25kN, followed by the second drop down to around 10kN till eventual failure. For the soil at the upper position of the slope surface, the trend is similar to that of lower surface points, but the settlement largely develops to approximately 14mm under maximum loading. For the soil at the middle of the slope crest, the maximum load is achieved at larger displacement of 26mm as compared with the slope surface measuring points, and soil particles experience longer-time settlement with significant displacement value in the whole failure process.

In conclusion, the whole slope undergoes two times of free falling when bearing loading is 25kN at three-quarter of displacement as well as 10kN at the end of the test. In these two circumstances, loading force remains unchanged while displacement increases, and the reason is that the slope reaches critical point and the failure surface is generated with major stress redistribution taken place within the soil mass at that time then the slope experiences complete collapse. The settlement at the lower parts of the slope surface appears earlier than that at the crest, however, the maximum final settlement of 40mm is located at the slope middle crest which is underneath the loading plate and develops larger than the lower positions at the slope surface. In comparison with the laboratory test results as shown in Figure 4.8, the trend of three curves are basically similar, and the final failure loading of 35kN from the laboratory test was also close to the value 37kN from the DEM analysis.

For the post-failure results, the matching between the DEM model and the laboratory test is less satisfactory quantitatively. In theory, better matching may be achieved by choosing other types of contact rule or other micro-parameters, and the micro-parameters

may even be changed after the maximum load has been reached. The authors have not carried out such numerical calibration for this study, and the prediction by using some acceptable micro-parameters appear to be more important than fitting the test results by tuning of various parameters beyond failure. Even though the matching is not good quantitatively, the load displacement relation from DEM analysis and the model test are similar qualitatively. Based on the comparison as mentioned above, the results of numerical modeling are generally effective and acceptable.

4.5 Conclusion and discussion

In this chapter, a laboratory slope model test is carried out with the corresponding three-dimensional numerical simulation using discrete element method. The complete progressive failure mechanism of slope under a local surcharge is determined both from the model test and numerical analysis for comparison. Furthermore, both qualitative and quantitative studies for a full scale 3D numerical modeling have been carried out in the present study which is virtually not found in literature.

For the physical modeling of soil slope under locally external surcharge, the main observations from the failure process are as follows. The first crack was found at the surrounding of the loading plate, and it extended towards each boundary with an angle of approximately 45°. After four-hour hydraulic loading, the sands at the middle top of the slope is pressed to form a big hollow zone, while the largest cracks are generated at the critical failure surface within the slope body. Then the soil mass contained within the critical failure

surface is pushed down with a complete failure. The failure process from the physical slope model is gradually and eventually generated. The failure surface after removal of the failed mass is found to fit nicely with the classical general shear failure mechanism as discussed by Cheng and Au (2005d).

For the three-dimensional analysis of the particle flow model under local loading, loading wall pattern is used to simulate the loading applied by hydraulic jack by applying a velocity to the model loading plate. The failure process of particle flow slope model is generally similar to that of the physical model in most respects. It is observed that an obvious collapse is noticed at the middle of slope crest where the loading plate falls down gradually forming a depression zone at the top. At the same time, sands at the two crest corners fall with a high velocity at the beginning and slow down to achieve equilibrium at the later stage. The failed soil mass moves down and accumulate at the slope toe. Many surface cracks directing towards the loading plate are found during the loading process. Finally, a critical failure surface basically conforming to the classical theory has formed followed by a major collapse of the soil mass.

In comparing the physical modeling and numerical simulation, deformation at the center of loading plate develops greater than the lower parts of the slope surface in laboratory test, while the underneath settlement happens earlier than the middle both in the laboratory test and numerical simulation. The relations between the force against displacement curves are basically similar between the physical model test and the numerical model, and the final failure loadings are also very close which is not accomplished in other previous studies. Although there are some discrepancy between the load-displacement results for the DEM

analysis and laboratory test after the initiation of failure, DEM can still produce a reasonable qualitative assessment of the post-failure response of the slope for the considerations of the engineers. These results have useful contributions to the better understanding about the complete slope failure mechanism and the effect and spread of the slope failure which is not possible for other classical methods.

CHAPTER 5 ANALYSIS OF THE INFLUENCE OF CURVATURE ON SLOPE STABILITY BY THREE-DIMENSIONAL DISTINCT ELEMENT METHOD

5.1 Introduction

All slope failures are three-dimensional (3D) in nature, but two dimensional (2D) modeling is usually adopted as this greatly simplifies the analysis. 2D analysis is also sufficient for many engineering design works, and a slightly smaller factor of safety is also beneficial for routine analysis and design works. There are however also cases where the geometry is highly complicated and the use of 3D analysis is required for a proper analysis. Most of the 3D LEM methods including those by Hovland (1977), Chen and Chameau (1983), Zhang (1988), Ugai (1988), Lam and Fredlund (1993), Chang (2002), Chen et al. (2003a) adopt the assumption of symmetrical slip surface with a zero sliding direction. Such methods are basically the extension of 2D methods, where the interslice force relationship is extended to intercolumn force assumptions and corresponding equilibrium equations are considered in 3D framework. Cheng and Yip (2007) developed a truly asymmetric model prescribing only one sliding direction for the whole failure mass, and the sliding direction can be determined by the equilibrium condition without any arbitrary assumption. 3D NURBS surface and the simulated annealing method proposed by Cheng et al. (2005) are incorporated to locate the 3D critical slip surface, and the convergence problem under transverse load in the Huang and Tsai formulation (2000) has been overcome by the new formulation.

On the other hand, 3D analysis by SRM is robust provided computer time and the amount of time to prepare the computer model can be tolerated. A large number of researchers have considered complex slope conditions to investigate the 3D slope stability. Ugai and Leshchinsky (1995) included a pseudo-static seismic force component in their 3D SRM analysis for vertical cuts. Zheng et al. (2005) used program ANSYS and conducted an extensive SRM analysis in slope, tunnel, and ultimate bearing capacity of foundations. Griffiths and Marquez (2007) considered both vertical and inclined boundaries to investigate the constraint effect of slopes with finite length in several 3D slope examples by SRM. Deng et al. (2007) also conducted 3D SRM to analyze stability of a pre-existing landslide with multiple sliding directions.

Many highway slopes, due to route selection based on existing geometry, geology, neighbor constructions and other necessary considerations, are commonly curved in geometry. For many highway slopes where there are curvatures, the use of simplified 2D analysis can be far from realistic, and the use of three-dimensional slope stability analysis becomes necessary as this will increase the accuracy in the analysis. Among the 3D analysis methods, few research works can be found on the curvature effect of curvilinear slope. Rassam and Williams (1999) conducted a survey on the curvature effect on fill slope stability with concave and convex faces were considered by using SRM in FLAC2D. At present, there are only limited works devoted to the effect of curvature on the factor of safety using LEM and SRM. Practically, there is no previous studies about the post-failure conditions and progressive failure mode of 3D slope with curvature with DEM analysis.

It is well known that curvature has a distinct influence on the stability of the slopes. Moreover, to the author's knowledge, there is no previous application of DEM to the study of the influence of curvature on slope stability at present. This chapter investigates the curvature influence on the stability and failure mode of concave slopes by three-dimensional Distinct Element Method employing PFC3D. The special effects of the concavity and the progressive failure process have been studied for simple and local loaded slope with curvature in this chapter.

5.2 Curvature influence on slope stability in three-dimensional analysis

An axisymmetric model is generated for the analysis of a homogeneous concave slopes as shown in Figure 5.1. The radius of curvature of the concave slope is given by R_0/H_0 equals 0.857, where R_0 and H_0 are the radius of curvature and height of slope respectively. The slope angle in the numerical model is 45° with c'=0.5kPa and ϕ'=26.5°. Wall to ball friction in the five faces of boundary in PFC3D model is set to 0.5, which coincides with the soil friction as ball to ball friction in particle flow code. The model is simplified into cube in this numerical analysis so as to reduce the tremendous computer time required for analysis, however, in practical condition, the concave slope section is surrounded by continuous soil mass. That is to say, the boundary wall in numerical modeling is used as other soil particles around in reality. So the boundary condition is the crucial factor in a realistic analysis of the problem. Then the in-situ state of stress in the ground before any excavation or construction is generated by setting the initial conditions which is controlled by gravity in a particle flow

model. The in-situ stress state is also an important factor because it will influence the subsequent behavior of the model. Initial stresses, however, are not prescribed directly in PFC3D. The initial stress state must be derived from the initial conditions specified for the compaction of the ball assembly, and it is generated from the gravitational loading in particle flow analysis. Based on the procedures as mentioned above, the initial state of a cut concave slope is generated in Figure 5.1.

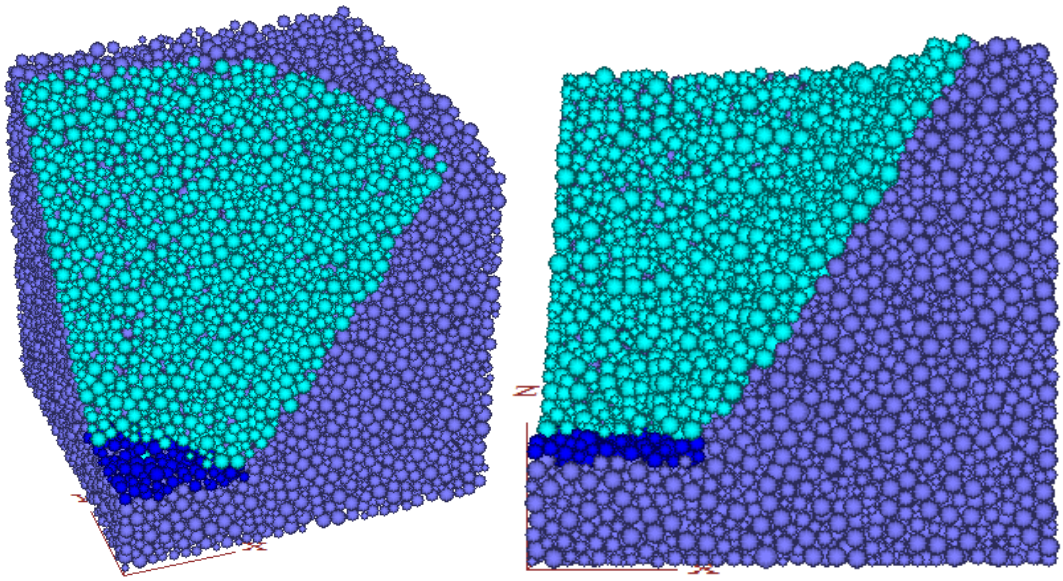

Figure 5.1 Initial state of a cut concave slope

The failure process of a concave slope with small cohesion under gravity is analyzed in Figure 5.2. In the beginning, the soils at the two corner side start to collapse while the soil at the middle of the slope crest remains basically stationary. With increasing settlement at the two corners, the soil in the middle part is dragged down gradually as shown in Figure 5.2(b). The failure started from partial sliding to global sliding, and in the end the whole slope crest crumbles as illustrated in Figure 5.2(d). From the above investigations on simple slope, the 3D curvature effect is basically symmetric about rotation axis with an axi-symmetrical shear

failure throughout the corner side of the slope, and a distinct 3D failure surface can be noticed from the displacement graph in Figure 5.8(d).

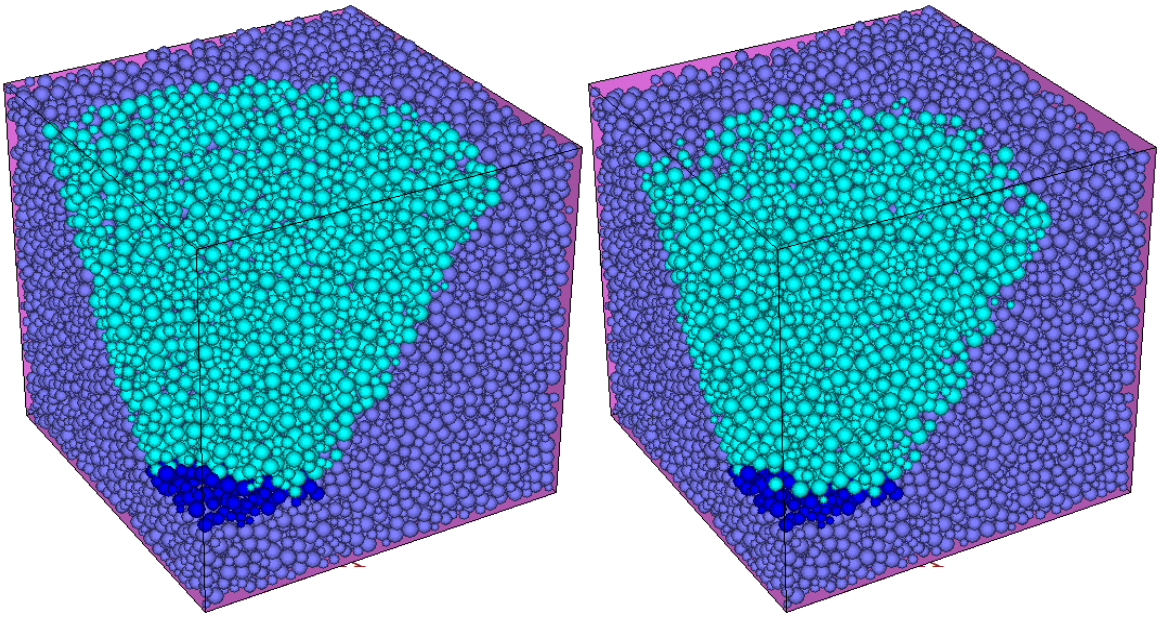

(a) After 1000 step (b) After 3000 step

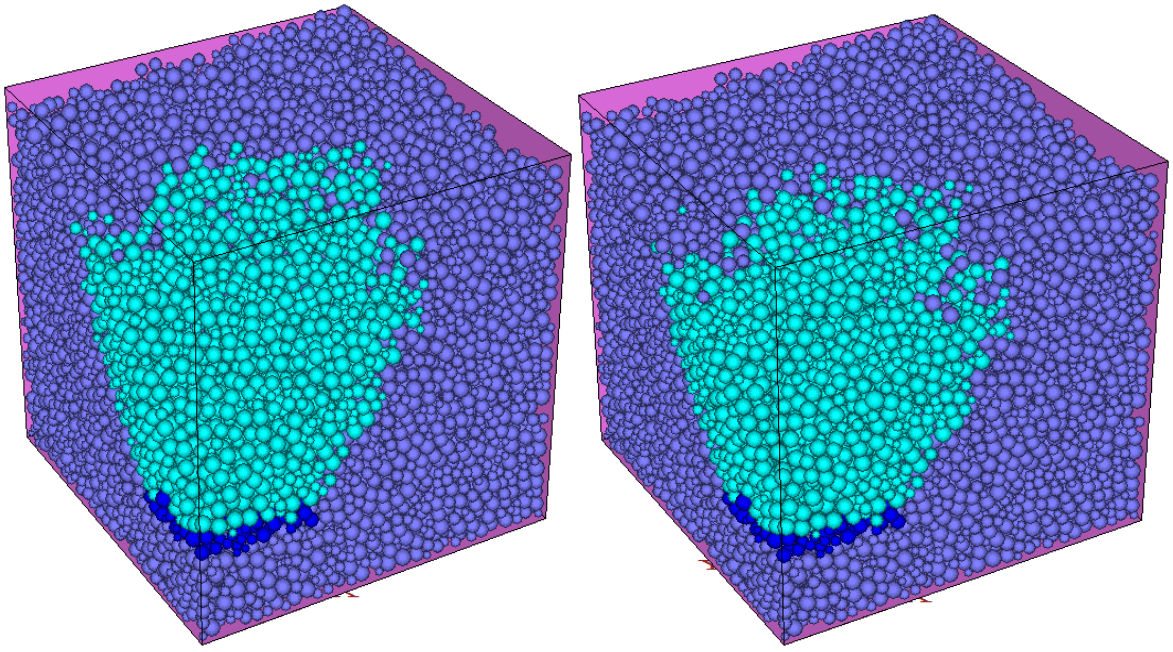

(c) After 1 x10^4 step (d) After 11 x10^4 step

Figure 5.2 Failure process of concave slope with lower cohesion under gravity

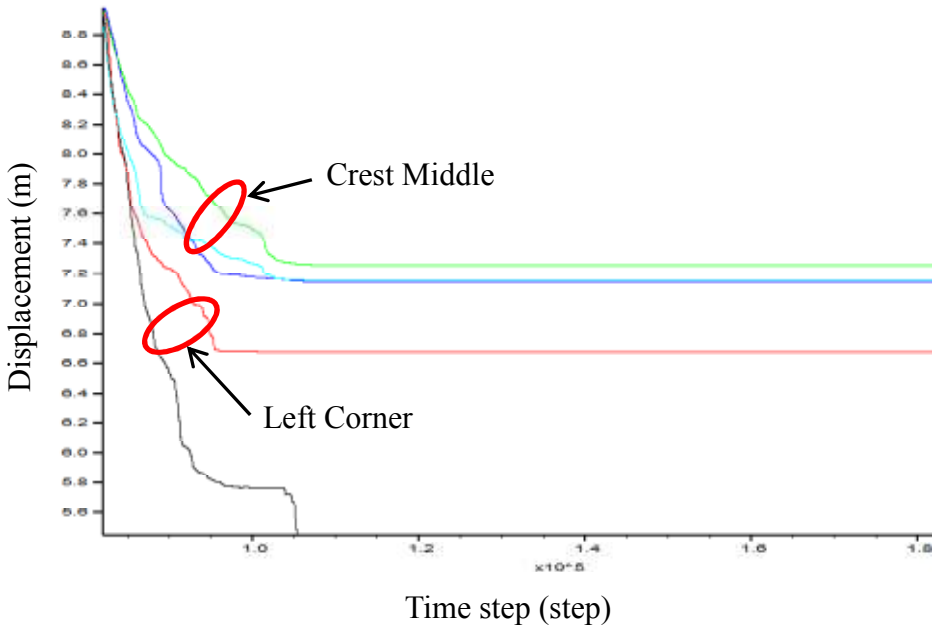

Figure 5.3 Settlements for balls in the Crest Left Corner VS Crest Middle of concave slope under gravity

In this slope failure with small cohesion, the soil particles at left corner move faster so that the curves for the balls at the left corner has steeper gradient than other curves for the particle at crest middle, which can be noticed in Figure 5.3. The soil mass at the two corners experience a deeper falling, due to the influence of the arching effect that brings thrust forces to restrain cracking on middle part of slope crest. Also the impact of side effect is dragging the corner balls away as well as downward.

5.3 Stability analysis of slope with curvature under local surcharge

If a local surcharge is applied on the top of a curvilinear slope, the symmetry of failure

will be disturbed and local failure instead of a global failure will take place. In Figure 5.4, a concave slope with a local loading from a raft footing is illustrated. The slope angle is also 45° with c'=3kPa and ϕ'=26.5°, and it has been tested to remain stable under gravity loading with the given soil parameters, so the failure is mainly induced by the application of the local load. A force of 1.0×10^5N is applied on the 2m×2m square footing at the top and 1m away from the crest of the slope. The red balls are connected by parallel bonds of high strength and high stiffness, and behave as a rigid footing. An external loading force is imposed to each ball comprising the raft in the negative z-direction vertically. The raft is constrained from movement in the x- and y-directions horizontally by initializing velocities to zero and fixing the x- and y-displacement.

The failure mode of this concave slope is shown in Figure 5.5. The footing presses on the soil mass and a cave is formed at the loaded area at the affecting area after 1000 time-step of loading. In DEM modeling, force is applied through contact propagation, and this is different from the physical modeling in the laboratory which is a displacement controlled test. Under force controlled analysis, massive displacement happens at the influenced area after a short time of load application, which can be seen as instantaneous disturbance in Figure 5.5(b), while other parts remain unchanged due to slow propagation of external loading through contact mode between discrete elements in particle flow code. Because of this hysteresis phenomenon, the failure process between physical model tests and DEM numerical model test is different in some ways, which are mentioned in section 3 of Chapter 4 above.

After an obvious hollow zone is generated partially in affecting area, soils at the two side corners remain stable due to high cohesive strength of slope, which is shown in Figure 5.5(c). The particles bond tightly, so that no obvious displacement occurs at the corner areas. Disturbance to the soil around the central axis in middle is evoked extremely, which can be noticed in Figure 5.6 that the average velocity curve in red representing the middle part of the crest has tremendous fluctuation compared with slight movement at the corner side. Finally, it can be seen from Figure 5.5(d) that the failure turns to be very local around the loaded area as anticipated. Since only local failure has occurred, there is no obvious shear failure through the toe.

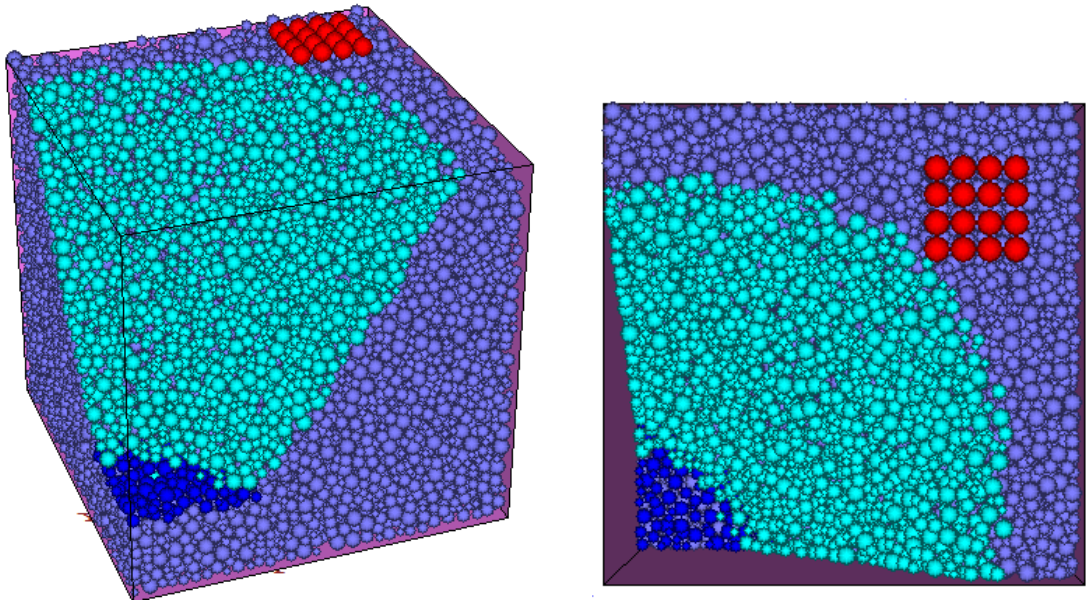

(1) Basic view of slope model in initial state (2) Top view of slope model in X-Y direction

Figure 5.4 Model of concave slope with local loading impacted by Raft Footing

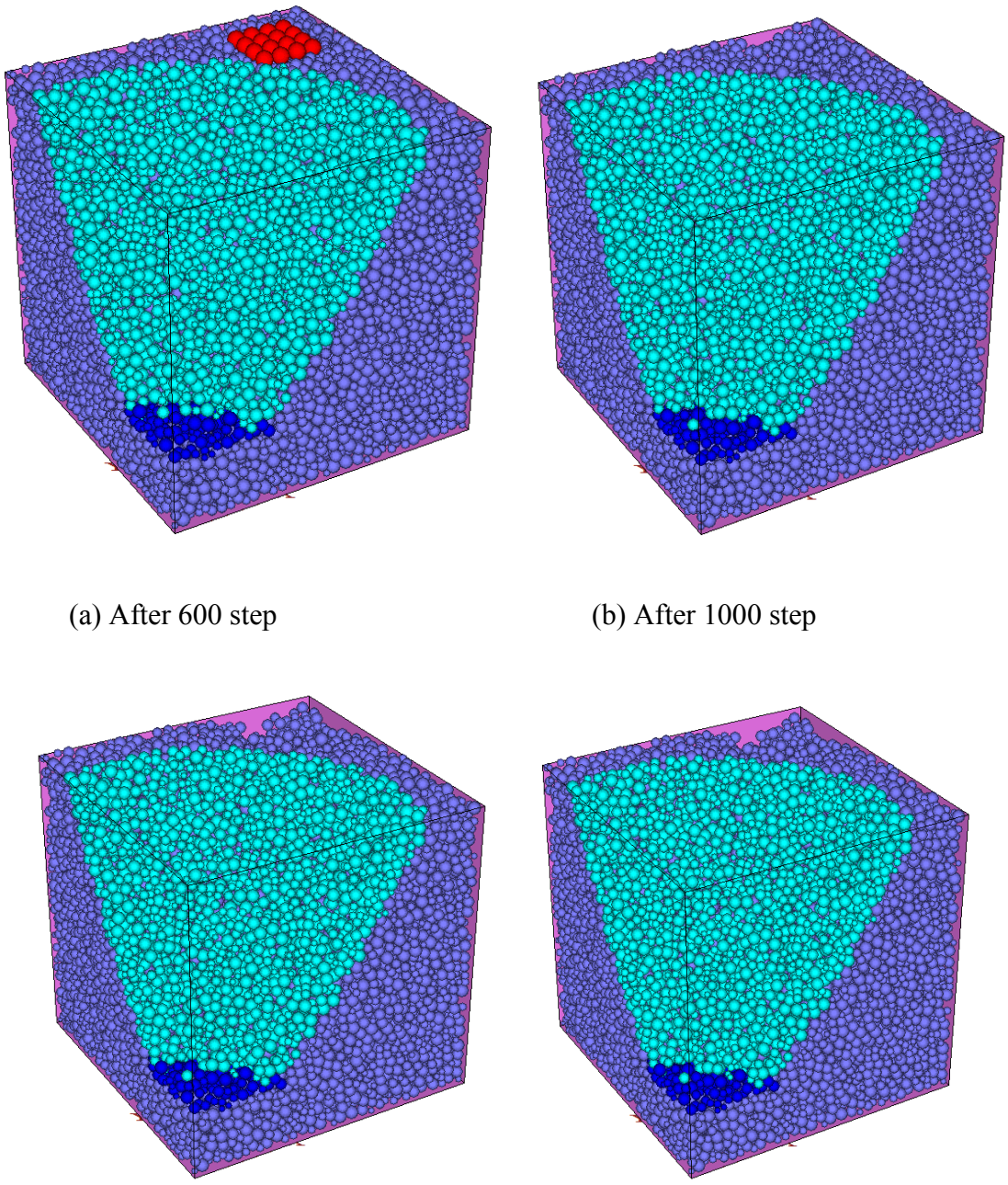

(a) After 600 step (b) After 1000 step

(c) After 6000 step (d) After 11 x10^4 step

Figure 5.5 Failure process of concave slope with local loading

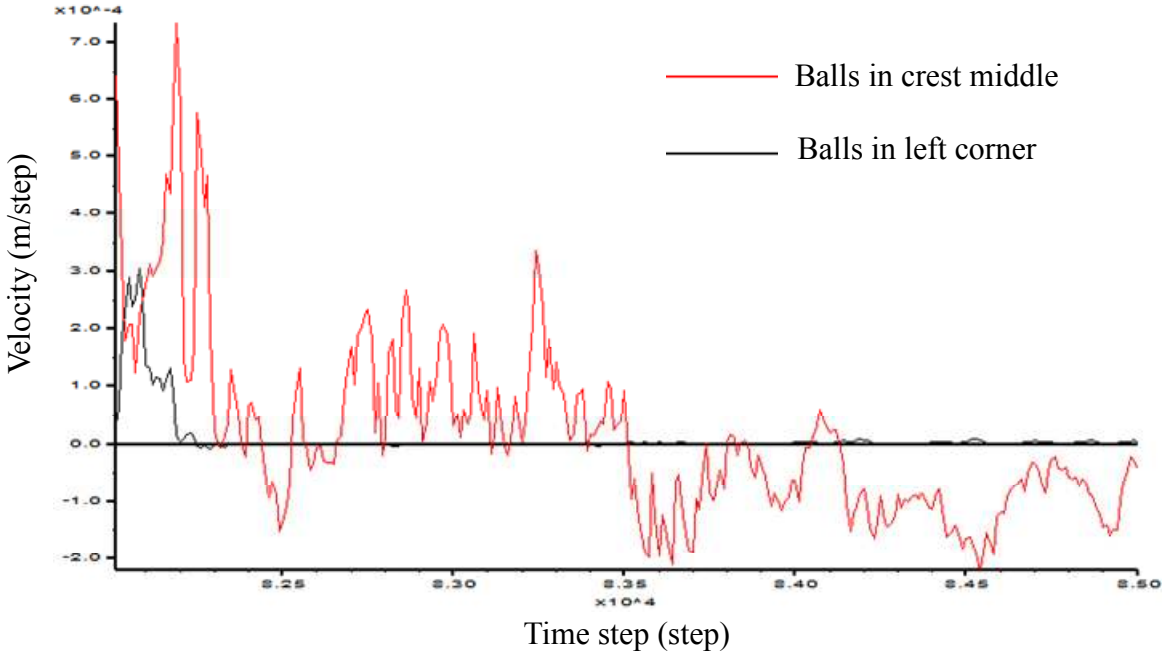

Figure 5.6 Average velocity history for balls at the left corner and middle part of crest

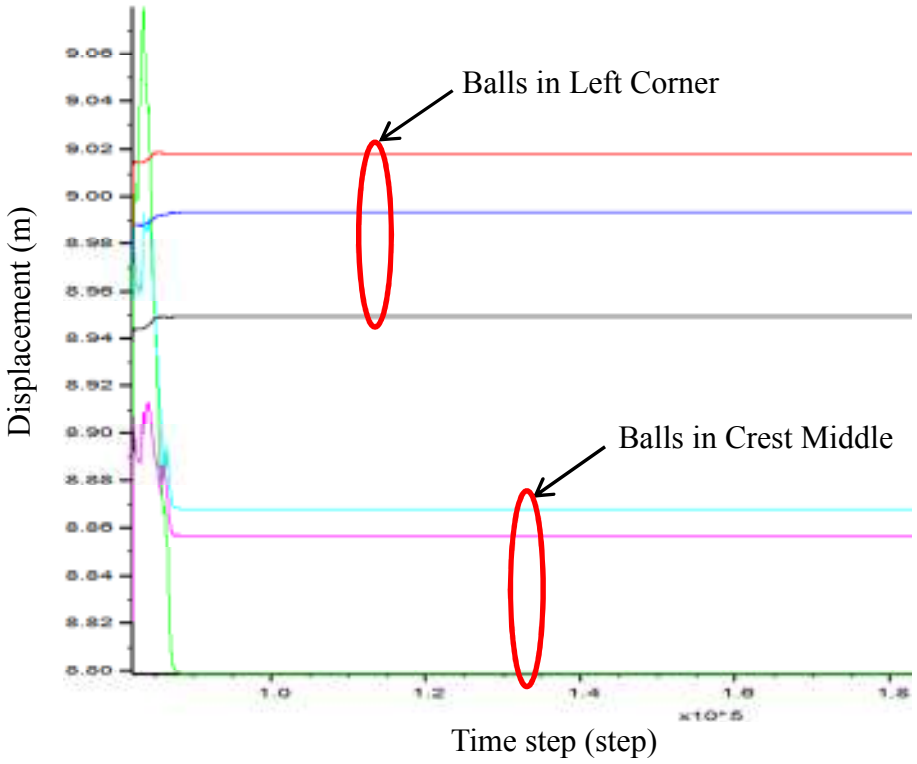

Figure 5.7 Displacement for balls in the Crest Left Corner VS Crest Middle of concave slope under local loading

With the external loading applied, the soil particles at the crest middle experience a vertical displacement of about 0.2m in 6000 time-step where this instant model is illustrated in Figure 5.5(c). Soil mass at corner side of the slope experiences slight upheaval at the same time when the top of the slope is compressed in middle, which can be seen as unchangeable. So distinct difference of two curves is noticed in Figure 5.7. After that, due to the large cohesion strength, soil mass is bonded tightly together as a whole, and slope reaches to equilibrium for the following time.

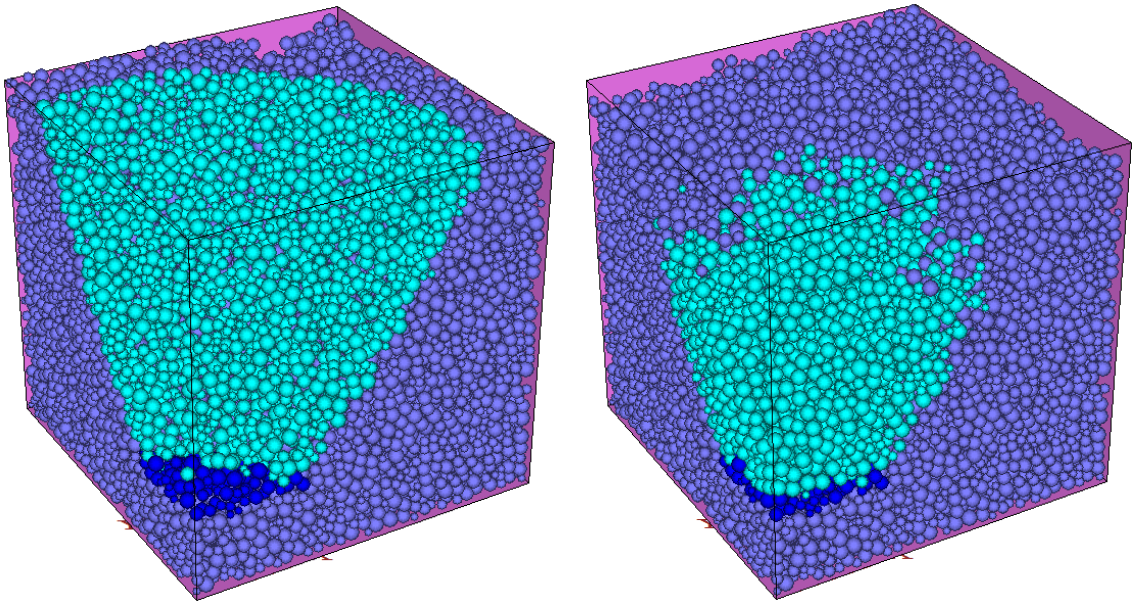

(a) Eventual failure of Raft Loading slope (b) Eventual failure of slope under gravity

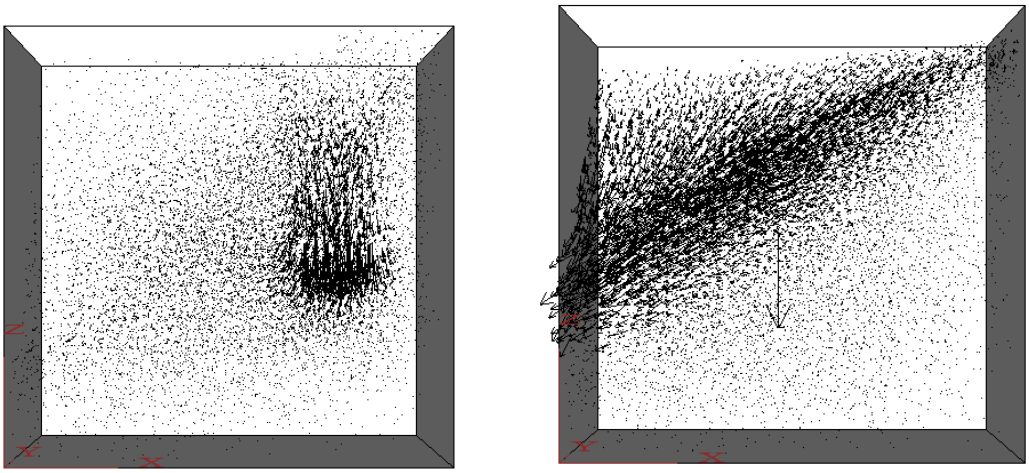

(c) Displacement vector of Raft loading slope (d) Displacement vector of slope under gravity

Figure 5.8 Comparison of concave slope with high and low cohesion strength

Two basic cases of concave slope is analyzed respectively above, which are slope under gravity with low cohesion strength and slope under raft loading with high bond strength. Comparison of these two cases is made while the eventual failure states and the displacement vectors relations are illustrated in Figure 5.8. From the discussion as mentioned in previous section, the side effect induces the soil particles at the corners of the slope crest move forward faster than the particles at the middle of the crest, while the soil from the corners accumulate at the bottom of slope toe with larger displacement than the soil at the middle as shown in Figure 5.8(b) which is the final failure state of the slope under gravity with low cohesion strength, and this result also proves the influence of the arching effect due to the curvature effect. An apparent shear failure surface can be figured out from the displacement vectors results in Figure 5.8(d). Meanwhile, an obvious disturbance is imposed by the loading plate for the second case, which is followed by a local collapse for the raft loading slope. There is

however no sign of global failure which is noticed in Figure 5.8(c) because of the high cohesion strength for the raft loading slope.

For concave slope, due to the influence of the arching effect, only partial/localized failure happens in concave slope under local loading as noticed from Figures 5.5 and 5.7 above. Thrust forces are generated by the soil particles at the two sides, which is the resistance to the slope failure at the middle part. However, different phenomenon occurs in normal plane slope under local loading (with no arching effect) which experiences larger collapse at the middle compared with that at the two sides. An obvious hollow zone appears at the loaded area, and the soil mass near to the disturbance area where the raft footing goes by as well as that in the inclined surface are all driven down and move forward in plane slope, and global collapse is initiated eventually. In the case of plane slope under local loading analyzed previously in Chapter 4, soil mass compressed by the loading plate experiences a large settlement of 2m at the middle part of the slope, compared with 1.6m of particle settlement at the left corner as shown in Figure 5.9. This results of settlement are highly different from those in Figure 5.7, but the settlements at crest middle are larger than those at the edges for plane and concave slope. Thus, more attention should be paid to reinforce the area near to the footing in both plane and concave cutting slope.

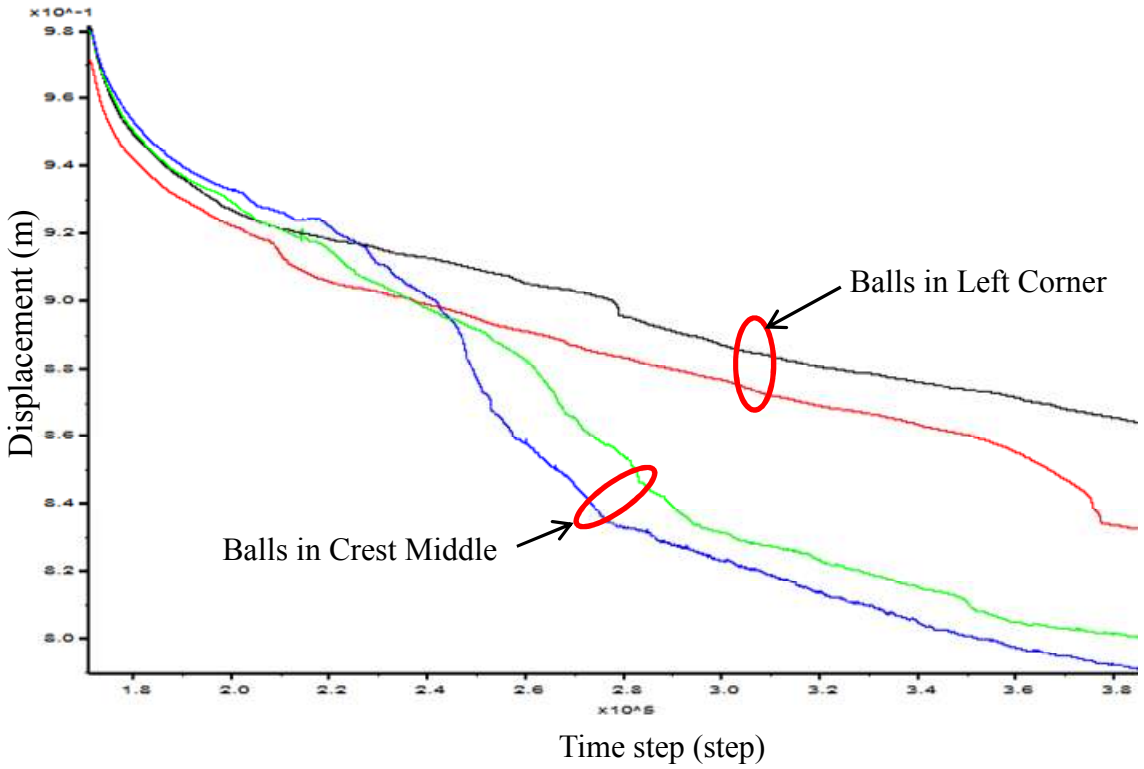

Figure 5.9 Settlement curves of soil in Flat Slope between Left corner and Middle crest

5.4 Conclusion and discussion

In this chapter, the effect of curvature with or without localized loading on slope stability is studied with discrete element method which is a pioneer work without any previous study. It is clearly demonstrated that curvature has a beneficial effect on the global stability of concave slopes, especially when the bonding strength of the soil is relatively high so that a higher arching effect can be developed. This well-known fact is clearly illustrated by the use of DEM in this chapter.

For three-dimensional curvature influence on slope stability with or without localized loading, the study has shown that the curvature specified by R_0/H_0 is a beneficial effect on the

global stability of concave slopes, especially when the resistance of soil is relatively high. Arching effect is illustrated clearly for concave slope. As a result, only partial/localized failure is initiated in concave slope under local loading. While collapse at the two corners of concave slope under gravity develops more obviously in final failure, the eventual settlement of crest middle is smaller than that of crest corner. Such result however may not be totally correct, as only limited domain is specified to generated the model and should not be taken as the true phenomenon. The failure mechanism is not greatly affected by the end effect, and the conclusion on the failure mechanism should be the true phenomenon which is also an obvious result.

From the results of analysis, it can be concluded that more attention should be paid to reinforce the area near to the footing for concave cutting slope. Also, the concave slope with high soil properties with radial oriented nails (if necessary) is a good option for the support selection.

CHAPTER 6 SUMMARY, CONCLUSIONS AND SUGGESTIONS FOR FUTURE WORK

6.1 Summary of main work and contributions

The present study is devoted to study of the failure mechanism and post-failure soil movement and stress changes of slope under the action of self-weight, soil nail, rainfall induced water flow, local loading and also curvature effect on curvilinear three-dimensional slope. Both two-dimensional and three-dimensional numerical simulations are carried out together with physical laboratory tests. Many important and new results are obtained, and these results are both innovative and new and have useful contributions to the better understanding about the complete slope failure mechanism. The summary is grouped under four main areas as below.

(1) Large displacement simulation of slope failure by two-dimensional distinct element method is carried out firstly. The failure mechanism of simple slope and soil-nail reinforced slope are analyzed in Chapter 3. The main observations from the two-dimensional DEM simulation are:

- For a slope with cohesionless soil, failure firstly occurs at the crest of the slope, and gradually extends to the base of the slope until finally the slope angle is equal to the friction angle of the soil.
- The overall particles flow reveals that the downward movement of the particles at the crest induces tensile failure, and tension crack may also be found at the crest of the slope.

The deposition of the particles at the toe causes the failure in forms of sliding out and upheaval; and the middle of the slope actually turns into a shear failure zone due to the continuous sliding of soil.

- For a slope with cohesive soil, if the cohesive strength is relatively high, the instability can be reduced and the displacement is limited.
- Soil nails can effectively reinforce the slope stability, especially when nail head is used, and the overall stability is greatly enhanced. Failure for soil nailed slope is hence generally comprised of the tensile failure at the crest and the shear failure at the base.

(2) The effect of water flow in slope stability problem by DEM is considered also in Chapter 3, which is more complicated in nature and is seldom studied before. The author has devised the method of inclined body forces to simulate such effect which is another innovative work from the present study. Four influencing factors are taken into account in this part for the study of the failure mode influenced by rainfall induced water flow: buoyant effect of ground water, seepage effect, strength reduction during slope failure and persistent rainfall effect. Also, different seepage flow patterns are tried and illustrated. The main observations from the simulation results are:

- The slope crest is scoured smoothly under continuous effect of rainfall induced water flow. More obvious settlements at the top, extended failure zone and noticeable upheaval at the toe are developed compared with normal failure.

- Rainfall induced water flow not only accelerates slope failure and results an obvious decrease in the stability of the slope, but also causes further thorough collapse at the end.

Based on the above study on the failure mechanism of slope under several conditions by two-dimensional distinct element method, contributions are summarized as follows:

- The analysis in this section successfully simulates the whole flow process of simple slope failure, which is one contribution in this study.
- The stabilization of the stress changes by the action of soil nail even when soil movement has been mobilized is a new finding which cannot be assessed by classical finite element or limit equilibrium analysis.
- This comprehensive analysis reveals the failure patterns of simple slope under the effect of self-weight, reinforced action of soil nails, buoyant force and seepage of water flow, which is seldom considered in the previous research and can be viewed as new work in slope stability using distinct element method.

(3) A laboratory slope model test is carried out with the corresponding three-dimensional numerical simulation using discrete element method in Chapter 4. The complete progressive failure mechanism of slope under a local surcharge is determined both from the model test and numerical analysis for comparison. Furthermore, both qualitative and quantitative studies for a full scale 3D numerical modeling have been carried out in the present study which is virtually not found in literature.

For physical modeling of soil slope under locally external surcharge, the main observations from the failure process are:

- The first crack was found at the surrounding of the loading plate, and it extended towards each boundary with an angle of approximately 45°.
- The sand at the top middle of the slope is pressed to form a big hollow zone after four-hour of hydraulic loading, while the largest cracks are generated at the critical failure surface within the slope body.
- The soil mass contained within the critical failure surface is then pushed down with a complete failure. The failure surface after removal of the failed mass is found to fit nicely with the classical general shear failure mechanism as discussed by Cheng and Au (2005d).

For three-dimensional particle flow analysis under local loading, the loading wall pattern is used to simulate the loading applied by hydraulic jack by applying a velocity to the model loading plate. The failure process of the particle flow numerical slope model is similar to the physical model in most respects, which are observed as follows:

- An obvious collapse is noticed at the middle of slope crest where the loading plate falls down gradually forming a hole at the top. At the same time, sands at the two crest corners fall with a large velocity at the beginning and slow down to achieve equilibrium at the later stage.

- Other soil mass runs down to accumulate at the slope toe. As time goes by, small cracks are generated to form the critical failure surface followed by an instant collapse.

In comparing the physical modeling and numerical simulation, several observations can be made:

- The deformation at the center of loading plate develops greater than the lower parts of the slope surface in laboratory test, while the underneath settlement happens earlier than the middle both in the laboratory test and numerical simulation.
- The relations between the force against displacement curves are basically similar between the physical model test and the numerical model, and the final failure loadings are also very close which is not accomplished in other previous studies.

(4) For the influence of three-dimensional curvature on slope stability with or without localized loading, it is studied in Chapter 5 with discrete element method which is another pioneer work without any previous study.

The observations from simulation show that the curvature defined by R_0/H_0 has a beneficial effect on the global stability of concave slopes, especially when the resistance of soil is relatively high. Arching effect is illustrated clearly for concave slope. As a result, only partial/localized failure is initiated in concave slope under local loading.

6.2 Conclusions

The conclusions of the present study can be summarized as follows:

- For the simple cut slope, slope failure occurs firstly at the crest (unless there is nail to stabilize the crest) because of insufficient resistance to driving forces like gravity or combined influence of gravity and water.
- Soil nail can provide the resistance to soil movement by mobilizing the shear strength along the nail and massive movement of soil is restrained and limited. The stabilization effect is still observed even when major soil movement has initiated.
- The soil particles slide down continuously and enlarge the extent of failure to the lower part of the slope and eventually sliding out at the toe. Sliding out can further decrease the support to the upper soil mass and promote the whole failure, especially for the cases where water takes effect. The actual failure of the slope involves major soil movement and distortion of the geometry before the global failure surface is formed.
- The stability of the toe is also an important factor in maintaining the overall stability of a slope which is also noticed by many engineers. Toe failure under the action of rainfall commonly observed in Hong Kong is also predicted by the use of DEM in the present study.
- Particle flow analysis which is a pioneer work in slope stability analysis is demonstrated to be basically reasonable, acceptable and useful, after comparing the physical modeling and three-dimensional DEM simulation of slope under external surcharge.

- For the influence of curvature on slope stability by three-dimensional distinct element method, it indicates that more attention should be paid to reinforce the area near to the toe of slope in concave cutting slope. Also, the concave slope with high soil properties with radial oriented nails (if necessary) is a good option for the support selection.

6.3 Recommendations and suggestions for the future work

For the future study, quantitative analysis can be further carried out by micro parameters calibration by generating the numerical model based on a local discontinuous description to reproduce the macro behavior of a granular material in a quantitative manner. The macro-mechanical response of the physical material including dilatancy, strain localization and others can be reproduced by determining the micro-properties of the material including the normal, tangential and rolling stiffness, local friction and non-dimensional plastic coefficient of the contacts.

Besides, soil-nail enforcement effect on plane cut slope and concave/convex slope can also be analyzed in three-dimensional discrete element method based particle flow code program PFC3D on the basis of two-dimensional simulation results in this study. Three-dimensional effect will be analyzed on the soil-nailed slope which might be different from two-dimensional simulation. A more comprehensive view will be seen in 3D qualitative simulation. Also different way of soil nail installation can be modeled, studied and compared. Generally soil nails are installed into the slope in parallel mode in rows. For slope with flat facing, nails are parallel to each other and also perpendicular to the facing. On slope with

curved facing, however, nailing perpendicularly to the facing corresponds to the state that nailing is in the radial direction with regard to the rotation axis of slope facing. So it is expected that two nailing mode might be investigated under Distinct Element Method in PFC3D, which are radial mode and parallel mode.

Moreover, rainfall induced unsaturated slope stability can be considered by a comprehensive and appropriate fluid scheme using other existing Coupled Computational Fluid Scheme. It may also be considered by the use of secondary development of FISH language in particle flow code program in the future, but such work is possibly highly complicated and difficult so that such effect is seldom considered in the literature.

REFERENCES

Au S.W.C. (1998), Rain-induced slope instability in Hong Kong, Engineering Geology, 51, 1–36

Brand E.W. (1981), Some thoughts on rain-induced slope failures. Proceedings of the 10th International Conference on Soil Mechanics and Foundation Engineering, Stockholm 1981, 03:373–6.

Brand E.W. (1984), Relationship between rainfall and landslides in Hong Kong. Proceedings of the 4th International Symposium on Landslides in Toronto, Canada 1984, 01:377–84.

Chinniah G, Clemence SP. Thurairajah A. (1994), Slope stability in residual soils: an overview, Proceedings of the International Conference on Landslides, Slope Stability and the Safety of Infrastructures, Malaysia, 1994.

Chen H. and Lee C.F. (2004), Geohazards of slope mass movement and its prevention in Hong Kong, Engineering Geology, 76, 3–25

Cheng, Y. P., Nakata, Y. and Bolton, M. D. (2003). Distinct element simulation of crushable soil. Geotechnique 53, No. 7, 633–641.

Cheng Y.M. (1998), Advancement and Improvements in Discontinuous Deformation Analysis, Computers and Geotechnics, vol. 22, no.2, 153-163.

Cheng Y.M. and Zhang Y.H. (1998a), The Extension and Application of DDA Method, The Chinese Journal of Geotechnical Engineering, vol.20, no.3, 109-111.

Cheng Y.M. and Zhang Y.H. (1998b), Block Rotation in DDA and Its Application to Rolling Stone, Chinese Journal of Rock Mechanics and Engineering, vol. 17, p.834-839.

Cheng Y.M. and Zhang Y.H. (2000a), Rigid Body Rotation and Internal Block Discretization in DDA Analysis, International Journal for Numerical and Analytical Methods in Geomechanics, vol. 24, p.567-578.

Cheng Y.M., Zhang Y.H. and Wang K.J. (2000b), Coupling of Fem and DDA methods in engineering, Journal of Geotechnical Engineering, vol. 22, p. 727-730.

Cheng Y.M., Zhang Y.H. and Cheng W.S. (2002a), Wilson non-conforming Element in Numerical Manifold Method, Communications in Numerical Methods in Engineering, vol.18, 877-884.

Cheng Y.M., Chen W.S. and Guo X.R. (2002b), Distinct Element Analysis of Ground Deformation arising from Underground Mining, Chinese Journal of Rock Mechanics and Engineering, vol.21, no.8, p.1130-1135.

Cheng Y.M., Chen W.S. and Guo X.R. (2002c), Object Oriented Data Structure for Three-Dimensional Joint Representation, Chinese Journal of Rock Mechanics and Engineering, vol.23, no.1, 55-59.

Cheng Y.M. and Zhang Y.H. (2002d), Coupling of FEM and DDA Methods, International Journal of Geomechanics, ASCE, vol.2, no.4, 503-517.

Cheng Y.M., Chen W.S. and Guo X.R. (2002e), Procedure to the detect of three-dimensional blocks using penetration edges method, Geotechnical Special Publication no. 117, ASCE, 79-85.

Cheng Y.M. (2003b), Locations of Critical Failure Surface and some Further Studies on Slope Stability Analysis, Computers and Geotechnics, 30: 255-267.

Cheng Y.M. and Liu H.T. (2005a), Location of critical three-dimensional non-spherical failure surface with applications to highway slopes', Computers and Geotechnics, 32:387-399.

Cheng Y.M. and Zhu L.J. (2005b), Unified Formulation for Two Dimensional Slope Stability Analysis and Limitations in Factor of Safety Determination, Soils and Foundations, 44(6):121-128.

Cheng Y.M. and Lansivaara T. (2005c), Some precautions in slope stability analysis, Proceedings of the 25th Annual Seminar, Geotechnical Division, The HKIE, 4th May, p.50-57.

Cheng Y.M. and Au S.K. (2005d), Slip line solution of bearing capacity problems with inclined ground, Canadian Geotechnical Journal, vol.42, 1232-1241.

Cheng Y.M., Chen W.S. and Zhang Y.H. (2006a), A robust method for the detection of contacts for three-dimensional blocks, International Journal for Geomechanics, ASCE, 6(5):303-310.

Cheng Y.M, Wei W.B. and Lansivaara T. (2006b), Factors of safety by Limit equilibrium and strength reduction methods, The 6th Conference on Numerical Methods in geotechnical Engineering, Austria, 485-490.

Cheng Y.M., Li L., Chi S.C., Wei W.B. (2007a), Particle swarm optimization algorithm for location of a critical non-circular failure surface in two-dimensional slope stability analysis, Computers and Geotechnics, 34(2):92-103.

Cheng Y.M., Li L. and Chi S.C. (2007b), Studies on six heuristic global optimization methods in the location of critical slip surface for soil slopes, Computers and Geotechnics, vol34, 462-484.

Cheng Y.M. (2007c), Global optimization analysis of slope stability by simulated annealing with dynamic bounds and Dirac function, Engineering Optimization, 39(1):17-32.

Cheng Y M, Lansivaara T, Wei W B (2007d), Two-dimensional Slope Stability Analysis by Limit Equilibrium and Strength Reduction Methods, Computers and Geotechincs, 34:137-150.

Cheng Y.M., and Lansivaara T. (2007e), Slope Stability Analysis by improved solution procedures, Analyse de la stabilité des pentes avec procédures de solution améliorées', ECSMFE Madrid, 851-856.

Cheng Y.M. and Yip C, J.T (2007f), Three-dimensional asymmetrical slope stability analysis, Journal of Geotechnical and Geoenvironmental Engineering, ASCE, 133(12):1544-1555.

Yeung T., Cheng Y.M., Tham L.G., Au S.K., So T.C., and Choi Y.K. (2007g), Field Evaluation of a Glass-Fiber Soil Reinforcement System, Journal of Performance of Constructed facilities, ASCE, 21(1), 26-34.

Cheng Y.M., Lansivaara T and Siu J.M. (2008a), Impact of Convergence on Slope Stability Analysis and Design, Computers and Geotechnics, 35(1), pp.105-115.

Cheng Y.M., Li L. and Chi S.C. (2008b), Determination of critical slip surface using artificial fish swarms algorithm, Journal of Geotechnical and Geoenvironmental Engineering, ASCE, 134(2):244-251.

Cheng Y.M., Li L., Lansivaara T., Chi S. C. and Sun Y.J., (2008c), Minimization of factor of safety using different slip surface generation methods and an improved harmony search minimization algorithm, Engineering Optimization, vol.40, 95-115.

Cheng Y.M., Lansivaara T. and Wei W.B. (2008d), Comments on 'Two-dimensional slope stability analysis by limit equilibrium and strength reduction methods', Computers and Geotechnics, vol.35, 309-311.

Cheng Y.M., Yeung T., Tham L.G., Au S.K., So T.C., Choi Y.K., Chen J. (2008e), New soil nail material – pilot study of grouted GFRP pipe nails in Korea and Hong Kong, Journal of Civil Engineering Materials, ASCE, 21(3), 93-102.

Cheng Y.M. and Zhang Y.H. (2008f), Three-dimensional Numerical Manifold Method - Tetrahedron and Hexahedron Mesh, International for Rock Mechanics and Rock Engineering, 41(4):601-628

Cheng Y.M. and Lau C.K. (2008g), Soil Slope stability analysis and stabilization – new methods and insights, Francis and Taylors, Spon Press.

Cheng Y.M. (2009a), Music inspired harmony search algorithm, chapter 9, Springer Verlag, USA.

Cheng Y.M, Liu Z. N., Song W.D. and Au S.K. (2009b), Laboratory test and Particle Flow Simulation of the Movement of Loess Cover during Ore Drawing, Journal of Geotechnical and Geoenvironmental Engineering, ASCE, 135:1754-1761.

Cheng Y.M., Chau K.T., Xiao L.J. and Li N. (2010a), Flow pattern for silo with two layers of materials with single and double openings, Journal of Geotechnical and Geoenvironmental Engineering, ASCE, 136(9):1278:1286.

Cheng Y.M., Zhao Z.H., Sun Y.J. (2010b), Evaluation of interslice force function and discussion on convergence in slope stability analysis by the lower bound method, Journal of Geotechnical and Geoenvironmental Engineering, ASCE, 136(8):1103-1113.

Cheng Y.M. and Li N. (2011), Particle flow pattern for silos with single opening, The 14th Asian Regional Conference on Soil Mechanics and Geotechnical Engineering, Hong Kong, China, 23 - 27 May 2011.

Cheng Y.M., Lansivaara T., Baker R. and Li N. (2013) The use of internal and external variables and extremum principle in limit equilibrium formulations with application to bearing capacity and slope stability problems, Soils and Foundation, 53(1):130-143.

Calvetti, F., 2008, Discrete modelling of granular materials and geotechnical problems: European Journal of Environmental and Civil Engineering, v. 12, p. 951-965.

Cundall P.A. and Strack O.D.L. (1979), A discrete model for granular assemblies, Geotechnique 29(1):47-65.

Gabrielia F., Cola S. and Calvetti F. (2009), Use of an up-scaled DEM model for analysing the behaviour of a shallow foundation on a model slope, Geomechanics and Geoengineering 4 (2), 109–122.

Cheuk C.Y., Ng C.W.W., Sun H.W. (2005) Numerical experiments of soil nails in loose fill slopes subjected to rainfall infiltration effects, Computers and Geotechnics, 32, 290–303.

Cho S.E. and Lee S.R. (2002), Evaluation of surficial stability for homogeneous slopes considering rainfall characteristics. J of Geotech And Geoenv ASCE, 128(9): 756-763.

Dai F.C. and Lee C.F. (2001), Terrain-based mapping of landslide susceptibility using a geographical information system: a case study. Can. Geotech. J., 38: 911-923.

Eberhardt, Erik (2003), Rock Slope Stability Analysis - Utilization of Advanced Numerical Techniques, Vancouver, Canada: Earth and Ocean Sciences, University of British Columbia

Fourie A.B. (1996), Predicting rainfall-induced slope instability. Proceedings of Institution of Civil Engineers, Geotechnical Engineering, 119:211–8.

Fredlund D.G. (1979), Appropriate concepts and technology for unsaturated soils. Canadian Geotechnical Journal, 16:121–39.

Hong Kong Institution of Engineers (2003), Soil nails in loose fill slopes, Hong Kong.

Horner, D. A., J. Peters, and A. R. Carrillo (2001).Large scale discrete element modeling of vehicle-soil interaction, ASCE Journal of Engineering Mechanics 127 (10), 1027–1032.

Itasca (1999), PFC2D/3D – Particle Flow Code in 2 Dimensions, Itasca Consulting Group Inc., Minneapolis.

Itasca (2000), UDEC – Universal Distinct Element Code (Version 3.1), Itasca Consulting Group Inc., Minneapolis.

Itasca (2008). PFC3D 4.0 Particle Flow Code in Three Dimensions, Theory and Implementation Volume. Minneapolis, Minnesota.

Jenck, O., Dias D. and Kastner R. (2009), Discrete element modeling of a granular platform supported by piles in soft soil validation on a small scale model test and comparison to a numerical analysis in a continuum, Computers and Geotechnics 36, 917–927.

Khazai B. and Sitar N. (2000), Assessment of seismic slope stability using GIS modeling, Geographic Information Sciences, 5(2):121-128.

Law K.T., Yu T.K. and Cheung S.C.H. (2001), Washing Out of Fines in Recompacted Fill Slopes. In: International Conference on Landslides: Causes, Impacts and Countermeasures, Davos, Switzerland P.169-178

Li J. (2003), Field study of a soil nailed fill slopes, Ph.D. thesis, University of Hong Kong.

Lu, M., and McDowell, G.R., 2010, Discrete element modelling of railway ballast under monotonic and cyclic triaxial loading: Geotechnique, v. 60, p. 459-467.

Ng C.W. W. and Shi Q. (1998), A numerical investigation of the stability of unsaturated soil slopes subjected to transient seepage. Computers and Geotechnics, (1).

Qiu C., Esaki T., Xie M., Mitani Y., Wang C.X. (2007a). Spatio-temporal estimation of shallow landslide hazard triggered by rainfall using a three-dimensional model, Environmental Geology, 52(8): 1569-1579.

O'Sullivan C. (2011a), Particle-Based Discrete Element Modeling: Geomechanics Perspective: International Journal of Geomechanics, v. 11:449-464.

O'Sullivan C. (2011b), Particulate Discrete Element Modelling: A Geomechanics Perspectives, Spon Press.

Rahardojo H., Li X.W., Toll D.G. and Leong E.C. (2001), The effect of antecedent rainfall on slope stability, Geotechnical and Geological Engineering, 19, 371–399

Rahardjo H, Leong EC, Deutcher MS, Gasmo JM, Tang SK. (2000), Rainfall-induced slope failures, Geotechnical Engineering Monograph 3, NTU-PWD Geotechnical Research Centre, Nanyang Technological University Singapore, p. 86, ISBN 981-04-2928-2.

Wei W.B., Cheng Y.M. and Li L (2008), Three-dimensional slope failure by strength reduction and limit equilibrium methods, Computers and Geotechnics, 36:70-80.

Wei W.B. and Cheng Y.M. (2010), Soil nailed slope by strength reduction and limit equilibrium methods, Computers and Geotechnics, 37:602-618

Xie M, Esaki T, Cai M. (2004c), A time-space based approach for mapping rainfall-induced shallow landslide hazard. Environmental Geology, 2004, 46(6-7): 840-850.

Xie, M., Esaki, T., Qiu, C., Wang (2006c), Geographical information system-based computational implementation and application of spatial three-dimensional slope, Computers and Geotechnics, 33 (4), p.260-274.

Yuen C.F. (2008), Physical modeling of two dimensional non-homogeneous slopes with soil nails and without soil nails, B.Eng Thesis, Hong Kong Polytechnic University.

Zhang L.L., Zhang L.M. and Tang W.H. (2005), Rainfall-induced slope failure considering variability of soil properties, Gotechnique, 55(2), 183–188

Zhou W.H. (2008), Experimental and theoretical study on pullout resistance of grouted soil nails, Ph.D. Thesis, Hong Kong Polytechnic University.

Zhu, H.P., Zhou, Z.Y., Yang, R.Y., and Yu, A.B., 2007, Discrete particle simulation of particulate systems: Theoretical developments: Chemical Engineering Science, v. 62, p. 3378-3396.